

UNCLASSIFIED

AD 410540

DEFENSE DOCUMENTATION CENTER

FOR

SCIENTIFIC AND TECHNICAL INFORMATION

CAMERON STATION, ALEXANDRIA, VIRGINIA



UNCLASSIFIED

NOTICE: When government or other drawings, specifications or other data are used for any purpose other than in connection with a definitely related government procurement operation, the U. S. Government thereby incurs no responsibility, nor any obligation whatsoever; and the fact that the Government may have formulated, furnished, or in any way supplied the said drawings, specifications, or other data is not to be regarded by implication or otherwise as in any manner licensing the holder or any other person or corporation, or conveying any rights or permission to manufacture, use or sell any patented invention that may in any way be related thereto.

N-63-4-3

CATALOGED BY DDC  
410540  
AS AD No. \_\_\_\_\_

ASD-TDR-63-194

## ELECTROMAGNETIC SHIELDING FEASIBILITY STUDY

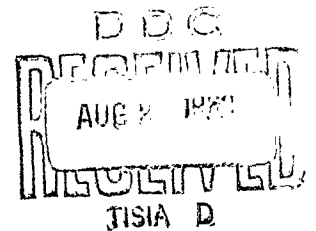
TECHNICAL DOCUMENTARY REPORT NO. ASD-TDR-63-194

May 1963

Directorate of Advanced Systems Planning  
Aeronautical Systems Division  
Air Force Systems Command  
United States Air Force  
Wright-Patterson Air Force Base, Ohio

Project No. 1395, Task No. 139502

410540



(Prepared under Contract No. AF 33(616)-8489  
by the Armour Research Foundation, Chicago, Illinois;  
Robert F. Tooper, Author.)

## NOTICES

When Government drawings, specifications, or other data are used for any purpose other than in connection with a definitely related Government procurement operation, the United States Government thereby incurs no responsibility nor any obligation whatsoever; and the fact that the Government may have formulated, furnished, or in any way supplied the said drawings, specifications, or other data, is not to be regarded by implication or otherwise as in any manner licensing the holder or any other person or corporation, or conveying any rights or permission to manufacture, use, or sell any patented invention that may in any way be related thereto.

Qualified requesters may obtain copies of this report from the Armed Services Technical Information Agency, (ASTIA), Arlington Hall Station, Arlington 12, Virginia.

This report has been released to the Office of Technical Services, U.S. Department of Commerce, Washington 25, D. C. , in stock quantities for sale to the general public.

Copies of this report should not be returned to the Aeronautical Systems Division unless return is required by security considerations, contractual obligations, or notice on a specific document.

## FOREWORD

This report was prepared by the Armour Research Foundation, Chicago, Illinois, under USAF Contract No. AF 33(616)-8489. This contract was performed under Project No. 1395, "Flight Vehicle Design", Task No. 139502, "Radiation Shield Weight Study". The work was administered under the direction of the Directorate of Advanced Systems Planning, Deputy for Technology, Aeronautical Systems Division with Sheldon B. Simmons\* succeeded by H. G. Kasten and in turn succeeded by Thomas J. McGuire, acting as project engineer.

The study presented began in June 1961 and concluded in September 1962 after a time-extension. The aim of the program was to conduct a comprehensive research study into the field of spacecraft crew shielding for the Van Allen radiation belt and solar flare environment by means of electrostatic and magnetostatic devices, and, based on 1970 state-of-the-art, to determine the feasibility of magnetostatic and electrostatic shielding.

The work reported herein was done under the direction of Robert F. Tooper, Research Physicist in the Plasma and Electron Physics Section, Physics Division, Armour Research Foundation of Illinois Institute of Technology. Important contributions to this report have been made by others. The section dealing with the mass of the structure was largely written by Sidney W. Kash. Parts of the chapter on charged particles in space were written by Thomas G. Stinchcomb and Raymond C. Barrall. The section on shielding effectiveness in Chapter 4 was written by William O. Davies. Thomas N. Casselman made contributions to the chapter on electrostatic shielding, as did S. W. Kash and Richard L. Watkins. The author wishes to thank Thomas Engelhart for his valuable suggestions concerning the transformation of Eqs. (4.29) into a form suitable for numerical integration and for his able programming of the system (4.49) with initial conditions (4.50) (4.54) (4.58) (4.63) for the UNIVAC 1105 computer, and Richard Steck for establishing a preliminary shielded-volume program for the IBM 7090, by means of which data leading to Figs. 4.13 and 4.14 were obtained. Eugene Titus kindly checked the derivation of the formula (4.80) for the vector potential of a cylindrical solenoid. The figures were drawn by Emil S. Burger, Charles R. Camplin, Chester F. Gawlik and Hugo E. Nelson. The manuscript was carried through many difficult drafts by Mrs. Betty Williams, who also did the final typing.

---

\* Deceased

## ABSTRACT

This report discusses the shielding of personnel against charged particles in space using electric or magnetic fields. The energy distribution and other characteristics of charged particles in space are summarized. The operation and stability of an electrostatic shield (two concentric charged conducting spheres) for protection against 1-Mev electrons and 500-Mev protons is discussed. Shielded regions for charges in a magnetic dipole field are described. A method is given for calculating trajectories of particles incident on a magnetic dipole in a parallel beam, with sample trajectories illustrated. The vector potential of a cylindrical solenoid is used to get the shielded region for  $L/R = 1.00$ ,  $R/C_{st} = 0.40$ . The mass of conductors and structure of superconducting solenoids are calculated in terms of the geometry and dipole moment. A non-optimum sample design has a magnetic moment  $5.66 \times 10^{12}$  gauss  $\text{cm}^3$ , radius and length 4 meters, weighs 417,000 lb, and protects  $\sim 50$  meters<sup>3</sup> from 1-Bev protons. A single-turn magnetic shield could be made 1/10 the mass of a comparable passive shield for 1-Bev protons. Structural considerations and preliminary shielded volume studies indicate that further decrease in mass could be obtained using an optimized cylindrical solenoid. Recommendations for future work emphasize further studies of cylindrical solenoids and other current configurations.

This technical documentary report has been reviewed and is approved.

*Fred D. Orazio, Sr.*

FRED D. ORAZIO, SR.

Technical Director

Directorate of Advanced Systems Planning

Deputy for Technology

## TABLE OF CONTENTS

	Page
1. INTRODUCTION	1
2. CHARACTERISTICS OF CHARGED PARTICLE RADIATION IN SPACE	7
Primary Cosmic Ray Particles	7
Particles From Solar Flares	15
Van Allen Particles	21
Effects of Short Time Exposures of Man to the Radiation in Space	24
3. ELECTROSTATIC SHIELDING	29
Operation of Two Concentric Charged Spheres	31
Stability of Two Concentric Charged Spheres	37
4. MAGNETIC SHIELDING—BASIC CONSIDERATIONS	46
Motion of Charged Particles in a Magnetic Field	46
Generation of Magnetic Fields	48
Comparison With Electrostatic Shielding	49
Motion in a Dipole Field	50
Forbidden Regions	60
Shielding Effectiveness	66
Particle Trajectories—Numerical Integration	70
Extension to General Axisymmetric Fields	94
5. MAGNETIC SHIELDING—MAGNET DESIGN	105
Characteristics of Superconducting Materials	105
Solenoid Parameters	110
Mass of the Conductors	113
Mass of the Structure	117
6. CONCLUSIONS	129
Feasibility	129
Comparison With Passive Shielding	131
Recommendations for Future Work	132
REFERENCES	135

# LIST OF FIGURES (CONTINUED)

	Page
Fig. 4. 13 Vector Potential of a Cylindrical Solenoid in the Equatorial Plane as a Function of Radial Distance.	103
Fig. 4. 14 Shielded Regions for a Cylindrical Solenoid Whose Dimensions are Comparable With the Störmer Radius, for $\gamma = -1.03$ .	104
Fig. 5. 1 Critical Current Density vs. Applied Magnetic Field for Some Niobium-Zirconium Alloys.	106
Fig. 5. 2 Critical Current vs. Applied Magnetic Field for $\text{Nb}_3\text{Sn}$ "Wires".	108
Fig. 5. 3 Definition of Coordinates and Geometrical Parameters for a Cylindrical Solenoid.	112
Fig. 5. 4 Variation of Magnetic Field With Radial Distance for a Cylindrical Solenoid.	114
Fig. 5. 5 Magnetic Pressure as a Function of Magnetic Field Strength.	116
Fig. 5. 6 Ratios of Working Stress to Azimuthal Stress and Longitudinal Stress to Azimuthal Stress for Cylindrical Solenoid Structures as Functions of $L/R$ .	122
Fig. 5. 7 Mass of the Cylindrical Structure $C_1$ as a Function of $L/R$ .	123

## LIST OF FIGURES

	Page
Fig. 2. 1 Kinetic Energy as a Function of Velocity for Relativistic and Nonrelativistic Particles.	13
Fig. 3. 1 Geometry of an Electrostatic System Capable of Shielding Against Both Positive and Negative Charged Particles.	30
Fig. 3. 2 Electrostatic Potential and Field as a Function of Radial Distance for Two Concentric Charged Spherical Conductors of Negligible Thickness.	32
Fig. 3. 3 Geometry of the Off-Center Spheres.	38
Fig. 4. 1 Geometrical Relationships Between Cartesian, Cylindrical Polar, and Spherical Polar Coordinates Used in This Report.	52
Fig. 4. 2 A Typical Line of Force of the Dipole Field.	53
Fig. 4. 3 Störmer Unit as a Function of Kinetic Energy of Protons and Electrons for Various Values of Dipole Moment.	56
Fig. 4. 4 Definition of Impact Parameters for Scattering of a Charged Particle by the Field of a Magnetic Dipole.	59
Fig. 4. 5 Regions Forbidden to Particles of a Single Energy Moving in a Magnetic Dipole Field for Various Values of the Angular Momentum Constant $\gamma$ .	63
Fig. 4. 6 Completely and Partially Shielded Regions for Particles of a Single Energy Moving in a Magnetic Dipole Field.	65
Fig. 4. 7 Trajectories in the Equatorial Plane of the Dipole.	87
Fig. 4. 8 Trajectories Incident Parallel to the Dipole Axis.	89
Fig. 4. 9 Trajectories of Particles Incident at an Angle of $22\frac{1}{2}^\circ$ With the Dipole Axis.	90
Fig. 4. 10 Trajectories of Particles Incident at an Angle of $45^\circ$ With the Dipole Axis.	91
Fig. 4. 11 Trajectories of Particles Incident at an Angle of $67\frac{1}{2}^\circ$ With the Dipole Axis.	92
Fig. 4. 12 Trajectories of Particles Incident at Right Angles to the Dipole Axis (Parallel to the Equatorial Plane).	93

## LIST OF TABLES

	Page
Table 2.1 Nuclear Abundances, Based Upon an Abundance of 100 for Hydrogen or Hydrogen Nuclei.	11
Table 2.2 Solar Proton Events.	19
Table 2.3 Integral Energy Spectrum of Particles in the Van Allen Zones.	22
Table 2.4 Effects of Radiation Doses.	26
Table 4.1 Limiting Values of Energy for Complete and Partial Shielding as a Function of Latitude for a Dipole Field.	69
Table 6.1 Parameters of Four Sample Solenoids.	130

## LIST OF PRINCIPAL SYMBOLS

### English Letter Symbols

$\vec{A}$	Magnetic vector potential
$A_\phi$	Azimuthal component of $\vec{A}$
$A(\gamma)$	Notation for inner forbidden region
$a$	Radius of inner sphere (Chapter 3)
$\vec{a}$	Magnetic dipole moment (Chapter 4)
$a$	Magnitude of $\vec{a}$ (Chapter 4)
$A$	Constant in expression for $V_i(r, \theta)$ (Chapter 3)
$A$	Constant in expression for $I(\xi)$ (Chapter 4)
$B(\gamma)$	Notation for outer forbidden region
$b$	Radius of outer sphere
$B$	Constant in expression for $V_i(r, \theta)$ (Chapter 3)
$B$	Constant in expression for $I(\xi)$ (Chapter 4)
$C_{11}$	Coefficient of capacitance
$C_{12}$	Coefficient of capacitance
$C_{21}$	Coefficient of capacitance
$C_{22}$	Coefficient of capacitance
$C_{st}$	Stormer radius
$c$	Speed of light
$D$	Constant in expression for $V_i(r, \theta)$ (Chapter 3)
$D$	Constant in expression for $I(\xi)$ (Chapter 4)
$E$	Total energy of a particle (kinetic energy plus rest energy)
$E_{ao}$	Electric field just outside the inner sphere
$E_{bi}$	Electric field just inside the outer sphere
$E_{bo}$	Electric field just outside the outer sphere

$E_{\text{elec}}$	Electrostatic energy
$E(\psi, k)$	Incomplete elliptic integral of the second kind
$E(k)$	Complete elliptic integral of the second kind
$E_{\text{kin}}$	Kinetic energy of a particle
$E_{\text{mag}}$	Magnetic energy
$E_{\text{max}}$	Vacuum-breakdown-limited electric field
$E_{\text{max}}$	Upper limiting energy for shielding effectiveness
$E_{\text{min}}$	Lower limiting energy for shielding effectiveness
$E_{\text{max}}^{\text{kin}}$	Kinetic energy corresponding to $E_{\text{max}}$
$E_{\text{min}}^{\text{kin}}$	Kinetic energy corresponding to $E_{\text{min}}$
$E(r)$	Radial electric field intensity as function of radial distance $r$
$e$	Charge of a particle
$\hat{e}_x$ , etc.	Unit vectors in direction of increasing $x$ , etc.
$E_0$	Constant in integral energy spectrum (Chapter 2)
$E$	Constant in expression for $V_i(r, \theta)$ (Chapter 3)
$\vec{F}$	Force on a particle
$F(\psi, k)$	Incomplete elliptic integral of the first kind
$F$	Constant in expression for $V_i(r, \theta)$ (Chapter 3)
$F$	Force on inner sphere due to displacement from concentricity (Chapter 3)
$\vec{H}$	Magnetic field intensity
$H$	Magnitude of $\vec{H}$
$I$	Current in a single turn
$I(\xi)$	Integrals appearing in the evaluation of vector potential from a cylindrical solenoid
$I_1(\xi)$	Integral appearing in the evaluation of vector potential from a cylindrical solenoid

$I_2(\xi)$	Integral appearing in the evaluation of vector potential from a cylindrical solenoid
$I_3(\xi)$	Integral appearing in the evaluation of vector potential from a cylindrical solenoid
$I_c$	Critical current
$j_c$	Critical current density
$K(k)$	Complete elliptic integral of the first kind
$k, k'$	Arguments of elliptic integrals (defined where they occur)
$k$	Constant in integral energy spectrum (Chapter 2)
$L$	Length of cylindrical solenoid
$\mathcal{L}$	Inductance of a cylindrical solenoid (Chapter 5)
$\mathcal{L}$	Lagrangian function (Chapter 4)
$m$	Relativistic mass of a particle
$m_0$	Rest mass of a particle
$m_{st}$	Mass of structure
$m_w$	Mass of superconducting wire
$N$	Number of turns
$n$	Differential directional intensity of a beam of particles
$N$	Particle flux (Chapter 2)
$N_e$	Electron flux
$N_p$	Proton flux
$n$	Constant in integral energy spectrum (Chapter 2)
$P_a$	Stress on inner sphere
$P_b$	Stress on outer sphere
$P_\phi$	Canonical angular momentum conjugate to the $\phi$ -coordinate
$P_1(\cos \theta)$	Legendre polynomial
$P$	Pressure
$P_0$	Impact parameter

$P$	$\xi/C_{st}$ (Chapter 4)
$Q$	Ratio of $\phi$ -component of velocity to total speed (in discussions of shielded regions)
$Q_o$	Impact parameter
$q_a$	Charge on inner sphere
$q_b$	Charge on outer sphere
$Q$	$\eta/C_{st}$ (Chapter 4)
$R$	Radius of cylindrical solenoid
$r$	Radial distance
$r'$	Radial coordinate with respect to the displaced center of the outer sphere
$r_0$	Constant in equation for dipole field line
$R$	$\xi/C_{st}$ (Chapter 4)
$R$	Radius of circular particle orbit (Chapter 4)
$s$	Arc length
$S_L$	Axial stress in cylindrical solenoid structure
$S_t$	Tensile stress
$S_y$	Yield strength
$S$	$s/C_{st}$ (Chapter 4)
$t$	Thickness of cylindrical shell
$t_d$	Total thickness of disks in cylinder-disk structure
$V_1$	Potential of inner sphere after displacement
$V_2$	Potential of outer sphere after displacement
$V_i(r')$	Potential between the two spheres in terms of $r$
$V_i(r, \theta)$	Potential between the two spheres
$V_o(r')$	Potential outside the outer sphere
$V(r)$	Electrostatic potential as function of radial distance $r$
$V_a$	Potential of inner sphere before displacement
$V_b$	Potential of outer sphere before displacement
$v$	Speed of a particle (magnitude of velocity vector)

$\vec{v}$	Vector velocity of a particle
$x$	Off-center distance when spheres are displaced slightly
$\vec{X}$	Position vector
$x, y, z$	Cartesian coordinates
$z$	Axial cylindrical coordinate

#### Greek Letter Symbols

$\beta$	$ \xi/(\omega - R) $
$\Upsilon$	Störmer angular momentum constant
$\theta$	Angular spherical coordinate
$\Lambda_0(\psi, k)$	Heuman's lambda function
$\mu$	Transformed dependent variable for particle trajectories [Cf. Eq. (4.36)]
$\xi, \eta, \zeta$	Rotated Cartesian coordinates
$\xi^+$	$z + \frac{1}{2} L$
$\xi^-$	$z - \frac{1}{2} L$
$\Pi(-\beta^2, k^2, k)$	Complete elliptic integral of the third kind
$\rho_{st}$	Density of structural material
$\rho_w$	Density of superconducting wire
$\sigma$	Transformed independent variable for particle trajectories [Cf. Eq. (4.37)]
$\sigma_a$	Surface charge density on inner sphere
$\sigma_b$	Surface charge density on outer sphere
$\sigma_w$	Cross sectional area of superconducting wire
$\phi$	Azimuthal cylindrical coordinate (also a spherical coordinate with identical meaning)
$\chi$	Impact angle for a particle approaching a magnetic dipole
$\varpi$	Cylindrical radial coordinate

## 1. INTRODUCTION

An important problem in manned space flight is to protect the crew from ambient charged particle radiation. In the Van Allen zones or during a Class 2 or higher solar flare dosage rates from ionizing radiation may reach such a level as to cause acute sudden radiation injury. Because of this, interest in shielding requirements and methods of shielding has been high. Several authors have discussed protection of personnel from the environmental radiation danger during space missions (see for example References 10, 15, 16, 29, 31, 32), but most have considered only the use of passive shielding materials. Whereas on earth protection against an arbitrarily strong radiation field can be achieved simply by using large quantities of shielding material, in space bulk shielding is restricted strongly by the payload-lifting capabilities of boosters.

Since most of the high-energy particles in space are electrically charged, electric or magnetic fields could be used to deflect the particles away from some protected area. Thus shielding would be accomplished by "active" instead of "passive" means, and the possibility exists that a saving in payload weight for the same shielded volume could be affected thereby. The purpose of this study was to determine the feasibility of active shielding methods both for space missions in the vicinity of the earth (lunar or cislunar missions) and for interplanetary voyages.

The primary purpose of considering active as opposed to passive shielding is weight reduction for systems stopping the primary charged particles or reducing their energy, but this picture is complicated by the following effects. First, a shielding system which degrades the energy of incoming particles may increase the effective dosage rate because low-energy particles have a higher relative biological effectiveness (RBE). Thus it is desirable to have a shield which reduces the flux of charged particles in certain regions without decreasing the particle energies. Second, the stopping or slowing of charged particles in passive shielding materials produces "secondaries" which add to the dose rate. Protons on interacting with matter produce neutrons and mesons; electrons on passing near atomic nuclei produce deceleration

---

Manuscript released by the author January 1963 for publication as an ASD Technical Documentary Report.

electromagnetic radiation (Bremmstrahlung) which appears in the form of high energy photons or x-rays. Both neutrons and Bremmstrahlung x-rays are uncharged and hence have great penetrating power when passing through matter; also they are not easily deflected by electromagnetic fields. A fair comparison between passive and active shielding methods should include the effect of secondaries. In some cases it is possible that the use of a passive shield without extra provision for stopping the secondaries would give rise to a higher dose rate than if no shielding at all were used. In practice the calculation of effects due to secondary production is difficult and is not carried out in the majority of treatments. A significant advantage of active shielding is that either large volumes of bulk material are not required or else the system can be designed so that bulky parts are not exposed to primary particles. Secondaries would be much less of a problem in active shielding devices than with passive systems.

At the outset it would seem simplest to use electrostatic fields to deflect charged particles. For example, a uniformly charged spherical conducting shell could be used to repel an omnidirectional flux of particles below a certain energy if the particles all have charges of the same sign. It can be shown that it is feasible to build and charge such an electrode and that the device will provide adequate shielding if all particles have charges of the same sign. But both positive and negative charged particles are found in the actual space environment. For instance, both protons and electrons occur in the Van Allen belts. Although one ordinarily thinks of solar flares as producing only high energy protons and possibly nuclei of the lighter elements, interplanetary space is filled with low energy plasma streaming out from the sun in the form of the "solar wind". The solar plasma contains an approximately equal number of electrons and positive ions so that the material as a whole is electrically neutral. Now a spherical electrostatic shield stopping, say, 500 Mev protons would accelerate either Van Allen electrons or electrons in the solar wind to energies slightly over 500 Mev. Such a device, although shielding against the protons, would produce a concentrated flux of high energy electrons. These electrons would not of themselves have any great penetrating power but would produce very dangerous x-rays on interacting with matter, whether spacecraft cabin or human tissue.

In principle an electrostatic shield consisting of two concentric charged spheres could be used as a shield against both positive and negative particles. Suppose one wishes to use such a shield for protection against 500 Mev protons and 1 Mev electrons (nominal values for the Van Allen belt). The outer sphere is charged to 500 million volts potential; this is just sufficient to stop the incoming protons, but accelerates the electrons until they have energies of 501 Mev per particle, which enables them to pass through the thin outer sphere with little energy loss or secondary production. Now suppose the inner sphere is given a potential with respect to the outer sphere of minus 501 million volts, or minus one million volts with respect to infinity. Then the electrons will have their energy reduced to zero, and the protons will not be accelerated since the potential at a point outside the outer sphere is independent of the potential on the inner sphere. Thus shielding against both protons and electrons would be achieved with little secondary production.

Practical considerations make the concentric sphere electrostatic shield unfeasible. It is difficult to charge two isolated bodies to predetermined potentials, and even harder to maintain those potentials when the electrodes are subject to continual bombardment by a beam of charged particles. Both spheres must be very large, and the outer sphere must be much larger than the inner, in order that the electric field in the intervening region may be less than the breakdown field. Since a system of charged conductors cannot remain in stable mechanical equilibrium, supports are required to keep the spheres concentric. Because of the high potential difference between the inner and outer spheres, the forces exerted by the supports against even a small displacement (less than one percent) must be very large. This ignores kinds of instability other than the spheres becoming off-center; for instance buckling would almost certainly occur in both spherical shells. Lastly, there are the openings in the spheres for access to the passenger compartments, and external equipment such as radio antennas with sharp corners, all of which would provide convenient places for the initiation of electrical breakdown.

More complicated electrostatic devices have been considered by Dow.<sup>78</sup> These have the disadvantage that they will work only for beams of particles incident from one or two directions, but may prove useful in the rare cases of

unidirectional fluxes. The flux of both Van Allen and solar flare particles after the first few minutes of the flare are omnidirectional. This is caused by the spiralling of charged particles in the geomagnetic field and interaction with turbulent interplanetary magnetic fields. The designs of Dow moreover require additional study with respect to electrostatic breakdown.

Magnetic fields may also be used to deflect charged particles away from certain regions and thus provide shielding. The action of a magnetic field on charged particles differs from that of an electrostatic field in several ways. The energy of a charged particle is not changed by the magnetic field, except for trivial amounts lost by radiation. The magnetic force on a charge does not lie in the direction of the field, and it depends on the particle velocity. The quantitative features of the particle's motion do not depend on the sign of the charge, the only difference being that a trajectory for a negative particle is the mirror image of some other trajectory for a positive particle. Thus magnetic shielding can be used for particles of both charge. Since the energy of particles not deflected from the protected area is not degraded, the RBE would not be increased by using magnetic shielding.

Until recently it appeared that, although magnetic shielding was possible in principle, it would not be possible in practice because high magnetic fields spread out over unusually large volumes would be required. Magnetic fields must be generated by electric currents, and even the use of very heavy conductors carrying large currents in coils wound around ferromagnetic materials would not result in fields sufficiently high for shielding against particles of a few hundred Mev. Besides the heavy conductors and core material, large amounts of electrical power and cooling water would be required. The weight and power requirements would clearly put the magnetic system at a disadvantage with respect to passive shielding if ordinary conductors were to be used. Also, the large amounts of conducting material and core material would provide an ideal medium for the production of secondaries.

The discovery in 1961 of superconducting materials which maintain their superconductivity in the presence of high magnetic fields has changed this situation. Because superconductors have no electrical resistance, currents can be kept flowing without the expenditure of electrical power provided that the coils are kept at the (very low) liquid helium temperature. The weight of

a superconducting coil giving the same field would be much less than that of a corresponding copper or silver coil. Because of the high currents, strong magnetic fields can be achieved without the use of iron or other ferromagnetic core material. Since ferromagnetic materials saturate at a field of about 20,000 gauss, the use of these materials is not even an advantage for fields of the order of 100,000 gauss. Secondaries are not a problem in magnetic shielding, since no core materials are required and the bulk of the superconducting material is relatively small.

Magnetic shielding using superconductors would have certain disadvantages. The coils producing the magnetic field must be kept at liquid helium temperature; thus some sort of cryogenic refrigerator or liquid helium dewar would be required. The system would be somewhat vulnerable to electrical and mechanical damage. Additional structure would have to be provided to protect the system against damage through interaction with its own magnetic field. Calculations show that this structure will comprise about ninety percent of the mass. The high magnetic fields involved will certainly have some effect on instrumentation, and electrical apparatus aboard a space vehicle using magnetic shielding would have to be designed with the magnetic field in mind. It is felt that evidence of severe d-c magnetic effects on living beings is not well-founded at present, and that exposure of a spacecraft crew to a strong magnetic field constant in time need not be a disadvantage. Nevertheless, such a threat must be considered extant until proved otherwise.

This report begins with a description of the charged particle radiation environment in space. The characteristics of the three principal forms of space radiation (primary extrasolar cosmic rays, solar flare particles, and geomagnetically trapped (Van Allen) particles) are given, with emphasis on energy range, intensity, and dosage to unshielded man. The proposed electrostatic shield is analyzed, and reasons are given and supported quantitatively for concluding that the electrostatic system is not practical. The major part of the report is devoted to a discussion of magnetic shielding using dipole-like magnetic fields produced by cylindrical air-core (or vacuum core) solenoids. It is shown that, provided the problems of fabricating superconductors into wire coils can be solved, the magnetic shield of the type described can offer a weight-saving advantage over passive shields giving

protection from equally energetic particles over equal volumes.

Studies of magnetic shielding have been carried out and reported by Dow,<sup>78</sup> Levy,<sup>77</sup> Brown,<sup>79</sup> and members of our group.<sup>74, 80</sup> It was shown by Dow that if ordinary conductors are used for the shielding coils, the system would weigh more than a passive shield giving the same protection. Levy considered a magnetic field produced by a single turn of superconducting wire carrying a high current, and showed that this system would have less weight than a corresponding passive shield if protection against high energy particles ( $\sim 1$  Bev), which one would encounter on long missions, is desired. Levy and Brown have pointed out that the prospects of magnetic shielding may be expected to improve with the development of superconducting materials having higher critical fields, critical current densities, and strength-to-weight ratios, whereas there is little room for improvement of passive systems. Both Dow and Brown have considered magnetic shields in which the deflection of particles occurs within the magnetic structure, while Levy and our group have considered systems in which the deflection takes place outside the magnet. The systems considered in this report are of the latter kind.

It is felt that the uncontained field designs are better than the contained field devices because of less problems with secondaries and more efficient utilization of the magnetic energy over larger regions of space. But it is probably too early to attempt to make a selection of one magnetic shield over the others at this time, and we will be concerned here with establishing the feasibility of such a system rather than giving a detailed design.

## 2. CHARACTERISTICS OF CHARGED PARTICLE RADIATION IN SPACE

### Primary Cosmic Ray Particles

For at least a generation the existence of primary cosmic rays has been known, and studies of their characteristics have been made not only from the standpoint of regarding them as a natural beam of high-energy particles, but also toward understanding their place of origin and the mechanism for their acceleration. These studies were very difficult in the past because very few cosmic ray particles are observed near the surface of the earth. Indeed, for a long time it was not known that the various secondary particles found near the earth's surface are products of the interaction of primary cosmic ray particles with components of the atmosphere. In the last decade cosmic-ray research has advanced greatly because high-altitude balloons, rockets, and satellites have been available for use in the upper atmosphere and beyond.

The peculiar characteristics, of which perhaps the most important is the very high energy, of cosmic rays have given rise to a number of theories concerning their origin. Some of these theories postulated that the cosmic rays are remnants of the original state of the universe before the stars were formed, or proceed from some unknown nuclear events of spontaneous decay. The central idea of these theories was that the problem of cosmic-ray origin is part of a larger cosmological problem concerning the origin and evolution of the universe as a whole, rather than explainable in terms of specific mechanisms. Recent developments which provide a key toward establishing such model theories include

1. The beam of primary cosmic ray particles is, to first approximation, a sample of the nuclei of elements found in the stars proportional to their natural abundances. These nuclei have energy in the Bev range. However, electrons and gamma rays having these energies are virtually nonexistent in the cosmic ray beam. The energies which the heavier nuclei possess are thousands of times greater than that which can be acquired by the disintegration of atomic nuclei. This seems to imply that the particles acquired their energy by some adiabatic process, proceeding over a long time, rather than

by some suddenly occurring event. Since particles which dissociate when they interact with electromagnetic fields are nearly absent, it seems reasonable to conclude that electromagnetic processes have been active in controlling the history of the particles.

2. Magnetic fields in the solar atmosphere and in interplanetary space have been found to be very important with respect to time variation of the cosmic ray flux. As a matter of fact one of the best ways of getting information about these magnetic fields is through study of cosmic rays, because the fields are too weak to be investigated by more conventional means such as the Zeeman effect.

3. It has been found that many astrophysical phenomena, such as radio emission and the polarization of starlight which has passed through the region of our galaxy, arise through the interaction of electromagnetic fields with the ionized interstellar medium.

4. The presence of large numbers of relativistic particles of high energy in such objects as the Crab nebula has been confirmed by both optical and radio astronomy.

Based on information such as the above, it may be seen that cosmic ray primaries form an important tool for gaining information about the structure of the universe in the large. Present models for the origin of cosmic rays are still sketchy for want of observational information. This condition is accentuated by our poor understanding of nonlinear hydromagnetic processes and our lack of knowledge about the interstellar and intergalactic media and the neighborhoods of supernovae or other energetic objects. But in spite of these gaps in our knowledge, probably an understanding of the origin of cosmic rays can be gained without postulating any new or rare physical processes.

One of the most recent model theories of the origin of cosmic rays is that of Morrison.<sup>30</sup> In this theory there is a wide variety of sources, each contributing to the cosmic ray flux. For cosmic rays of low energy especially, a large number of mechanisms in stellar atmospheres or based on interstellar gas motion could give rise to the observed intensities. The particles whose energies are several Mev probably have their origins in streams of

gas from the sun or other stars. Particles having energies in the 10 to 100 Bev range probably originate in stars with mass ejection and in magnetic instabilities located in spiral arms of the galaxy. Particles with energies in the  $10^3$  to  $10^5$  Bev range may originate in explosive stars, such as novae and supernovae. These stars may now be extinct, since the particles can be trapped in the galactic magnetic field long enough to go back to early stages of the galaxy. Finally, particles in the very high energy range from  $10^7$  to  $10^8$  Bev may have come from unusual very energetic extragalactic objects, such as the "jet" in the spherical galaxy NGC 4486.

We turn to a description of the properties of the cosmic radiation, including the energy distributions (References 6, 7, 30). As indicated previously one of the most important features of primary cosmic-ray particles is their high energy, which extends to at least a few times  $10^8$  Bev or  $10^{17}$  ev. It is interesting to note that a single particle of energy  $10^{17}$  ev has an energy of about  $1.6 \times 10^5$  ergs or  $1.6 \times 10^{-2}$  joules in macroscopic units.

It is a general property of the cosmic ray beam that, apart from minor fluctuations of a few percent, the flux of primary particles above the 10 Bev remains constant in time except during very large solar flares. Since the earth turns on its axis and cosmic particles undergo complex motions in the geomagnetic field, the observed constancy of the flux with time implies the uniformity of the flux over all directions of space. Particles of the lowest energies (below 2 or 3 Bev) do not follow this rule. Such particles are rare in years of strong solar activity and are present in their full intensity only near minimum of the eleven year sunspot cycle. It may be concluded that cosmic ray particles of such low energy originate in the sun and derive their energy from solar activity.

The flux of cosmic ray particles seems to remain essentially constant for periods of the order of ten thousand years. This is shown by agreement between documentary and radiocarbon dating of old historical events, for which a correction taking into account background cosmic radiation must be made. Considerations such as these give information about particles of 2 to 10 Bev energy only, but the bulk of the incoming energy lies in this range. Measurements performed on cosmic-ray-produced isotopes in meteors show that, within an order of magnitude, the flux of cosmic ray particles having

these typical energies has not changed for several hundred million years. One may thus accept, as a fundamental feature of cosmic ray phenomena, the statement that the portion of the cosmic ray flux not influenced by the sun or the earth has remained essentially constant over times comparable with geological ages. For energies below about 30 Bev the geomagnetic and solar effects increase with decreasing energy, and below a few Bev the phase of solar activity determines the observed flux.

The isotropy of the flux for particle energies above those attributable to solar activity is important. It implies that there are no strong local sources of cosmic radiation except for the sun. Now it is unlikely that the true sources of cosmic rays are isotropically situated about the earth, so we conclude that the trajectories of primary particles are influenced in such a way as to obscure the direction of their sources.

The primary cosmic ray particles are mostly protons, but there are also alpha particles and heavy nuclei up the periodic table at least as high as iron. The number of electrons and gamma ray photons is below one percent of the total. The abundances of various nuclei in the cosmic ray beam are compared with the solar system abundances of the same elements in Table 2. 1.

The overall similarity between the abundance of nuclei in the cosmic ray beam and the abundance of elements in the solar system (including the sun) is striking. Perhaps the cosmic ray beam is richer than the sun in the heavier elements, but only by a factor less than an order of magnitude. From studies of the structure and composition of stars we know that astronomical abundances are not universal but vary from object to object, depending on what thermonuclear processes are going on in a particular star. The cosmic-ray beam may provide us in the future with clues to its origin after both its composition and the composition of possible sources are known with greater precision.

Another striking property of the cosmic ray particles is their energy spectra. Using a number of different experimental methods, the primary particles have been shown to extend in kinetic energy from less than a tenth of their rest energy to as much as  $10^9$  times their rest energy. The total

**Table 2.1.** Nuclear abundances, based upon an abundance of 100 for hydrogen or hydrogen nuclei (after Reference 30).

	Cosmic ray beam (mainly below 10 Bev)	Adjusted solar system composition ("cosmic" abundances)
H	100	100
He	15	15
Li		$4 \times 10^{-7}$
Be	0 to 0.4	$1 \times 10^{-7}$
B		$1 \times 10^{-7}$
C	$1.2 \pm 0.4$	0.037
N		0.016
O		0.10
F		
Ne	0.2	0.003
Mg	0.09	0.003
Si	0.07	0.004
Fe, Co, Ni	0.06	$6 \times 10^{-4}$ up to 0.004
Beyond Ni	less than $10^{-5}$	$10^{-6}$

energy (kinetic energy plus rest mass energy) of a relativistic particle is given by

$$E = mc^2 = \frac{m_0 c^2}{(1 - v^2/c^2)^{1/2}}, \quad (2.1)$$

where  $m_0$  is the rest mass of the particle,  $m$  is its "relativistic mass",  $v$  is the speed of the particle, and  $c$  is the speed of light. If the speed of the particle is small compared with the speed of light, then the right hand side of Eq. (2.1) may be expanded in a Taylor series; retaining only the leading terms, we get

$$E \approx m_0 c^2 + \frac{1}{2} m_0 v^2. \quad (2.2)$$

This expression, except for the rest energy term  $m_0 c^2$ , is a nonrelativistic expression for the kinetic energy of a particle. Thus the kinetic energy of a relativistic particle is the quantity  $E - m_0 c^2$ .

The kinetic energy in units of rest mass energy is plotted as a function of velocity in Fig. 2.1 according to both relativistic and nonrelativistic theory. In the relativistic case at velocities near the velocity of light, the increase in energy is due to increase in mass rather than increase in velocity. For velocities of the order of  $0.75 c$ , corresponding to a relativistic kinetic energy of about half the rest energy  $m_0 c^2$ , and above, the nonrelativistic theory is to be regarded as inadequate. The rest energies of electrons and protons are

$$m_0 c^2 = \begin{cases} 511 \text{ kev for electrons,} \\ 938 \text{ Mev for protons.} \end{cases} \quad (2.3)$$

The differential directional intensity, or flux per unit energy, of a stream of particles is defined in the following way. Consider a surface in space, and upon this surface consider a differential area  $dA$  and a normal to  $dA$ . Further, consider a cone subtended an infinitesimal solid angle  $d\Omega$  centered about the normal to  $dA$ . Then  $\underline{n}$ , the differential directional intensity, is the number of particles  $dN$  crossing the unit area  $dA$  which have energy in the interval  $\underline{E}$  to  $\underline{E} + dE$ , the direction of whose velocity vectors fall in the solid angle  $d\Omega$ , per unit time  $dt$ , i. e.,

$$\underline{n} = \frac{dN}{d\Omega dA dE dt}. \quad (2.4)$$

A typical unit for  $\underline{n}$  might be protons/Mev  $\text{cm}^2$  sec steradian.

It is a consequence of Liouville's theorem of statistical mechanics that the directional intensity of a beam of charged particles moving in a constant magnetic field is constant along the path of the particles (Reference 6, pp. 267-269). Applications of this result to motion in the geomagnetic field have been made by Lemaitre and Vallarta.<sup>61-65</sup>

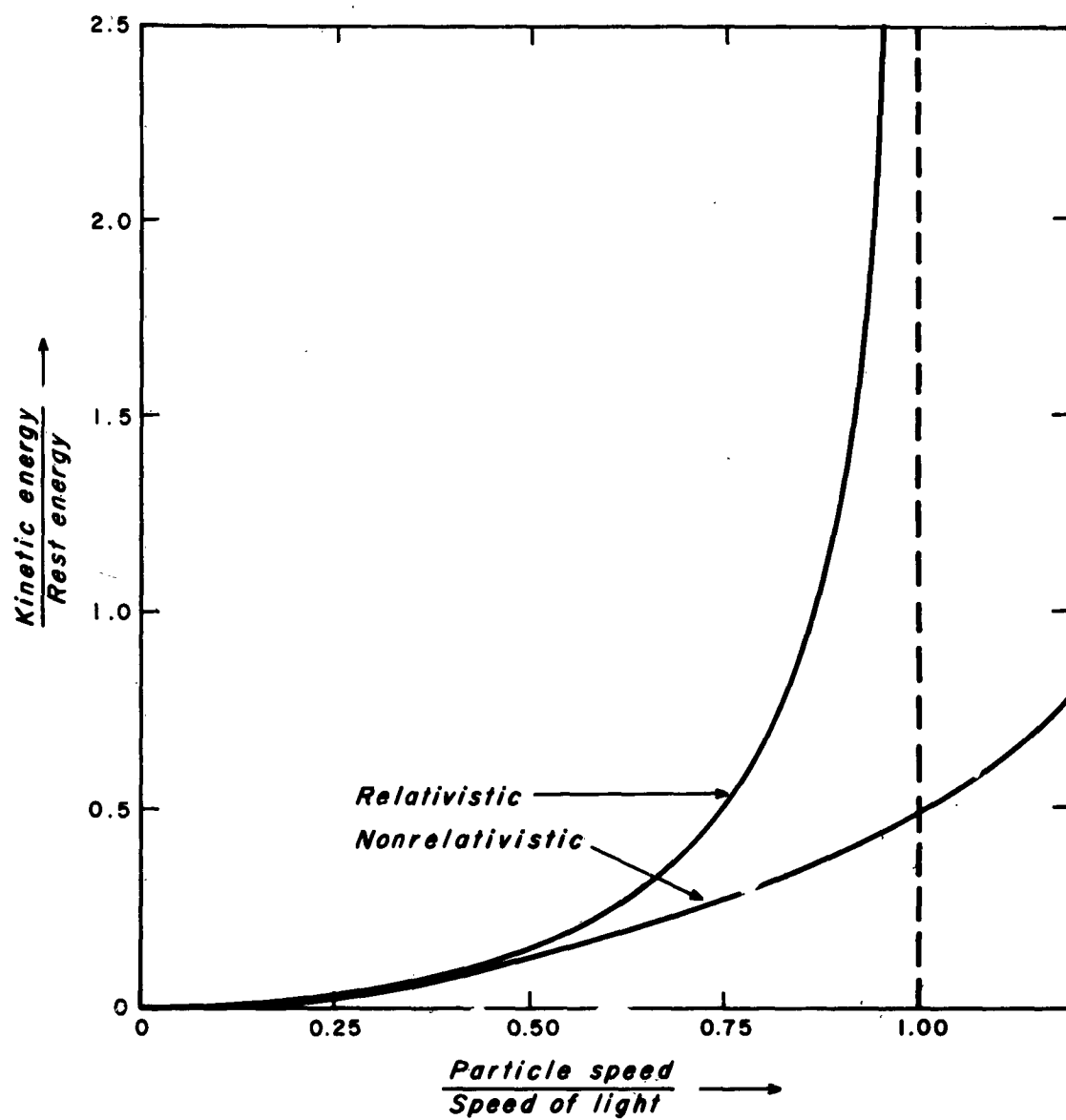


Fig. 2.1 Kinetic Energy as a Function of Velocity for Relativistic and Nonrelativistic Particles.

The intensity will in general be a function of energy:  $n = n(E)$ . The flux of particles is obtained by integrating the differential directional intensity over all values of the energy:

$$N(>E) = \int_E^{\infty} n(E) dE. \quad (2.5)$$

This gives the number of particles per unit area per second with total energies greater than  $\underline{E}$ .

The integral energy spectrum of the cosmic ray protons is well represented by the empirical formula<sup>30</sup>

$$N(>E) = 0.3 E^{-3/2} \quad (500 \text{ Mev} < E < 20 \text{ Bev}), \quad (2.6)$$

where  $N(>E)$  is measured in protons/cm<sup>2</sup> sec steradian and  $\underline{E}$  must be given in Mev. The spectrum extends up to extreme energies of at least  $10^{18}$  ev. The low energy limit is less than 100 Mev. The energy flux falling on the surface of the earth from a solid angle of  $2\pi$  steradians near the poles, where it is unaffected by geomagnetic shielding, is about  $7 \times 10^{-3}$  ergs/cm<sup>2</sup> sec. The exponent in the denominator of the formula (2.6) for the spectrum is not strictly a constant  $3/2$  but varies somewhat both with energy and with time. At sunspot maximum it goes down to  $1.2 \pm 0.1$ .

Though the sources of cosmic radiation are apparently outside our planetary system, it has become clear that conditions inside the system do affect the amount of this radiation reaching the space around the earth. Such effects as have been observed so far are decreases in the cosmic radiation. "Forbush decreases" are very sudden decreases which follow strong solar disturbances and which last several days or weeks. Presumably the plasma thrown out during the flare carries a magnetic field with it which deflects the cosmic ray particles. Another type of decrease is correlated with the eleven year solar cycle. In 1959 the intensity during the solar maximum was about half that during the solar minimum around 1954.

The cosmic ray beam is strongly shielded by the dipole magnetic field of the earth. The full cosmic ray intensity comes into the earth in the regions near the poles. But near the equator the less energetic cosmic rays are bent away from the earth so that only those having energies greater than about 15 Bev can come in. Hence the intensity near the equator is only about five percent of that in the polar regions. Beyond the geomagnetic field the cosmic radiation is presumed to be isotropic. The geomagnetic field creates an east-west effect near the earth with a predominance of the particles coming from the west.

The radiation dosage due to cosmic rays which might be encountered during a manned space flight without shielding has been estimated to be about 5 to 12 rem per year and is not regarded as hazardous.<sup>31-32</sup>

#### Particles From Solar Flares

Sunspots and solar activity are important to space flight because of their relationship to solar flares. The mechanism for formation of sunspots is not well understood. It is believed that they are formed when solar gases flow into low-pressure areas, similarly to hurricanes on earth. Because of the high magnetic Reynold's number on the surface of the sun, sunspot regions have high magnetic fields generated by magnetohydrodynamic effects. The expansion of gases in the low pressure region results in cooling with resultant lower light emission which appears as a darkening. The dark central region of a sunspot is called the umbra. Surrounding the umbra is a filamentary lighter region called the penumbra.

Several days before the formation of a sunspot, a series of bright patches called faculae appear on the sun's surface. In a very short time (sometimes as small as a few hours), a hole forms in the facular area and a sunspot is born. The faculae continue to exist throughout the lifetime of the sunspot group and may persist for several weeks after the dark areas disappear.

Usually sunspots occur in pairs or groups elongated in the direction of the sun's rotation; occasionally they may occur singly. It is believed that sometimes one member of a sunspot pair is submerged below the solar surface, and is not visible except through its influence on the faculae. Sunspots occurring in pairs have opposite magnetic polarity. Moreover, if the preceding spots in

pairs in the sun's northern hemisphere have positive magnetic polarity, the preceding spots in the southern hemisphere have negative polarity. The polarities of long-lived spots appear to reverse with each 11-year sunspot cycle; thus the true cycle may be a double one having a period of 22 years.

The largest sunspots measure 20,000 miles or more across the penumbral region, a large double group may extend 100,000 miles across the penumbra, and complex multiple groups may be even larger. A spot with diameter larger than about 20,000 miles may be seen by the naked eye if proper filters are used.

In regions of the sun where sunspots exist, solar flares may occur. A solar flare is a brightening of the facular area surrounding a sunspot. Peak brightness of the flare is reached within a few minutes; decay occurs over a period of a half hour to several hours. Flares are classified according to size as Class 1, 2, 3, or 3+. The numbers indicate the area—in 10,000ths of the solar disk—of the increased brightness of the flare. Class 1 flares, the smallest, have a mean life of about 15 minutes. They occur every few hours during periods of maximum solar activity. The largest flares, Class 3+, have a mean life of about three hours, but occur only two or three times per year. Some extremely large Class 3+ flares have lasted longer than five hours.

Solar flares produce a number of effects in the neighborhood of the earth. Sudden Ionospheric Disturbances (SID's) are radio fadeouts which occur on the bright side of the earth practically simultaneously with the brightening of the flare. They are caused by an abrupt increase in the ionization of the ionospheric D-layer due to ultraviolet radiation from the sun during the flare. Although not all flares produce SID's, some fadeouts can last for several hours.

During some, but not all, solar flares the sun may emit a considerable amount of matter. Some of this consists of protons which have moderate energies (ten to several hundred Mev) and sometimes relativistic energies (several Bev or more). In addition a plasma consisting of low energy protons and electrons is emitted from the solar flare. The protons give rise to the increases in ionization above the normal ionization produced by galactic cosmic rays. These increases are observed in detectors in rockets, balloons and sometimes at sea level. The plasma emitted by solar flares may be the cause of violent fluctuations in the earth's magnetic field (geomagnetic storm).

The protons, upon entering the geomagnetic field, are subject to the force  $\vec{F} = (e/c)\vec{v} \times \vec{H}$ , which causes them to follow trajectories depending on the vector values of  $\vec{v}$  and  $\vec{H}$ . Analysis of this effect shows that it requires more energy for a proton to enter at the equator than at the poles. Associated with each geomagnetic latitude is a cutoff energy. Protons with energies below this cutoff cannot enter but are bent into trajectories that send them away from the earth.

The history of solar proton emissions varies with latitude due to the effect of the geomagnetic field. Within about twenty degrees of the geomagnetic poles, the magnetic effects are mostly negligible, and so the observations in these polar regions reflect the history of the solar proton emissions rather than the history of geomagnetic storms. The rise-time of proton storms varies from several hours (12 hours in the event of September 3, 1960) down to fraction of an hour (1/4 hour in the event of May 4, 1960). About one hour is a typical rise-time. The decay time varies from several days (4 days in the event of July 10, 1959) to several hours (3 hours in the event of May 4, 1960) with a typical value of about a day. Except for small times, the decay generally goes proportionally to  $t^{-2}$  where  $t$  is the time after maximum intensity. For large flares the decay may be slower (e.g., proportional to  $t^{-1.5}$ ), and for small flares it may be faster.

The latitude dependence of solar protons is determined by the geomagnetic field which at the time of these events may be subject to severe fluctuations. There have been occasions (e.g., May 12, 1959) when balloon-borne detectors at Minneapolis and Murmansk, Alaska have observed the solar protons at energies 100 to 400 Mev. These energies are below the energies permitted by the normal geomagnetic field at those latitudes. The greatest solar proton intensity always occurs near the geomagnetic poles.

At the beginning of a solar proton event, the angular distribution of protons at the top of the atmosphere is anisotropic. Directions determined by permissible orbits through the magnetic field connecting the solar point of emission with the point of observation are favored. But by the time the maximum intensity is reached the angular distribution seems to become isotropic. This is probably due to large random distortions of the magnetic field near the sun, near the earth, and beyond the earth. The angular dependence of protons at

any depth inside the atmosphere is determined by atmospheric absorption, which is high at large zenith angles.

The intensity and spectral distribution vary widely from one solar proton event to another. The energy distribution can usually be approximated by an integral spectrum of the form

$$N(>E) = k(E/E_0)^{-n}, \quad (2.7)$$

where  $N(>E)$  is the number of protons having energies greater than  $E$ . Table 2.2 shows the variation in energy distribution and shows that there are marked changes in this distribution during the course of a single event. In this table  $E_0$  is taken for convenience to be 100 Mev.

It has been estimated that for a typical solar flare ( $k$  from 10 to 100 protons/cm<sup>2</sup> sec ster,  $n$  from 3 to 5), the exposure level at maximum intensity may be from 10 to 100 rem/hr and the total integrated dose may be from 20 to 400 rem.<sup>31-32</sup>

The solar protons are usually produced during solar flares of Class 2 or greater. These flares occur at random in active sunspot regions. Usually the active sunspot region does not emit solar protons on its first pass across the visible side of the sun. Hence a requirement for a proton event seems to be the presence of active sunspot regions on the visible side of the sun which were in existence on prior passes across the visible side. If large flares occur in this active sunspot region, solar protons may be emitted and may reach the vicinity of the earth. But the likelihood of any reaching the vicinity of the earth is not great while the active region is just appearing on the east limb of the sun. It is greater several days later, when the region approaches the central regions of the sun's face and remains high as the region passes through the western side and around the west limb. Thus it may be possible to have several days advance notice of a period during which a solar proton event is likely.

Anderson<sup>9</sup> made a study of the relation of the probability of solar proton emission to the size of the penumbral region of an active sunspot group.

Table 2.2. Solar proton events

Universal Time	n	k (protons/cm <sup>2</sup> sec ster)	Energy of Particles Observed (Mev)	Observation Point
0430 August 23, 1958	4	80	100-500	Balloon; Fort Churchill, Canada
0200-1500 May 12, 1959	3.8	400	100-220	Balloon emulsions; Minneapolis
2300-0830 July 14-15, 1959	3.5	17	100-400	Balloon; College, Alaska
0500 July 15, 1959	5.5	45	200	Balloon; Minneapolis
1046 July 15, 1959	2.9	1500	88-300	Balloon; Minneapolis
1700 July 15, 1959	2.6	—	400	Balloon; Lindau, Germany
After flare of 2115 July 16, 1959	4	$1500/t^3$ $t > 1.2$ days	85-300	Balloon; Resolute Bay, Canada
1000 April 1, 1960	2.6	0.4	30	Satellite; Explorer 7
0900-1200 April 1, 1960	2.4	0.5	90-500	Balloon; Minneapolis
0400 September 3, 1960	0.12	—	100-250	Balloons; Minneapolis and Fort Churchill, Canada
1000 September 3, 1960	3.5	—	100-250	Balloons; Minneapolis and Fort Churchill, Canada

He found that solar proton emission occurs predominately when the penumbral area is greater than a certain minimum. Only two out of 40 solar proton events violated his criteria (i. e. , occurred during a time not included in the interval whose beginning time is when the penumbral area of a sunspot group begins to exceed that of the group of July, 1958 measured two days before the large flare of July 7, and whose ending time is when the sunspot group goes behind the west limb), whereas 13 out of the 40 would have been expected to violate it had the events been completely random. On the other hand, there were many periods during which the criteria were satisfied (times included in these intervals) but during which no solar proton events occurred.

Robey<sup>16</sup> has made a study of two giant solar flares and the hazards to which space travelers would be subject during such flares. A large Class 3+ solar flare would be dangerous to man in space at least as far out as the nearer major planets. The Class 3+ flare of May 10, 1959 was studied, and the flux densities, dosage rates for unshielded man, and passive shielding requirements were estimated. Also considered were the very high energy cosmic ray flares, which are in a different class, tentatively denoted by Class 4, from the Class 3+ flares. The flare of February 23, 1956 was in this class and was the largest flare ever recorded. Flares in this class are rare, averaging about one every three or four years. However, the prediction of flares of Class 3+ and above is very poor.

It was estimated by Robey that a flux of  $3 \times 10^4$  protons/cm<sup>2</sup> sec ster existed at one earth-distance from the sun for several hours following the flare of May 10, 1959. This gives an equivalent dose rate for unshielded man of 280 rem/hour, assuming an RBE of 2. The cosmic noise absorption, which is taken to indicate the arrival of particles, was observed 29.5 hours before balloon measurements were made. At the time of measurement the flux was decaying with time. Thus one is being optimistic in assuming that the dose rate was constant during the 29.5 hour period at 140 rep/hour. Under this assumption the total dose from the flare is 4,374 rep. The RBE is somewhere between the limits 2 and 10, which implies an effective biological dose between 8,544 and 43,740 rem. This is lethal in either case.

There are only five cases of extremely high energy solar flares (Class 4) on record of which the flare of February 23, 1956 is thought to be the largest.

Because of the large flux of particles in the Bev energy range, this flare represents one of the worst cases from the standpoint of radiation shielding. On the basis of an estimated  $10^{13}$  grams ejected by the sun over a solid angle of one steradian, the radiation dose to an unshielded man at the earth's distance from the sun was estimated to be  $10^3$  or  $10^4$  rem/ster. This has to be multiplied by  $4\pi$  (giving another order of magnitude), because the flux would be omnidirectional because of interactions with turbulent magnetic fields in interplanetary space. The weight of a spherical shield made of carbon with an inside radius of 90 cm and a wall thickness sufficient to reduce the proton dose to 25 rem was estimated to be 834,000 pounds, assuming an RBE of unity. Actually the RBE would be higher than this because many of the protons which would pass through the shield into the cavity would have their energies degraded to low values where the RBE approaches 10 or 20. With an RBE of ten assumed for a safety factor, the shield weight is increased to several million pounds. Without the safety factor the wall thickness is about 260 cm (8.5 feet). The additional dosage from secondary neutrons and mesons was not estimated; an inside lining of a good neutron monitor would also be required.

It may be concluded tentatively that for missions in space lasting for two or three years, during which time the probability of a giant solar flare is high, shields against protons in the Bev energy range would be required.

#### Van Allen Particles

The Van Allen "radiation" consists of charged particles trapped in the earth's magnetic field or "magnetosphere". The particles are concentrated in a toroidal region centered over the geomagnetic equator. Usually this is divided into the so-called "inner zone" and "outer zone" based on regions of maximum particle intensity. The inner zone remains constant in position and intensity; the outer zone varies in position and intensity depending on solar activity.

The inner part of the Van Allen belt contains predominately large numbers of protons of energy greater than 10 Mev although electrons are also found. For energies greater than 75 Mev the integral proton energy spectrum follows approximately an  $E^{-n}$  law with  $n$  equal to 0.84. Between 10 Mev and 20 Mev,  $n$  changes to about 3.5. The total number of protons having energies greater

than 40 Mev at the heart of the inner zone (2200 miles above the geomagnetic equator) is about  $2 \times 10^4$  protons/cm<sup>2</sup> sec or about 20 rem/hr. Also the inner belt contains electrons of low energy. These electrons are much more numerous than the protons but of such low energy that they contribute little to the ionization. They are difficult to detect, and in most of the preliminary experiments the information about them has been deduced from the secondary bremsstrahlung x-rays they produce. In the heart of the inner zone, the intensity of electrons of energy greater than 20 Kev is about  $2 \times 10^9$  electrons/cm<sup>2</sup> sec steradian (accuracy within a factor of 10) and the intensity of electrons of energy greater than 600 Kev is about  $10^7$  electrons/cm<sup>2</sup> sec steradian. The integral spectrum for electrons of energy greater than 200 Kev follows an  $E^{-n}$  law with  $n$  about 4 or 5. A summary of the integral energy spectra for Van Allen particles is given in Table 2.3.

Table 2.3 Flux (integral energy spectrum) of particles in the Van Allen zones (after Reference 29).

Peak of the Inner Zone (usual situation)

Electrons:  $N_e(>30 \text{ Kev}) \approx 2 \times 10^9$  electrons/cm<sup>2</sup> sec ster  
 $N_e(>600 \text{ Kev}) \approx 1 \times 10^7$  electrons/cm<sup>2</sup> sec ster  
 Protons:  $N_p(>40 \text{ Mev}) \approx 2 \times 10^4$  protons/cm<sup>2</sup> sec

Peak of the Outer Zone (situation of high intensity)

Electrons:  $N_e(>30 \text{ Kev}) \approx 1 \times 10^{11}$  electrons/cm<sup>2</sup> sec  
 $N_e(>200 \text{ Kev}) \leq 1 \times 10^8$  electrons/cm<sup>2</sup> sec  
 Protons:  $N_p(>60 \text{ Mev}) \leq 1 \times 10^2$  protons/cm<sup>2</sup> sec

For protons of energy less than 30 Mev, no significant information is available.

Dose rate in peak of the inner zone  $\approx 24$  rem/hour.

Dose rate in peak of the outer zone  $\approx 200$  rem/hour.

The outer part of the Van Allen belt contains primarily low-energy electrons. It may be divided into two subzones which have been designated<sup>42</sup>  $E_2$  and  $E_3$ . The inner  $E_2$  subzone has maximum intensity at about 6000-7000 miles above the geomagnetic equator and the outer  $E_3$  subzone at about 9000 to 12,000 miles above the geomagnetic equator. The intensity and position of

the  $E_3$  subzone varies depending on solar activity whereas the  $E_2$  subzone is relatively stable. The  $E_3$  subzone is the more intense zone with  $10^{10}$  or  $10^{11}$  electrons/cm<sup>2</sup> sec with energies greater than 20 Kev. Naugle<sup>32</sup> estimates 200 rem/hour for typical exposure in the heart of the outer zone.

Understanding the Van Allen radiation belts will involve the solution of several physical problems. There are questions concerning the source or sources of the radiation and the mechanism by which it is injected into the geomagnetic field. There is the problem of finding the trajectories followed by the particles of trapped radiation. And there are questions concerning the lifetime of the trapped radiation, energy-loss scattering, and other mechanisms by which particles are removed from the radiation belts. Let us discuss these questions briefly. Two possible sources for the Van Allen radiation have received the most consideration: the decay of neutrons from the cosmic ray albedo of the earth's atmosphere, and the radiation from solar storms.

Measurements of neutrons in the region of the radiation belts have been made by Hess and Starnes<sup>17</sup> using a boron trifluoride detector up to 1400 km altitude. Since such a detector is predominantly sensitive to neutrons of energy much lower than those whose decay is supposed to give rise to the measured Van Allen belt protons, these data do not readily yield the necessary source information for the proton radiation, although they do for the electron radiation. Neutron spectrum measurements in the energy range appropriate to gain source information for the Van Allen belt protons have been carried out by Hess and others in airplanes to 40,000 ft elevation. These results must be extrapolated to Van Allen belt elevations in order to be applicable. However, the neutron albedo source in the energy regions appropriate to the Van Allen electron radiation is more reliably known since the atmospheric measurements coupled with diffusion calculations are confirmed by outer-space measurements. On the basis of presently available information it has been concluded that neither the outer belt electron radiation nor the inner belt electron radiation is accounted for solely by injection of neutron decay electrons. The protons radiation may be accounted for by injection of neutron decay protons insofar as order of magnitude is concerned, but there is some lack of agreement in the shape of the spectrum.

Protons from solar flares may be the source of a part of the Van Allen proton radiation, although the fact that there are only small changes in the proton radiation level during a solar proton event tends to weaken this hypothesis. The radiation from solar flares is favored as a source for the Van Allen electron radiation because of the changes in intensity and position of the outer belt during solar emission. But this hypothesis is not consistent with the fact that no energetic electrons have been detected in the solar radiation. Also no adequate mechanism to provide acceleration of electrons to observed energies during these events is presently known.

Although the motion of particles trapped in a magnetic field is well understood, the application of these principles to charged particles in the earth's magnetic field becomes complicated mathematically. Computations of low-momentum trajectories are much simplified by adiabatic invariants. Calculated changes in intensity and angular distribution of the trapped radiation as functions of position in the geomagnetic field are consistent with such measurements as have been made. However, the trajectories of high momentum particles for which the Alfvén discriminant is of order of 0.1 or greater are not well understood because the method of adiabatic invariants fails in this case.

The time that a particle can remain trapped in the geomagnetic field depends on many considerations such as energy loss by collision with ions and neutral atoms, charge exchange, and nuclear interactions. Cross sections or the probability of occurrence for these processes are well known. The lifetimes can be calculated to the accuracy with which the composition of residual matter in these regions of space is known. Fluctuations such as hydromagnetic waves and magnetic storms in the magnetic fields will affect the lifetimes. Dust particles in space may also have some effect on the lifetimes of the particles.

#### Effects of Short-Time Exposures of Man to the Radiations in Space

It is of considerable interest to make an estimate of the radiation exposure which an individual might receive during space travel. Information currently available on the radiation levels in space make it clear that this problem is one which might best be described as "of major importance" in the planning of such travel.

Initial work in the field of radiation dosimetry led to the establishment and use of the roentgen as a basic unit of radiation dose. The roentgen is defined as that amount of radiation which produces in one cubic centimeter of air one electrostatic unit of charge of either sign. This is about 83 ergs/gram of air. This unit, while useful, presents certain difficulties which are removed in part by a unit called the rep. A rep, or "roentgen equivalent physical", is the amount of energy per gram of tissue which results from exposure to a radiation field of 1 roentgen. Measurements indicate that the rep is equal to 93 ergs/gram. Another unit which has become popular is the rad, which is simply 100 ergs/gram. These latter units have an advantage over the roentgen in that they characterize the radiation dose in terms of the energy deposited in tissue rather than merely describing an effect due to the passage of the radiation through air. The damage to tissue for a given amount of energy per gram is dependent upon the type of radiation and the energy of the primary radiation. In other words, the various radiations differ in their relative biological effectiveness (RBE). The rem, "roentgen equivalent man," equal to the product of rads times RBE is the most meaningful unit because it is in terms of the effects of radiation on human beings.

With this brief introduction to dosimetry, we turn now to the problem of determining how much radiation is too much. Like many problems in life sciences, a single definite answer is not available. There is nearly universal agreement that radiation is harmful. At high intensity, death or other effects occur with fairly definite probability and usually somewhat delayed in time. At low levels the exact effects are now known, although most experts are of the opinion that all radiation is harmful to some degree and might be manifested as a slightly shortened lifespan or other effect difficult to recognize.

The gross acute effects of radiation are also time-dependent. This is a consequence of the ability of the body to rebuild and repair. This could be of considerable importance for relatively long exposures such as might occur during prolonged space travel. A consideration of the time dependency of the effects of long exposures should precede extended space travel. However, we shall limit our considerations to the more immediate problem of shorter term exposures since shorter ventures into space are certain to precede longer missions. We must note, however, that even distributing the radiation exposure over a period of several days will somewhat reduce the observable effects.

As a more conservative estimate will result from neglecting this effect, it will not be taken into consideration at this time.

While there is not any amount of radiation which can be called completely safe, there are maximum permissible radiation exposures established by law. These standards allow routine exposures up to roughly 3 rem per calendar quarter provided that the total accumulated exposure does not exceed an average of 5 rem per year after age 18. The regulations also permit a single exposure of 25 rem "occurring only once in the lifetime of the person". It is clear that the scope of such recommendations and regulations was never intended to include travel in extraterrestrial space. Still, a limit must be selected and when one takes into consideration the other elements of risk which face the space traveler, a limit which is not unduly conservative would seem to be in order.

To aid in the selection of such a limit, a few of the effects of radiation are reviewed in Table 2. 4 in order to help suggest a limit and to illustrate the consequences of exceeding such a limit.

Table 2. 4 Effects of radiation doses

Dose (rem)	Major Effects From Short Exposures
600	Essentially no survivors.
400	Many symptoms; only 50% would survive 30 days with medical attention.
200	Few symptoms during the first two weeks; many symptoms beginning in the third week; perhaps 90% surviving 30 days with medical attention; the 90% probably making a rather complete recovery.
50	Transient changes in the blood cells. Essentially 100% survival. Ill effects at a later time not likely.
25	No effects observable.

It can be seen from Table 2. 4 that exposure to 25 rem would not be cause for alarm if lower exposures are not attainable. One must also take into consideration the possibility that additional shielding may increase the

hazard by adding to weight generally and possibly supplanting other features or items of equipment. However, any limit ultimately selected must also be influenced by the need for a safety factor which compensates for the uncertainty in dosimetry in this new field.

The protons in the Van Allen region are relatively high in energy by the usual standards. Van Allen<sup>29</sup> has estimated that a traverse of the radiation belts might result in a dose of the order of 10 roentgens. If one takes the data of Schaefer<sup>60</sup> indicating approximately 120 rep/hr at the peak of the inner radiation belt, and assumes travel through the belt at a velocity of 5 miles per second taking into account the change in intensity with distance, a dose of approximately 15 reps per traverse results. The above calculation assumes the electron dose to be negligible with very slight shielding afforded by structural materials. Schaefer has made a preliminary evaluation of the RBE of protons in the Van Allen radiation belt and obtained a value of about 1.2. He found the RBE for solar flare protons to be about 1.5. These factors are sufficiently close to 1.0 to be neglected for the present estimations in view of the fact that RBE is also a function of the proton energy.

From the foregoing it is obvious that the radiation levels would not allow a manned craft to remain in the Van Allen radiation belt for any appreciable time.

Another important aspect of the radiation hazard in space is that presented by solar flares. Solar flares have been observed to produce dose rates on the order of 200-300 rep/hour and to persist for several hours. In the case of only minimal shielding of  $2 \text{ gm/cm}^2$  such as would be expected for structural strength, the lethal consequences of being exposed to a solar flare is so obvious as to require no further comment. While efforts to increase the predictability of solar flares are continuing, it would appear unlikely that prediction will be satisfactory for the longer flights. Thus, shielding for solar flares appears to be mandatory. It is noted that this is not necessarily the case for the Van Allen belt since there are "polar cones" through which one might pass and the ability to predict the radiation dose within reasonable limits makes the hazard more acceptable. However, a departure over the polar caps could be hazardous if a large solar flare were to occur, in fact more hazardous than a departure through the Van Allen belt where the geomagnetic field offers some protection. Although the earth's magnetic field acts as a barrier to solar

flare particles in the lower latitudes, it will assist these particles to funnel down over the geomagnetic poles by the magnetic mirror effect. Thus the flux of solar flare protons would be high in the regions considered safe from Van Allen particles.

In conclusion, the most profitable shielding effort will be against solar flare protons. Besides being the source of the highest particle intensity, the proton energy spectrum contains more of the lower energy protons which have greater absorption coefficients. The RBE of these lower energy protons is higher because of the greater linear energy transfer (LET). The solar flare proton spectrum peaks at less than 50 Mev and decreases exponentially at energies greater than about 100 Mev. Assuming a minimal structural shielding of 2 grams/cm<sup>2</sup>, and using data from the solar flare of May 1959, one may determine graphically that about 80 percent of the protons have energies less than about 50 Mev; about 92 percent less than 75 Mev, 96 percent have energies less than 100 Mev; and 1 percent have energies in excess of 150 Mev.

As a preliminary estimate, it is necessary to shield against protons up to 150 Mev in order to achieve a shielding factor of about 100. Of course, in the interest of simplicity, we have passed over a number of problems which deserve more attention. Among these are the radiation damage potential in the lens of the eye, change in RBE as the proton energy penetrating the shield changes, and possible radiation effects not adequately predicted by measurements and calculations based only on ionization in tissue.

### 3. ELECTROSTATIC SHIELDING

One of the methods proposed for shielding a space vehicle against high energy charged particles is to use electrostatic fields. Such fields could be set up around the spacecraft by giving the vehicle an electric charge. The electric field would repel particles having the same charge polarity as the vehicle, but would attract particles having the opposite charge. It is also possible in principle to design electrostatic configurations which would shield against charged particles of both signs. The simplest such design is the two concentric spheres which will be discussed in the sequel.

Let us compare the advantages and disadvantages of the electrostatic shield with those of the uncontained or dipole-like magnetic shield. A single spherical charged conductor will attract all particles of opposite charge besides repelling all particles of the same charge. The shielding effect will be isotropic since the repulsion or attraction would not depend on the direction from which the particles approach the sphere. On the other hand, the magnetic shield is intrinsically effective against particles of both signs. Magnetic shielding is anisotropic because the forbidden regions for particles of the same energy depend on the direction from which particles approach and on their impact parameters.

Although simple conceptually, electrostatic shielding is impractical, primarily because of the high potentials required on the conducting surfaces. Extremely large and relatively smooth surfaces would be required to prevent electrical breakdown and charge leakage. Shielding against charged particles of both signs would require two concentric spheres. Such a system of charged conductors inherently unstable and, as will be shown later, the force resulting from a small off-center displacement tending to increase that displacement would have to be compensated by a structure adding considerably to the mass of the system and to the electrical breakdown problems. Finally, it is not clear how the high potentials required could be generated and maintained in interplanetary space, which is a relatively good electrical conductor.

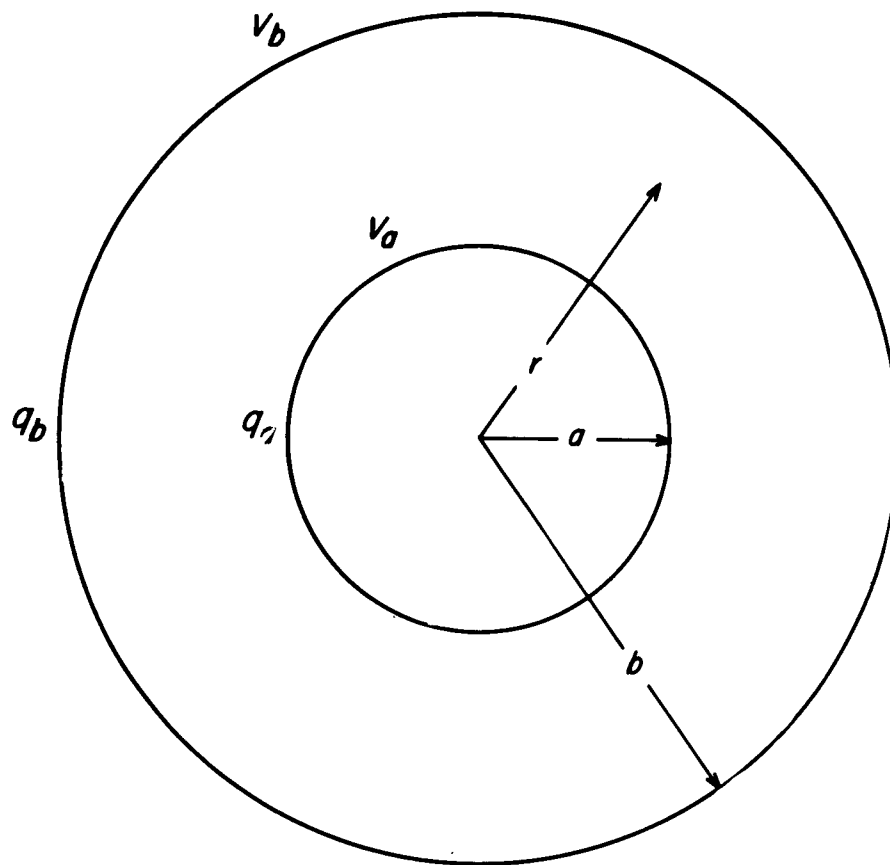


**Fig. 3.1 Geometry of an Electrostatic System Capable of Shielding Against Both Positive and Negative Charged Particles.**

### Operation of Two Concentric Charged Spheres

By using two concentric spheres charged to opposite polarities it is in principle possible to shield against both positive and negative charged particles. In this section we consider the way in which such a shield would operate and establish the dimensions of the system based on vacuum breakdown considerations. In the next section we study the stability of the system and calculate the force tending to increase an off-center displacement. A drawing of the system is shown in Fig. 3. 1. The region to be shielded is that within the inner sphere.

Let  $a$  and  $b$  represent the radii of the inner and outer spheres, and let  $q_a$ ,  $V_a$  and  $q_b$ ,  $V_b$  be the corresponding charges and potentials on the spheres. The electrostatic potential  $V(r)$  at a distance  $r$  from the common center of the two spheres is given by

$$V(r) = \begin{cases} V_a & (0 \leq r \leq a) \\ \frac{bV_b - aV_a}{b-a} - \frac{ab}{b-a} \frac{V_b - V_a}{r} & (a \leq r \leq b) \\ \frac{b}{r} V_b & (b \leq r) \end{cases} \quad (3.1)$$

in terms of  $V_a$ ,  $V_b$  or by

$$V(r) = \begin{cases} \frac{q_a}{a} + \frac{q_b}{b} & (0 \leq r \leq a) \\ \frac{q_a}{r} + \frac{q_b}{b} & (a \leq r \leq b) \\ \frac{q_a + q_b}{r} & (b \leq r) \end{cases} \quad (3.2)$$

in terms of the charges. \*

---

\* Equation (3. 2) is expressed in electrostatic units whereas Eq. (3. 1) can be regarded as independent of the system of units. In what follows we shall work in the esu system but some of our results will be stated in engineering units for the sake of familiarity.

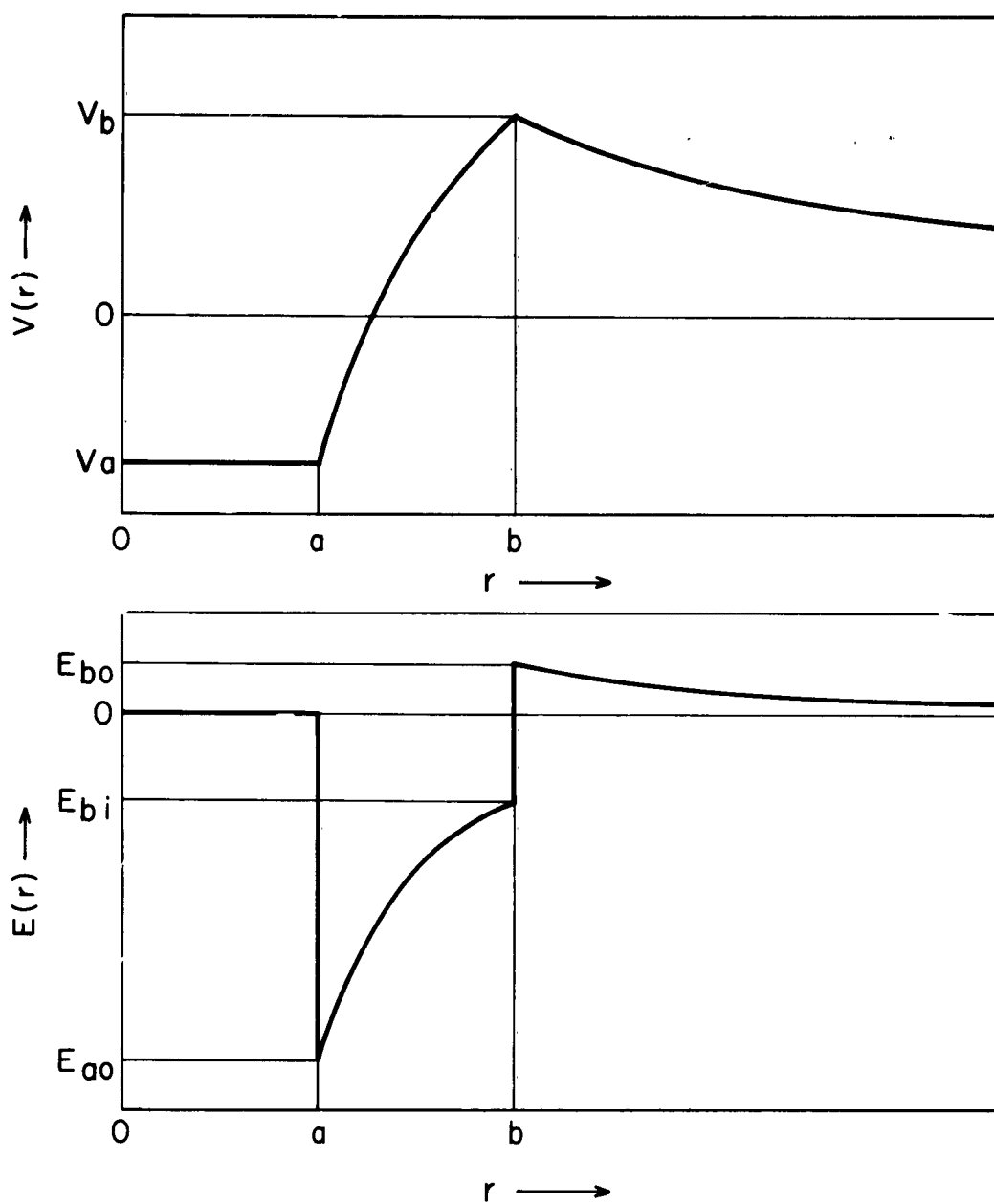


Fig. 3.2 Electrostatic Potential and Field as a Function of Radial Distance for Two Concentric Charged Spherical Conductors of Negligible Thickness.

The potentials are related to the charges by

$$\left. \begin{aligned} V_a &= \frac{q_a}{a} + \frac{q_b}{b} \\ V_b &= \frac{q_a + q_b}{b} \end{aligned} \right\}, \quad (3.3)$$

or, conversely, by

$$\left. \begin{aligned} q_a &= -\frac{ab}{b-a} (V_b - V_a) \\ q_b &= \frac{b(bV_b - aV_a)}{b-a} \end{aligned} \right\}. \quad (3.4)$$

A typical plot of the electrostatic potential (3.1) as a function of radial position is shown in the upper graph of Fig. 3.2. The potential function is continuous but contains two "corners", one at  $a$  and the other at  $b$ . An approaching proton of charge  $e$  aimed directly at the center of the spheres (zero angular momentum) with kinetic energy less than  $eV_b$  encounters a potential barrier and its turning point is outside the outer sphere ( $b < r_t$ ). An electron of charge  $-e$  and zero angular momentum with kinetic energy less than  $-eV_a$  also encounters a potential barrier, but its turning point is in the space between the two spheres ( $a < r_t < b$ ). In the foregoing and in the figure we have assumed that  $V_a$  is positive. The essential double potential barrier could also have been obtained by taking  $V_a$  positive and  $V_b$  negative, but we will show later that this situation is less advantageous from the standpoint of breakdown in view of the fact that in the space environment the protons are much more energetic than the electrons.

The electric field as a function of position is obtained by taking the negative derivative of the potential with respect to  $r$ . In terms of potentials,

the field is given by

$$E(r) = \begin{cases} 0 & (0 \leq r \leq a), \\ -\frac{a^3}{b-a} \frac{V_b - V_a}{r^2} & (a \leq r \leq b), \\ \frac{b}{r^2} V_b & (b \leq r). \end{cases} \quad (3.5)$$

This function has discontinuities at  $a$  and  $b$  (Cf. Fig. 3.2). Inside the smaller sphere the field is zero. Just outside the inner sphere it jumps to a value  $E_{ao}$  given by

$$E_{ao} = -\frac{b}{a} \frac{V_b - V_a}{b-a}. \quad (3.6)$$

The field then falls continuously in absolute value until a point just inside the larger sphere is reached; the field there is

$$E_{bi} = -\frac{a}{b} \frac{V_b - V_a}{b-a}. \quad (3.7)$$

Just outside the outer sphere it jumps to the value

$$E_{bo} = V_b/b. \quad (3.8)$$

As a result of the electric forces, the inner sphere will experience a pressure (independent of the sign of  $q_+$  and the value of  $q_b$ ) tending to expand it.

This pressure will be equal to

$$P_a = \frac{E_{ao}^2}{8\pi} = \frac{1}{8\pi} \left( \frac{b}{a} \frac{V_b - V_a}{b-a} \right)^2. \quad (3.9)$$

The outer sphere will experience a pressure or tension given by

$$P_b = \frac{E_{bo}^2 - E_{bi}^2}{8\pi}. \quad (3.10)$$

To avoid buckling instabilities in the outer sphere, it should be maintained under pressure ( $P_b > 0$ ) rather than tension ( $P_b < 0$ ); that is, we require  $|E_{bo}| > |E_{bi}|$ . This leads directly to the condition that

$$\frac{b}{a} > 2 - \left| \frac{V_a}{V_b} \right|. \quad (3.11)$$

Thus by the proper choice of  $b/a$  the outer sphere can be maintained subject to a slight outward pressure.

Let us at this point compare the electric fields just outside each of the two spheres:

$$\left| \frac{E_{ao}}{E_{bo}} \right| = - \frac{E_{ao}}{E_{bo}} = \frac{b^2}{a(b-a)} \left( 1 - \frac{V_a}{V_b} \right). \quad (3.12)$$

Generally the protons in space are considerably more energetic than the electrons. We have a choice between making (1) the inner sphere positive ( $V_a > 0$ ) to repel the protons and the outer sphere negative ( $V_b < 0$ ) to repel the electrons with  $|V_a| \gg |V_b|$  or (2) making the inner sphere negative ( $V_a < 0$ ) to repel the electrons and the outer sphere positive ( $V_b > 0$ ) to repel

the protons with  $|V_a| \ll |V_b|$ . In case (1) we have  $V_a/V_b \ll -1$  and in case (2) we have  $V_b/V_a \ll -1$ .

Suppose first that  $V_a/V_b \ll -1$ . Then Eq. (3.12) gives

$$\left| \frac{E_{ao}}{E_{bo}} \right| \gg \frac{2b^2}{a(b-a)} \quad (V_a \ll -V_b). \quad (3.13)$$

The right hand side of this expression has (for  $b > a$ ) a minimum (equal to 8) at  $b/a = 2$  and increases nearly linearly with large  $b/a$ . Hence

$$|E_{ao}| \gg 8 |E_{bo}| \quad (V_a \ll -V_b). \quad (3.14)$$

This condition is undesirable. Since the largest field  $|E_{ao}|$  in the system must be less than the breakdown field  $E_{\max}$ , the outside field  $|E_{bo}|$  must be much less than  $E_{\max}/8$ . This could only be achieved, for useful values of  $V_a - V_b$ , by making the outer sphere extremely large. But the inner sphere would have to be made large too in order to keep the ratio  $b/a$  near 2.

Now suppose  $V_b/V_a \ll -1$ . In this case Eq. (3.12) gives

$$\left| \frac{E_{ao}}{E_{bo}} \right| > \frac{b^2}{a(b-a)} \quad (V_b \ll -V_a). \quad (3.15)$$

This is a much more moderate condition on  $E_{ao}$  than (3.13). In particular by staying near  $b/a = 2$  we can keep the field  $|E_{ao}|$  near  $4 |E_{bo}|$ . Accordingly all our future discussions will be restricted to the case where the inner sphere is negative (to make a potential barrier for the electrons) and the outer sphere is positive (to make a potential barrier for the protons) (This is the case illustrated in Fig. 3.2).

In conclusion we require that the outer sphere be charged positively to the potential required to repel the protons. The inner sphere should have a radius slightly less than half the outer one, and it should be charged negatively to a potential sufficient to repel the electrons. It should be noted that if the electrons have initially a high enough energy so that they are not kept from the inner sphere, they will enter it with their kinetic energy decreased by an amount  $-eV_a$ . The electric field will be greatest just outside the inner sphere and will there be given approximately by

$$|E_{ao}| \xrightarrow{b=2a} (2/a)(V_b - V_a) \approx 4|E_{bo}|. \quad (3.16)$$

As an example, suppose the outer sphere is charged to a potential  $V_b = +5 \times 10^8$  volts and the inner sphere to a potential  $V_a = -10^6$  volts. This arrangement would provide shielding against protons of 500 Mev kinetic energy and 1-Mev electrons. Suppose further that the field  $|E_{ao}|$  is to be just equal to the field  $E_{\max} \approx 3 \times 10^7$  volts/meter at which vacuum breakdown occurs. Then using  $b = 2a$  to give a slight outward pressure to the outer sphere according to the condition (3.11), we find, from Eq. (3.6),

$$b - a = 2(V_b - V_a)/E_{\max} \approx 33.3 \text{ meters.}$$

Thus  $a = 33.3$  meters and  $b = 66.6$  meters. The fields  $|E_{bi}|$  and  $E_{bo}$  are nearly equal and have the approximate value  $7.5 \times 10^6$  volts/meter.

#### Stability of Two Concentric Charged Spheres

Besides the effects discussed above there is the problem of stability of an electrostatically charged concentric spherical system. Although we have already guarded against buckling instabilities by imposing the criterion (3.11), Earnshaw's theorem states that no electrostatic system can be in a state of stable equilibrium, and we must look into other type of instability that may occur. Now it is a characteristic of all linearized theories of equilibrium

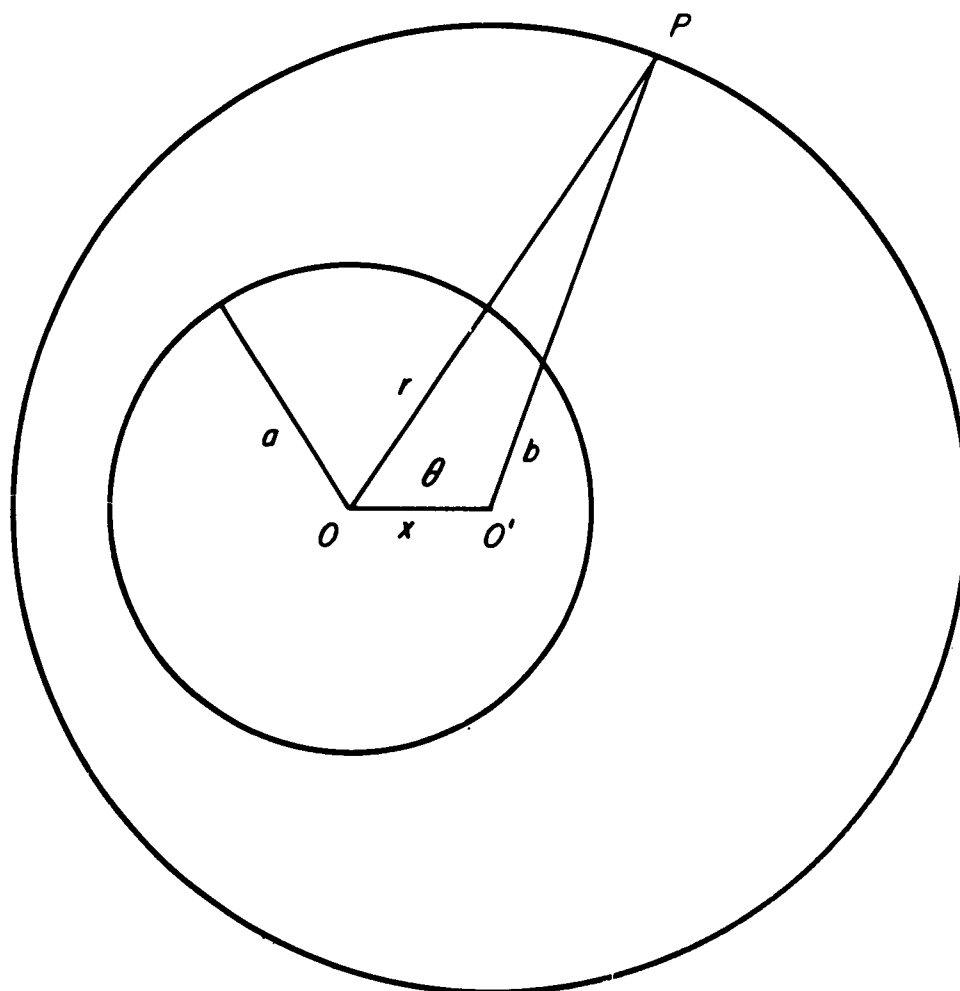


Fig. 3.3 Geometry of the Off-Center Spheres

that it is impossible to predict the form which an instability will take; the best that can be done is to assume some small departure of a specific type from the equilibrium state and calculate the forces tending either to restore the system to equilibrium (in which case the system is stable) or to increase the departure from equilibrium (in which case the equilibrium is unstable). In the case of the oppositely charged concentric spheres any change in their concentricity will give rise to a redistribution of charge on their surfaces such that there will be a net attractive force between them. Without some kind of supporting structure any movement away from concentricity will cause the spheres to collide. Accordingly we shall calculate the net force produced as a function of the off-center distance by extending a method given by Smythe (Reference 2, p. 141).

We first need to calculate the electrostatic potential as a function of position in the space between the two spheres when they are displaced a small distance  $x$ . We choose the origin  $O$  at the center of the inner sphere (Fig. 3.3); then the equation of the outer sphere of radius  $b$  with respect to the center of the inner is, to the second order in  $x/r$ ,

$$\frac{1}{b} \approx \frac{1}{r} \left[ 1 + \frac{x}{r} P_1(\cos \theta) + \frac{x^2}{r^2} P_2(\cos \theta) \right]. \quad (3.17)$$

Here  $P_1(\cos \theta) = \cos \theta$ ,  $P_2(\cos \theta) = (3 \cos^2 \theta - 1)/2$  are Legendre polynomials of the first and second order. Solving Eq. (3.17) for  $r$  we have approximately

$$r \approx b \left[ 1 + \frac{x}{b} \cos \theta - \frac{x^2}{2b^2} \sin^2 \theta \right]. \quad (3.18)$$

Since here the boundary conditions involve terms up to  $O(x^2/b^2)$  and since both  $r = 0$  and  $r = \infty$  are excluded from the field, the potential between the

two spheres must be of the form

$$V_i(r, \theta) = A + \frac{B}{r} + \left[ Cr + \frac{D}{r^2} \right] P_1(\cos \theta) + \left[ Er^2 + \frac{F}{r^3} \right] P_2(\cos \theta), \quad (3.19)$$

in which  $\underline{C}$ ,  $\underline{D}$  are correction terms proportional to  $\underline{x}$  and  $\underline{E}$ ,  $\underline{F}$  are correction terms proportional to  $\underline{x}^2$ . The boundary conditions are

$$V_i(a, \theta) = V_1, \quad (3.20a)$$

$$V_i\left(b \left[1 + (x/b)\cos \theta - (x^2/2b^2)\sin^2 \theta\right], \theta\right) = V_2. \quad (3.20b)$$

Application of the first boundary condition (3.20a) gives, on equating like powers of  $\cos \theta$ ,

$$A + \frac{B}{a} - \frac{a^2 E}{2} - \frac{F}{2a^3} = V_1, \quad (3.21a)$$

$$aC + \frac{D}{a^2} = 0, \quad (3.21b)$$

$$a^2 E + \frac{F}{a^3} = 0. \quad (3.21c)$$

Application of the second boundary condition (3.20b) gives, when terms of order higher than  $\underline{x}^2$  are neglected and coefficients of  $\cos \theta$  are set equal,

$$A + \left(\frac{1}{b} + \frac{x^2}{2b^3}\right)B - \frac{b^2 E}{2} - \frac{F}{2b^3} = V_2, \quad (3.21d)$$

$$-\frac{x B}{b^2} + b C + \frac{D}{b^2} = 0, \quad (3.21e)$$

$$\frac{x^2 B}{2b^3} + x C - \frac{2x D}{b^3} + \frac{3b^2 E}{2} + \frac{3F}{2b} = 0. \quad (3.21f)$$

Solving, we have

$$A = V_1 + \frac{b(b^3 - a^3)(V_2 - V_1)}{(b^3 - a^3)(b - a) - abx^2}, \quad (3.22a)$$

$$B = -\frac{ab(b^3 - a^3)(V_2 - V_1)}{(b^3 - a^3)(b - a) - abx^2}. \quad (3.22b)$$

It will appear that the other coefficients are not needed in calculating the force between the spheres.

The surface charge density on the inner sphere is given by

$$\begin{aligned} \sigma_a(\theta) &= -\frac{1}{4\pi} \left. \frac{\partial V_i}{\partial r} \right|_{r=a} \\ &\approx \frac{1}{4\pi} \left\{ \frac{B}{a^2} - \left( C - \frac{2D}{a^3} \right) P_1(\cos \theta) - \left( 2Ea - \frac{3F}{a^4} \right) P_2(\cos \theta) \right\}. \end{aligned} \quad (3.23)$$

When this is integrated over the surface of the sphere  $a$ , the terms in  $P_1(\cos \theta)$  and  $P_2(\cos \theta)$  give no contribution. Thus the charge on the inner sphere is

$$q_a \approx B \approx -\frac{ab(b^3 - a^3)(V_2 - V_1)}{(b^3 - a^3)(b - a) - abx^2}. \quad (3.24)$$

To get the charge on the outer sphere we must express the potential between the spheres in terms of the radius vector  $\underline{r}'$  of a field point with respect to the center  $O'$  of the outer sphere. This is related to  $\underline{r}$  by an equation analogous to (3.18), viz

$$r \approx r' \left( 1 + \frac{x}{r'} \cos \theta - \frac{x^2}{2r'^2} \sin^2 \theta \right). \quad (3.25)$$

The angle  $\theta$  remains the same when referred to the new origin in the order of approximation to which we are working. In terms of  $\underline{r}'$  the potential between the spheres becomes, to  $O(x^2)$ ,

$$\begin{aligned} V_i(r') \approx & A + \frac{B}{r'} \left[ 1 - \frac{x}{r'} \cos \theta + \frac{x^2}{2r'^2} (1 + \cos^2 \theta) \right] \\ & + C r' \left( 1 + \frac{x}{r'} \cos \theta \right) \cos \theta + \frac{D}{r'^2} \left( 1 - \frac{2x}{r'} \cos \theta \right) \cos \theta \\ & + \left( E r'^2 + \frac{F}{r'^3} \right) (3 \cos^2 \theta - 1)/2. \end{aligned} \quad (3.26)$$

The potential outside the outer sphere is, in terms of  $\underline{r}'$ ,

$$V_o(r') = \frac{b}{r'} V_2. \quad (3.27)$$

The surface charge density on the outer sphere is given by, according to Gauss' law,

$$\begin{aligned} \sigma_b(\theta) = & -\frac{1}{4\pi} \left\{ \frac{\partial V_o}{\partial r'} \bigg|_{r'=b} - \frac{\partial V_i}{\partial r'} \bigg|_{r'=b} \right\} \\ \approx & \frac{V_2}{4\pi b} - \frac{1}{4\pi} \left\{ \frac{B}{b^2} - \left( C - \frac{2D}{b^3} + \frac{2Bx}{b^3} \right) \cos \theta + \dots \right\} \end{aligned} \quad (3.28)$$

When this is integrated over the surface of the outer sphere, we get for the charge

$$q_b \approx bV_2 - B \approx \frac{b(bV_2 - aV_1)(b^3 - a^3)}{(b^3 - a^3)(b - a) - abx^2}. \quad (3.29)$$

From Eqs. (3.24) (3.29) the coefficients of capacitance are

$$\begin{aligned} C_{11} &= \frac{ab}{b-a} \Phi(x) & C_{12} &= -\frac{ab}{b-a} \Phi(x) \\ C_{21} &= -\frac{a^2}{b-a} \Phi(x) & C_{22} &= \frac{b^2}{b-a} \Phi(x), \end{aligned} \quad (3.30)$$

where

$$[\Phi(x)]^{-1} \equiv 1 - \frac{abx^2}{(b^3 - a^3)(b - a)}. \quad (3.31)$$

Now as the spheres are displaced by the distance  $x$ , the charges  $q_a$ ,  $q_b$  remain unchanged. Hence,

$$-\frac{ab(V_b - V_a)}{b-a} \approx q_a \approx -\frac{ab(V_2 - V_1)}{b-a} \Phi(x),$$

$$\frac{b(bV_b - aV_a)}{b-a} = q_b \approx \frac{b(bV_2 - aV_1)}{b-a} \Phi(x),$$

and the new potentials  $V_1$ ,  $V_2$  are given in terms of the potentials  $V_a$ ,  $V_b$

of the undisplaced spheres by

$$\left. \begin{aligned} V_1 &\approx V_a / \Phi(x) \\ V_2 &\approx V_b / \Phi(x) \end{aligned} \right\} \quad (3.32)$$

Thus we can calculate the electrostatic energy

$$E_{elec} = \frac{1}{2} (C_{11} V_1^2 + 2 C_{12} V_1 V_2 + C_{22} V_2^2) \quad (3.33)$$

and find

$$E_{elec} \approx \frac{ab V_a^2 - 2ab V_a V_b + b^2 V_b^2}{2 \Phi(x)(b-a)} \quad (3.34)$$

The force per unit small displacement  $x$  can then be obtained as follows.

$$\frac{F}{x} = - \frac{1}{x} \frac{\partial E_{elec}}{\partial x} = \frac{ab(ab V_a^2 - 2ab V_a V_b + b^2 V_b^2)}{(b^2 - a^2)(b-a)^2} \quad (3.35)$$

In view of considerations in the previous section we put  $b \approx 2a$  and  $|V_a| \ll |V_b|$ . Then Eq. (3.25) reduces to the approximate formula

$$\frac{F}{x} \approx \frac{8}{7} \frac{V_b^2}{a} \quad (3.36)$$

As an example of the magnitude of the instability force constant  $F/x$ , consider the previous case where the outer sphere was charged to a potential  $V_b = 5 \times 10^8$  volts  $= 1.67 \times 10^6$  statvolts and the inner sphere has radius

$a = 33.3 \text{ meters} = 3.33 \times 10^3 \text{ cm}$ . Then we find  $F/x$  is approximately  $0.958 \times 10^9 \text{ dynes/cm}$ , or about 5480 lbs/inch. This value is for small displacements only and may be expected to increase rapidly as the displacement increases. Furthermore, for light-weight non-rigid balloon-type structures, one may expect the off-center instability to be aggravated by other effects, such as distortions of the spheres.

#### 4. MAGNETIC SHIELDING—BASIC CONSIDERATIONS

##### Motion of Charged Particles in a Magnetic Field

The principles underlying the operation of a magnetic shield for a space vehicle are more subtle than those governing a passive shield or electrostatic shield. The action of any magnetic shielding system depends on the Lorentz force  $\vec{F} = (e/c)\vec{v} \times \vec{H}$  exerted on a particle of charge  $e$  moving with vector velocity  $\vec{v}$  in a magnetic field  $\vec{H}$ . (The force equation, like all equations in this chapter, is written in Gaussian units with  $c$  equal to the speed of light.) This force is proportional to the charge, the particle velocity, and the magnetic field strength. The line of action of the magnetic force is perpendicular to both the particle velocity and magnetic field. No force is exerted by the magnetic field on a charge at rest. Since the magnetic force is perpendicular to the velocity, no work is done on the particle and the kinetic energy remains constant.

In a uniform magnetic field, a charge moves in a helical path which spirals around a magnetic line of force. If the particle has no velocity component in the direction of the field, the spiral path becomes simply a circle of radius

$$R = \frac{E}{eH} \frac{v}{c} = \frac{1}{eH} (E_{\text{kin}}^2 + 2m_0c^2 E_{\text{kin}})^{1/2}. \quad (4.1)$$

Here  $v$  is the component of particle velocity normal to a line of force and  $E$  is the relativistic energy of the particle, equal to the sum of its kinetic energy  $E_{\text{kin}}$  and rest energy  $m_0c^2$ . For nonrelativistic (low energy) particles the kinetic energy is small compared to the rest energy. Neglecting the term  $E_{\text{kin}}^2$  by comparison with  $2m_0c^2 E_{\text{kin}}$  in Eq. (4.1) and putting  $E_{\text{kin}} \approx \frac{1}{2}m_0v^2$ , we obtain the nonrelativistic expression for the "cyclotron radius"

$$R \approx \frac{m_0cv}{eH} \quad (E_{\text{kin}} \ll m_0c^2). \quad (4.2)$$

The tendency of charged particles to move in spiral paths around a line or force is modified somewhat if the magnetic field is not uniform. Consider, for example, a monopole magnetic field whose lines of force are straight lines diverging radially outward from a single point. \* Those lines of force passing through given closed curves in space form surfaces, called "flux tubes". One possible set of flux tubes for the field under consideration is a family of right circular cones with vertices at the magnetic pole from which the lines of force radiate. The paths of charged particles in the field will be geodesics, or "straightest lines", on these conical flux tubes. Such geodesics spiral toward the apex of the cone, reach a certain distance from the apex depending on the sharpness of the cone (which in turn depends on the particle energy) and then spiral down the cone away from the apex. This may be illustrated by drawing a straight line on a sheet of thin paper or cellophane and rolling the sheet in the form of a cone. The operation of rolling transforms the straight lines drawn on a flat surface into geodesics on a cone. In a sense, the magnetic field performs geometrical operations on the path of a charged particle; the most important dynamical property, namely the energy, remains unchanged.

The tendency of charged particles in a nonuniform magnetic field to move like reversing conical helices is called the "magnetic mirror" effect. It occurs whenever the gradient of the field has a component in the direction of the field or equivalently, whenever flux tubes generated by circles decrease monotonically in cross-section.

The most characteristic features of charged particle motion in a magnetic field, namely a tendency toward circular or cylindrical helical motion in a nearly uniform magnetic field and magnetic mirroring in a field with gradients, may be used to synthesize magnetic radiation shields. Before discussing in more detail the way in which such devices would operate, we shall first consider how magnetic fields suitable for shielding might be produced.

---

\* This example may appear somewhat unrealistic, since magnetic fields in nature do not have sources or sinks; however, the lines of force of a bar magnet do not deviate very much from radially outward straight lines in regions near the poles, and the qualitative features of the particle motion about to be described are similar to those which occur whenever magnetic field lines converge or diverge. The field under discussion may be imagined to be that of a very long thin bar magnet in a region near one end.

### Generation of Magnetic Fields

Until recently, magnetic shielding of spacecraft against high energy charged particle radiation was ruled out by the large electric currents and massive conductors necessary to generate the very strong extensive magnetic fields that would be required. Iron-core electromagnets would not be useful for shielding because soft iron saturates at a field of about 20,000 gauss and, as will be shown later, field-strengths of the order of 100,000 gauss are needed for shielding. Air-core solenoids with very high currents must be used, since at high fields ferromagnetic materials offer no advantage and simply add weight. If solenoids are built using ordinary conductors (such as silver, copper, aluminum) the cross-section of the turns must be large in order to minimize the resistance. This makes the coil very heavy if a strong magnetic field spread over a large region is desired. A large power plant is needed to drive the currents through the coil. In spite of the rather low resistance of the coil, enormous amounts of energy would be converted to heat, since heating is proportional to the square of the current. This heat would have to be dissipated in cooling water flowing in tubes within the coil in order to prevent melting of the windings. An example of a copper solenoid magnet with fields of the order needed in magnetic shielding (but over a much smaller working space than would be needed in shielding applications) is the magnet used at Bell Laboratories for critical field experiments on superconductors.<sup>8b</sup> This magnet can generate a field of 88,000 gauss over a cylindrical working space 5 cm in diameter and 10 cm long, using 1.5 megawatts of electric power. A cooling system using 1000 gallons per minute of cold water is required to dissipate the power, almost all of which is converted into heat. The associated equipment (motor-generator set, switchgear, cooling towers, etc.) requires several large rooms and the total cost runs to several hundred thousand dollars. All this is required for a magnetic field far less extensive in space than that needed for space vehicle shielding. Magnetic shielding using ordinary conductors is clearly out of the question because of the inordinate weight, power and cooling requirements.

The prospects for making air-core solenoid magnets giving high field-strengths extending over large spatial volumes were considerably improved in 1961 by the discovery of superconducting materials which retain their properties in the presence of strong magnetic fields. It was discovered by

H. K. Onnes in 1911 that certain materials lose their electrical resistivity when cooled to within a few degrees of absolute zero.<sup>81-82</sup> Onnes almost immediately suggested that superconducting materials be used to construct air-core electromagnets, but his efforts led to little success because in the so-called "soft" superconductors available to him (lead, tin, and mercury) the superconducting state is destroyed by a small magnetic field (a few hundred gauss). It was later found that "hard" superconductors\* may have critical fields (magnetic fields above which the superconductivity is "quenched" or destroyed) of a few tens of thousands of gauss. Recently, it was discovered that certain hard superconductors, particularly the molybdenum-rhenium and niobium-zirconium alloys, and the niobium-tin and vanadium-gallium inter-metallic compounds,  $\text{Nb}_3\text{Sn}$  and  $\text{V}_3\text{Ga}$ , have critical magnetic fields of the order of 100,000 gauss or higher and are furthermore capable of carrying very high current densities.<sup>85</sup> The high current-carrying capacity of these hard superconductors, in contrast to that of soft superconductors where all the current must be carried in a thin layer near the surface, seems to be derived from currents flowing within the body of the conductor in superconducting filaments. These filaments are probably associated with dislocations in the crystalline material. Using solenoids made of hard superconductors with their high critical fields and current-carrying capacity, it is probably possible to generate, without the continuous expenditure of electrical power and without Joule heating, high magnetic fields over large regions, suitable for space vehicle shielding. This assumes that the by no means trivial technical problems associated with operation of superconducting materials in large volumes at high magnetic energies and cryogenic temperatures can be overcome.

#### Comparison With Electrostatic Shielding

Before going into the detailed discussion of magnetic shielding, it is well to discuss the advantages of electromagnetic shielding over the other type of active shielding proposed for space vehicles, the electrostatic system. First, shielding designs using magnetic fields are effective against both positive and negative charged particles. In fact, a magnetic shield designed to be effective against protons having a few hundred Mev kinetic energy will

---

\*The designations "hard" and "soft" as applied to superconductors refer to the mechanical hardness or softness of the material.

automatically be equally effective against electrons having that energy and much more effective against electrons of lower energy. Since in the actual space environment electrons are seldom found with energies much above 1 Mev, electrons and the bremsstrahlung x-rays they produce will never be a problem in a vehicle designed around an electromagnetic proton shield. By contrast an electrostatic system designed to shield against protons would produce a concentrated flux of very high energy electrons unless an unmanageably large dual electrode system with its attendant breakdown, charging, and stability problems were constructed and put into operation. Second, a properly designed magnetic shield can protect against particles of very high energy. Whereas a magnet providing shielding against solar flare protons of 1 or 2 Bev energy appears not impossible within the framework of future technology, the practical problems associated with the design of an electrostatic system capable of generating and sustaining potential differences of several billion volts appear so overwhelming as to completely rule this system out for high-energy particle shielding.

#### Motion in a Dipole Field

We shall consider only uncontained magnetic fields in this report. An uncontained field design is one in which a significant fraction of the magnetic energy is outside the device. The field falls off roughly as  $1/r^3$  at a large distance  $r$  from the coil producing the field, but is effective since a small deflection of an oncoming particle far from the coil will cause the particle to stay away from the protected area. For discussions of contained-field devices, see References 78 and 79.

At large distances from the current-elements producing the field, any uncontained magnetic field goes over to the dipole field. A dipole is a very short bar magnet with very high pole strengths or, equivalently, a very small coil carrying a very high longitudinal current. A reasonable idea of how an uncontained magnetic shield would perform can be obtained by considering the motion of charged particles in a dipole field, with departures from ideal behavior caused by the finite size of the coil to be explained later.

The motion of charged particles in the field of a magnetic dipole was first studied by Störmer<sup>75</sup> in connection with Birkeland's theory of the aurora.

Further work on this problem, directed primarily toward understanding the geomagnetic effects of cosmic radiation, was done by Lemaitre and Vallarta,<sup>61-65</sup> Dwight,<sup>66</sup> Schlüter,<sup>67</sup> Firor,<sup>68</sup> Jory,<sup>69</sup> Lüst,<sup>70</sup> Kelsall,<sup>72</sup> and Tooper.<sup>73</sup> The relationship of magnetic shielding to geomagnetic effects on cosmic radiation is not accidental, because the earth's magnetic field provides a very effective shield against solar cosmic ray particles in the energy range up to a few Bev.

A dipole with moment  $\vec{a} = \hat{e}_z a$  situated at the origin with axis in the z-direction gives a static magnetic field derived from the vector potential

$$\vec{A} = -\hat{e}_\phi a \frac{\tilde{\omega}}{(\tilde{\omega}^2 + z^2)^{3/2}} = -\hat{e}_\phi a \frac{\sin \theta}{r^2}. \quad (4.3)$$

The field components are found by differentiating the potential with respect to the three coordinates according to  $\vec{H} = \text{curl } \vec{A}$ . In Cartesian coordinates (x, y, z), cylindrical coordinates ( $\tilde{\omega}$ ,  $\phi$ , z) such that  $x = \tilde{\omega} \cos \phi$ ,  $y = \tilde{\omega} \sin \phi$ , and spherical coordinates (r,  $\theta$ ,  $\phi$ ) such that  $\tilde{\omega} = r \sin \theta$ ,  $z = r \cos \theta$  (Cf. Fig. 4.1), we obtain for the magnetic field

$$\begin{aligned} \vec{H} &= -\hat{e}_x a \frac{3xz}{r^5} - \hat{e}_y a \frac{3yz}{r^5} - \hat{e}_z a \frac{3z^2 - r^2}{r^5}, \quad r = (x^2 + y^2 + z^2)^{1/2}, \\ &= -\hat{e}_\omega a \frac{3\omega z}{r^5} + \hat{e}_z a \frac{\omega^2 - 2z^2}{r^5}, \quad r = (\tilde{\omega}^2 + z^2)^{1/2}, \\ &= -\hat{e}_r 2a \frac{\cos \theta}{r^3} - \hat{e}_\theta a \frac{\sin \theta}{r^3}. \end{aligned} \quad (4.4)$$

Here  $\hat{e}_x$ ,  $\hat{e}_y$ , etc. represent unit vectors in the directions of increasing x, y, etc. The differential equation of a magnetic line of force, or flux line, is

$$dr/H_r = r d\theta/H_\theta \quad (4.5)$$

Further work on this problem, directed primarily toward understanding the geomagnetic effects of cosmic radiation, was done by Lemaitre and Vallarta,<sup>61-65</sup> Dwight,<sup>66</sup> Schlüter,<sup>67</sup> Firor,<sup>68</sup> Jory,<sup>69</sup> Lüst,<sup>70</sup> Kelsall,<sup>72</sup> and Tooper.<sup>73</sup> The relationship of magnetic shielding to geomagnetic effects on cosmic radiation is not accidental, because the earth's magnetic field provides a very effective shield against solar cosmic ray particles in the energy range up to a few Bev.

A dipole with moment  $\vec{a} = \hat{e}_z a$  situated at the origin with axis in the z-direction gives a static magnetic field derived from the vector potential

$$\vec{A} = -\hat{e}_\phi a \frac{\tilde{\omega}}{(\tilde{\omega}^2 + z^2)^{3/2}} = -\hat{e}_\phi a \frac{\sin \theta}{r^2}. \quad (4.3)$$

The field components are found by differentiating the potential with respect to the three coordinates according to  $\vec{H} = \text{curl } \vec{A}$ . In Cartesian coordinates (x, y, z), cylindrical coordinates ( $\tilde{\omega}$ ,  $\phi$ , z) such that  $x = \tilde{\omega} \cos \phi$ ,  $y = \tilde{\omega} \sin \phi$ , and spherical coordinates (r,  $\theta$ ,  $\phi$ ) such that  $\tilde{\omega} = r \sin \theta$ ,  $z = r \cos \theta$  (Cf. Fig. 4.1), we obtain for the magnetic field

$$\begin{aligned} \vec{H} &= -\hat{e}_x a \frac{3xz}{r^5} - \hat{e}_y a \frac{3yz}{r^5} - \hat{e}_z a \frac{3z^2 - r^2}{r^5}, \quad r = (x^2 + y^2 + z^2)^{1/2}, \\ &= -\hat{e}_\omega a \frac{3\omega z}{r^5} + \hat{e}_z a \frac{\omega^2 - 2z^2}{r^5}, \quad r = (\tilde{\omega}^2 + z^2)^{1/2}, \\ &= -\hat{e}_r 2a \frac{\cos \theta}{r^3} - \hat{e}_\theta a \frac{\sin \theta}{r^3}. \end{aligned} \quad (4.4)$$

Here  $\hat{e}_x$ ,  $\hat{e}_y$ , etc. represent unit vectors in the directions of increasing x, y, etc. The differential equation of a magnetic line of force, or flux line, is

$$dr/H_r = r d\theta/H_\theta \quad (4.5)$$

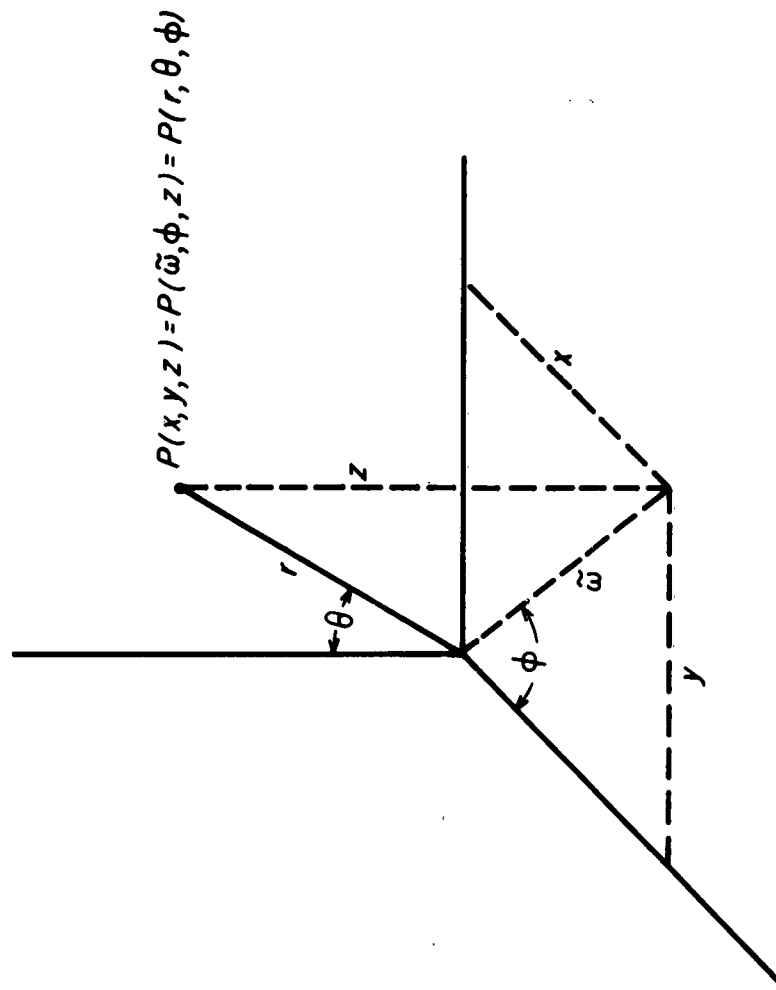


Fig. 4.1 Geometrical Relationships Between Cartesian, Cylindrical Polar, and Spherical Polar Coordinates Used in This Report.

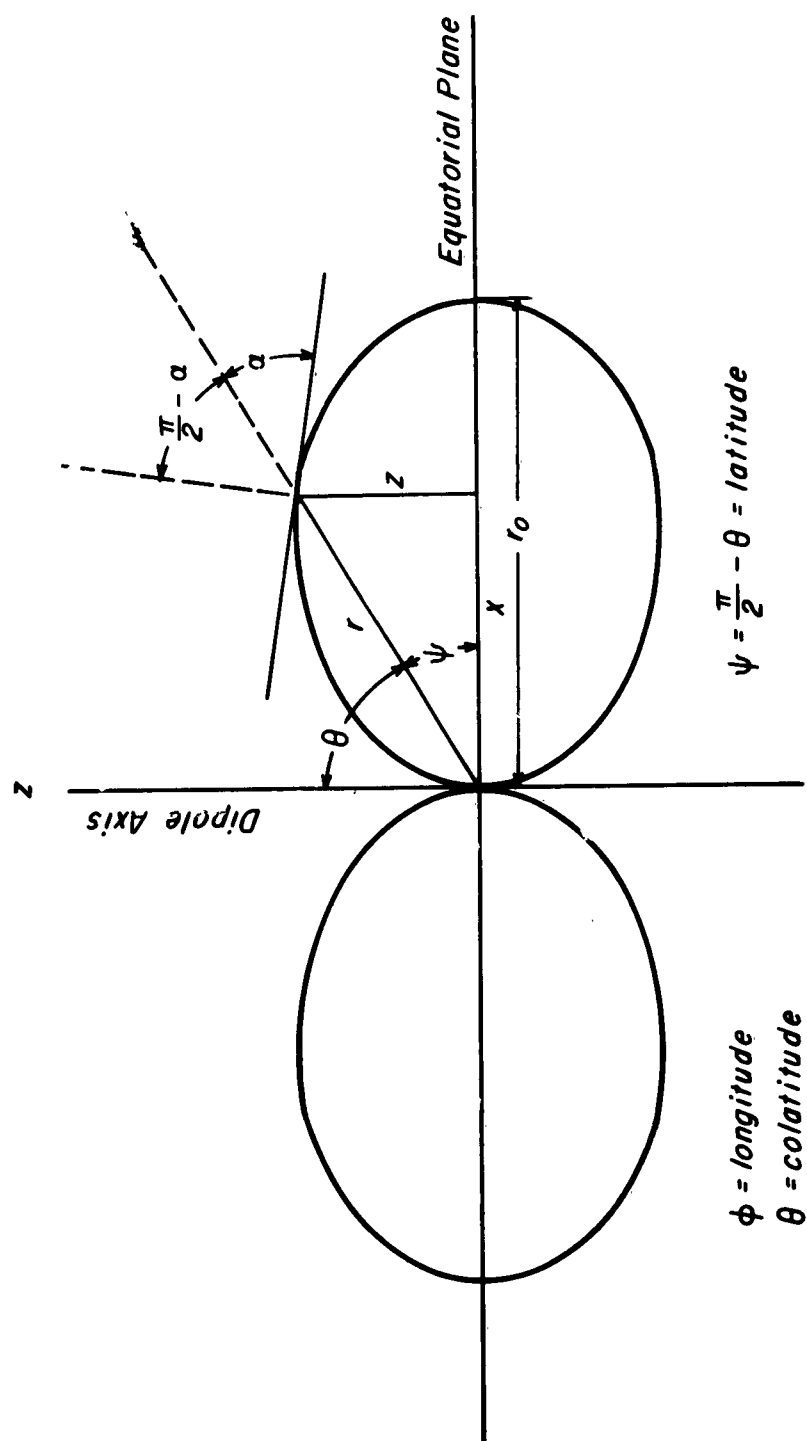


Fig. 4.2 A Typical Line of Force of the Dipole Field.

in spherical coordinates. Solutions of this equation are of the form

$$r = r_0 \sin^2 \theta, \quad \phi = \text{const.} \quad (4.6)$$

Here  $r_0$  is the distance from the dipole to the point where the flux line intersects the equatorial plane  $\theta = \pi/2$ . The shape of a line of force is independent of the dipole moment  $\underline{a}$ . A typical flux line for the dipole field is shown in Fig. 4.2.

The equation of motion of a relativistic particle having charge  $e$  and rest mass  $m_0$  moving with velocity  $\vec{v}$  in a magnetic field  $\vec{H}$  is, in Gaussian units with  $c$  equal to the speed of light,

$$\frac{d}{dt} \frac{m_0 \vec{v}}{(1 - v^2/c^2)^{1/2}} = \frac{e}{c} \vec{v} \times \vec{H}. \quad (4.7)$$

Since the force on a charged particle due to a magnetic field is always perpendicular to the velocity, the magnetic force does no work on the particle. This means that the energy—and hence the speed—of the particle remains constant. This can be shown formally as follows:

$$\begin{aligned} \frac{dE}{dt} &= \frac{d}{dt} \frac{m_0 c^2}{(1 - v^2/c^2)^{1/2}} = \vec{v} \cdot \frac{d}{dt} \frac{m_0 \vec{v}}{(1 - v^2/c^2)^{1/2}} \\ &= \frac{e}{c} \vec{v} \cdot (\vec{v} \times \vec{H}) = 0. \end{aligned}$$

Thus the energy  $E = m_0 c^2 / (1 - v^2/c^2)^{1/2}$  is a constant of the motion\* and so is the "relativistic mass"  $E/c^2$ . Accordingly the equation of motion can

---

\* Although the magnetic force does no work on a charged particle, the self-force does do work. It has been assumed here and will be assumed in the sequel that the particle does not lose energy by radiation. This is a good approximation except for extremely large values of particle energy and magnetic moment.

be written in the form

$$\frac{E}{c^2} \frac{d\vec{v}}{dt} = \frac{ea}{c} \vec{v} \times \text{curl} \left( -\hat{e}_\phi \frac{\sin\theta}{r^2} \right), \quad (4.8)$$

where Eq. (4.3) has been used to represent the dipole field.

Because the energy of the particle is conserved, the speed,  $v = |\vec{v}|$  remains constant. Write  $ds = v dt$ . The arc length  $s$  will be used instead of time  $t$  as independent variable in the equations of motion. Written this way, the parametric equations for the trajectories involve only geometrical quantities. Considering the components of the position vector  $\vec{x}$  as functions of  $s$ , we write the equations of motion as

$$\frac{d^2\vec{x}}{ds^2} = \frac{eac}{Ev} \frac{d\vec{x}}{ds} \times \text{curl} \left( -\hat{e}_\phi \frac{\sin\theta}{r^2} \right). \quad (4.9)$$

The quantity

$$C_{st} = \left( \frac{eac}{Ev} \right)^{1/2} = \left\{ \frac{ea}{E_{kin} + m_0c^2} \left[ 1 - \frac{m_0^2c^4}{(E_{kin} + m_0c^2)^2} \right]^{-1/2} \right\}^{1/2} \quad (4.10)$$

has dimensions of length and is called the Störmer length or Störmer radius corresponding to the particle energy  $E = E_{kin} + m_0c^2$  and dipole moment  $\underline{a}$ . The Störmer length represents the radius of a circular particle orbit in the equatorial plane of the dipole, found by equating the centripetal force to the magnetic force in the equatorial plane. Such motion is possible because to this particle the field appears uniform in intensity and direction. In the second way of writing Eq. (4.10), the particle speed has been found in terms of the energy and the energy resolved as a sum of the rest energy  $m_0c^2$  and the kinetic energy  $E_{kin}$ .

Numerical values of the Störmer unit are plotted for protons and electrons

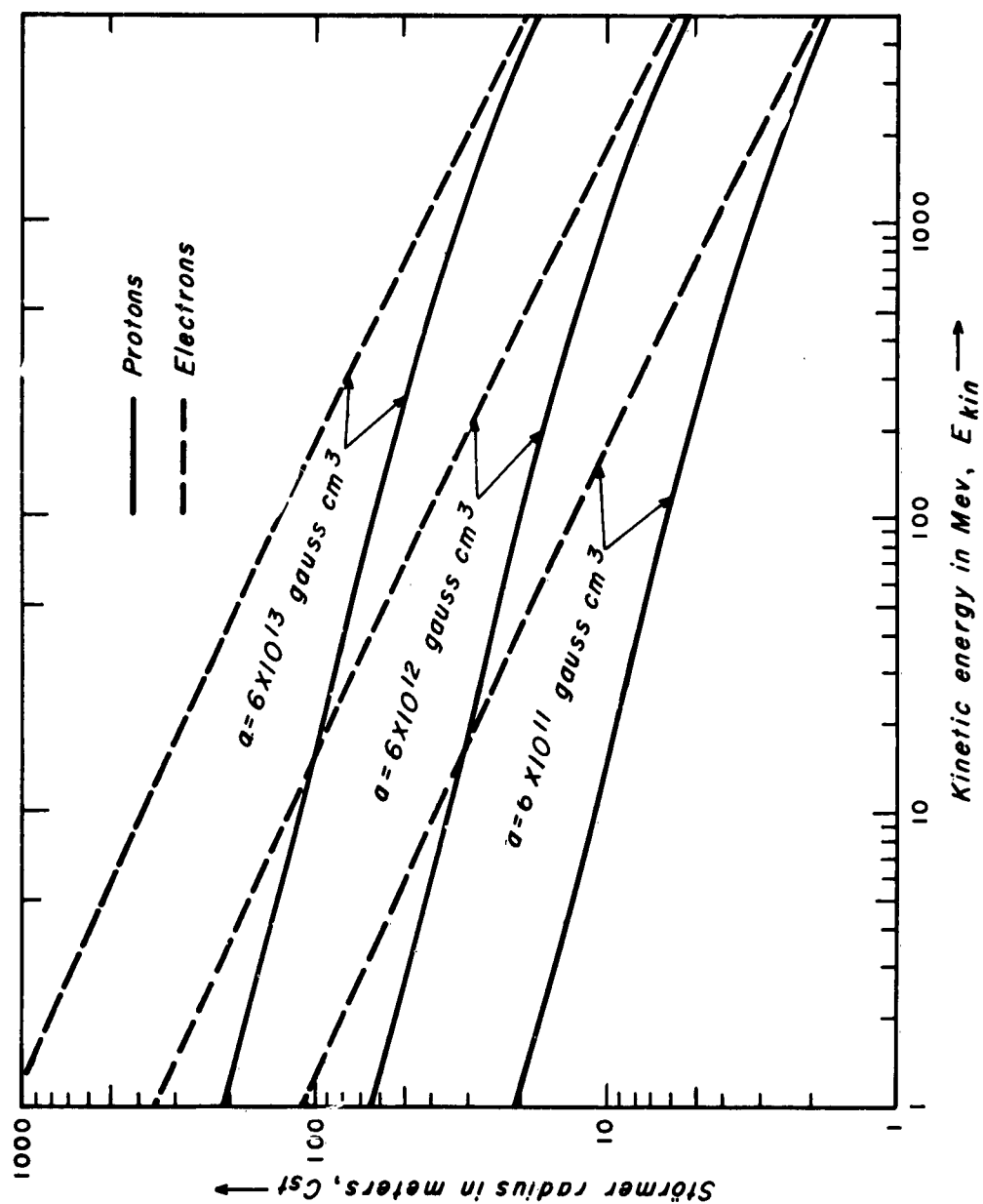


Fig. 4.3 Störmer Unit as a Function of Kinetic Energy of Protons and Electrons for Various Values of Dipole Moment.

as a function of kinetic energy and magnetic moment in Fig. 4.3. Values of magnetic moment of  $10^{11}$  or  $10^{12}$  gauss cm<sup>3</sup> correspond to what may reasonably be achieved aboard spacecraft using superconducting solenoids. The particle energies have been chosen so as to include Van Allen particles and solar flare protons. Notice that the Störmer radius at low kinetic energies is much greater for electrons than for protons; this is because the electron rest mass is smaller by a factor of  $10^3$ . For a given magnetic moment and particle energy, electrons are easier to shield against than protons.

Introduction of the Störmer unit permits the problem of motion in a dipole field to be scaled for all values of particle energy and dipole moment. All distances used need only be given as multiples of the Störmer radius.

The axial symmetry of the dipole field leads to a first integral of the  $\phi$ -component of the equation of motion (4.8). The fact that the vector potential (4.3) is independent of  $\phi$  gives rise immediately to a conservation theorem for the momentum conjugate to the  $\phi$ -coordinate. This canonical momentum has dimensions of angular momentum, but is not strictly the angular momentum of the particle. To see this, recall that the Lagrangian function for a charged relativistic particle moving in an electromagnetic field derivable from potentials  $\vec{A}$ ,  $\Phi$  is<sup>3, 4</sup>

$$\mathcal{L} = -m_0 c^2 (1 - v^2/c^2)^{1/2} + (e/c) \vec{A} \cdot \vec{v} - e\Phi. \quad (4.11)$$

Using the vector potential for the dipole field given by Eq. (4.3) and expressing the velocity components in spherical coordinates, we have for the Lagrangian of a charge in a magnetostatic dipole field,

$$\mathcal{L} = -m_0 c^2 \left[ 1 - \frac{1}{c^2} (\dot{r}^2 + r^2 \dot{\theta}^2 + r^2 \sin^2 \theta \dot{\phi}^2) \right]^{1/2} - \frac{ea}{c} \frac{\sin^2 \theta}{r} \dot{\phi}. \quad (4.12)$$

Here the dots denote differentiation with respect to time. The Lagrangian (4.12) is independent of  $\phi$ ; it follows directly from Lagrange's equations that the momentum conjugate to  $\phi$  is conserved.<sup>3</sup> This momentum is

$$p_{\phi} \equiv \frac{\partial \mathcal{L}}{\partial \dot{\phi}} = \frac{E}{c^2} \left[ r^2 \sin^2 \theta \dot{\phi} - v C_{st}^2 \frac{\sin^2 \theta}{r} \right]. \quad (4.13)$$

The conserved canonical momentum  $p_{\phi}$  has units of angular momentum. It may be expressed in terms of the angular momentum  $(E/c^2) v C_{st}$  of a particle moving in the equatorial plane of the dipole along a circle with center at the dipole and radius  $C_{st}$  by introducing the (dimensionless) Störmer constant

$$p_{\phi} = 2Y \frac{E}{c^2} v C_{st}. \quad (4.14)$$

The factor 2 has been inserted for the sake of simplicity in later equations.

It may be seen from (4.13) that  $p_{\phi}$  represents the angular momentum of the particle about the dipole axis if and when the particle is an infinite distance from the dipole. In such a case the second term in Eq. (4.13) arising from the vector potential goes to zero. This suggests the following interpretation of  $p_{\phi}$  and  $Y$  in terms of impact parameters.

Consider a particle incident on the dipole from infinity, and the straight line asymptotic to the orbit at infinity (i. e., the straight line the particle follows before it is deflected by the magnetic field of the dipole). The asymptotic line will pass a certain distance  $P_0$  from the dipole axis (see (Fig. 4.4). This is because the asymptote and the dipole axis form in general two nonintersecting skew lines in space. A minimum distance between two skew lines can be defined; it is equal to the length of their unique common perpendicular. The distance  $|P_0|$  may be thought of as an "impact parameter". The common perpendicular between the asymptote and the dipole axis together with the asymptote determine a plane (Fig. 4.4). Suppose that a line is constructed in this plane parallel to the asymptote and passing through the dipole axis. This line and the dipole axis determine a second plane which is perpendicular to the first. Let  $\chi$  be the angle in this plane between the dipole axis and the line parallel to the orbit's asymptote. The angular

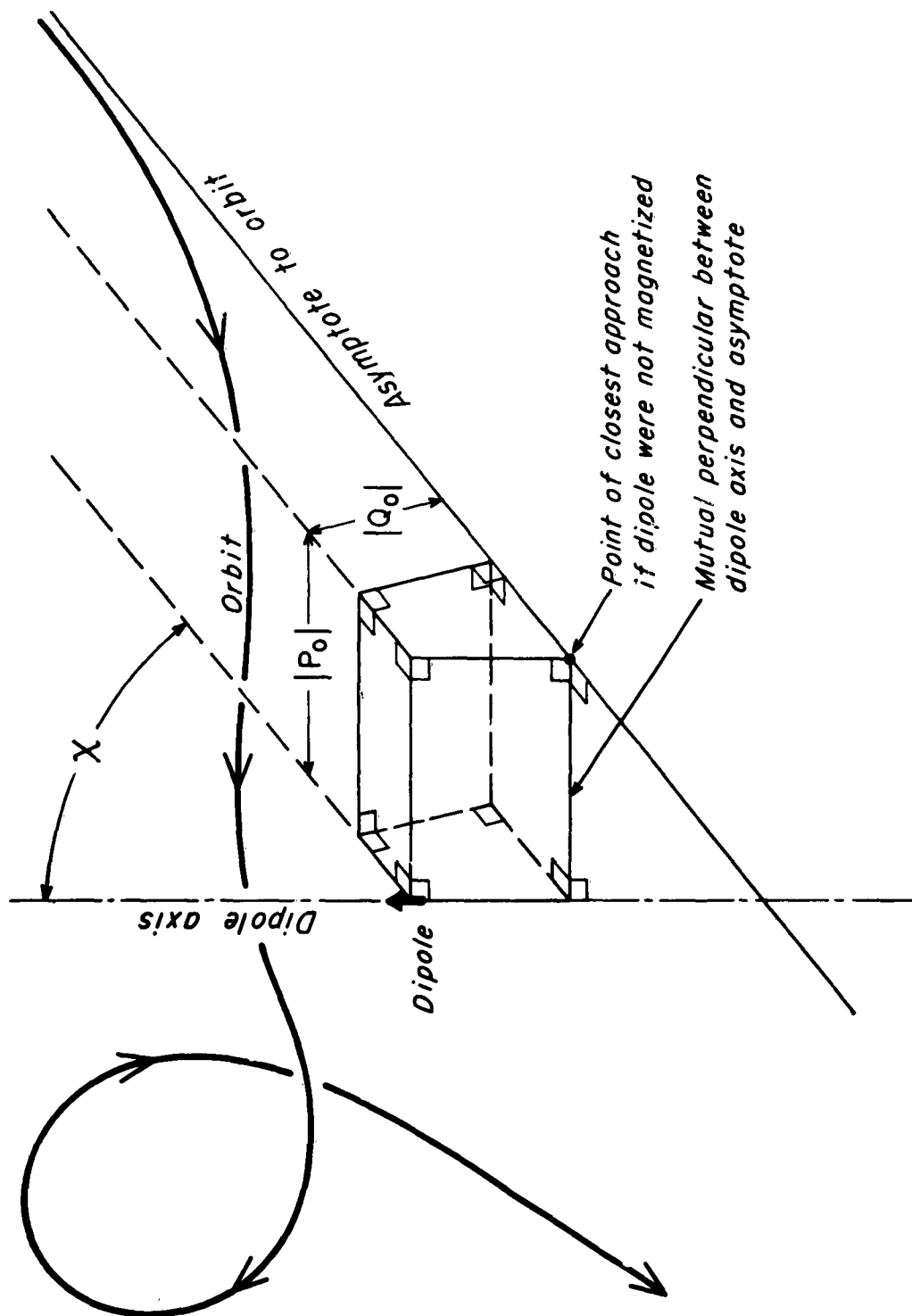


Fig. 4.4 Definition of Impact Parameters for Scattering of a Charged Particle by the Field of a Magnetic Dipole.

momentum (at infinity) about the dipole axis is, in terms of the impact parameters,

$$P_\phi(r \rightarrow \infty) = -\frac{E}{c^2} v P_0 \sin \chi. \quad (4.15)$$

Comparing (4.14) with (4.15) we see that the dimensionless constant is given in terms of the Stormer distant  $C_{st}$  and the impact parameter  $P_0$  by the relation

$$2Y = - (P_0 / C_{st}) \sin \chi \quad (4.16)$$

The negative sign has been attached to  $P_0$  in Eqs. (4.15) (4.16) because  $Y$  can be either positive or negative depending on the sign of the angular momentum at infinity. The sign is chosen so that the angular momentum will have a positive or negative sign according as  $\dot{\phi} = d\phi/dt$  is initially positive or negative. The motion depends strongly on which side of the dipole axis the particle is aimed initially. The magnetic field influencing the particle will be either "generally upward" or "generally downward" with respect to an imaginary observer standing on the equatorial plane. The force on the particle will be in the same general direction regardless to which side of the dipole axis the particle was initially directed. This is in sharp contrast to the behavior of a particle under the influence of a central force, where the force is directed either toward or away from some fixed center like a charged nucleus. Depending on the sign of the impact parameter, the particle may be either forced away from or attracted into the region of the dipole. Different behavior of the trajectories is to be expected for different signs as well as different absolute values of the integration constant.

#### Forbidden Regions

Further information about the trajectories can be obtained from the conservation of canonical angular momentum expressed in the form (4.13)

(4.14). It is possible to find regions forbidden to particles having various initial values of angular momentum because they cannot enter them without violating the conservation law for  $p_\phi$ . The size of these regions depends on the Störmer length and hence on the particle energy and dipole moment. For a given Störmer unit there is also an axially symmetric region which particles incident from infinity cannot enter (even though it is accessible to bound particles) no matter what their value of angular momentum. The "absolutely shielded region" can be determined without explicit knowledge of the trajectories.

The forbidden regions corresponding to various values of angular momentum (and hence to various values of the Störmer constant  $\gamma$ ) may be determined by writing Eqs. (4.13) (4.14) together in the form

$$Q \equiv \frac{r \sin \theta \dot{\phi}}{v} = \frac{C_{st}^2}{r^2} \sin \theta + 2\gamma \frac{C_{st}}{r \sin \theta}. \quad (4.17)$$

The quantity  $Q$  is the ratio of the  $\phi$ -component of velocity to the total speed, and so its absolute value must be less than, or at most equal to, unity. We obtain a violation of this condition by putting  $Q > 1$  in Eq. (4.17), or

$$\sin \theta \frac{r^2}{C_{st}^2} - 2\gamma \frac{r}{C_{st}} - \sin^2 \theta < 0.$$

Thus, for  $Q > 1$ , the quantity  $r/C_{st}$  must lie in the range

$$\frac{\gamma - (\gamma^2 + \sin^2 \theta)^{1/2}}{\sin \theta} < \frac{r}{C_{st}} < \frac{\gamma + (\gamma^2 + \sin^2 \theta)^{1/2}}{\sin \theta}.$$

We need consider only  $\sin \theta > 0$  and  $r > 0$  since octants other than the first may be obtained by reflection through the dipole axis and equatorial plane. With this condition, the root with the negative sign is always negative, so we discard it. Thus, for each value of  $\gamma$ , whether positive or negative, there is

a forbidden region given by

$$A(\gamma): \quad \frac{r}{C_{st}} < \frac{\gamma + (\gamma^2 + \sin^2 \theta)^{1/2}}{\sin \theta}. \quad (4.17a)$$

Another violation of the condition  $|Q| \leq 1$  is obtained by putting  $Q < -1$  in Eq. (4.17). This implies

$$\sin \theta \frac{r^2}{C_{st}^2} + 2\gamma \frac{r}{C_{st}} + \sin^2 \theta < 0,$$

whence  $r/C_{st}$  must fall in the interval

$$B(\gamma): \quad \frac{-\gamma - (\gamma^2 - \sin^2 \theta)^{1/2}}{\sin \theta} < \frac{r}{C_{st}} < \frac{-\gamma + (\gamma^2 - \sin^2 \theta)^{1/2}}{\sin \theta}. \quad (4.17b)$$

This gives a second forbidden region lying outside the first which, however, exists only for negative values of  $\gamma$ .

The inner forbidden regions  $A(\gamma)$  and the outer forbidden regions  $B(\gamma)$  for the dipole field are shown in Fig. 4.5. The outer forbidden regions have the interesting property that, in cross-section, a segment AFB of a line drawn from the dipole such that it intersects the boundary of  $B(\gamma)$  at points A and B will be bisected by a line parallel to the dipole axis at a distance  $-\gamma C_{st}$  from it. Thus  $AF = FB$ . This property is evident from the inequalities (4.17) defining  $B(\gamma)$  and the observation that  $r \sin \theta$  is the projection of  $\underline{r}$  on the equatorial plane.

The inner forbidden regions  $A(\gamma)$  increase monotonically in size with increasing  $\gamma$ . For values of  $\gamma$  less than  $-1$ , the outer forbidden region  $B(\gamma)$  completely surrounds the inner region  $A(\gamma)$ , and the space between these two regions can only be occupied by bound particles which have either started out in this intervening space or which have had their energy degraded in some way. For values of  $\gamma$  greater than  $-1$ ,  $B(\gamma)$  no longer surrounds  $A(\gamma)$ , but

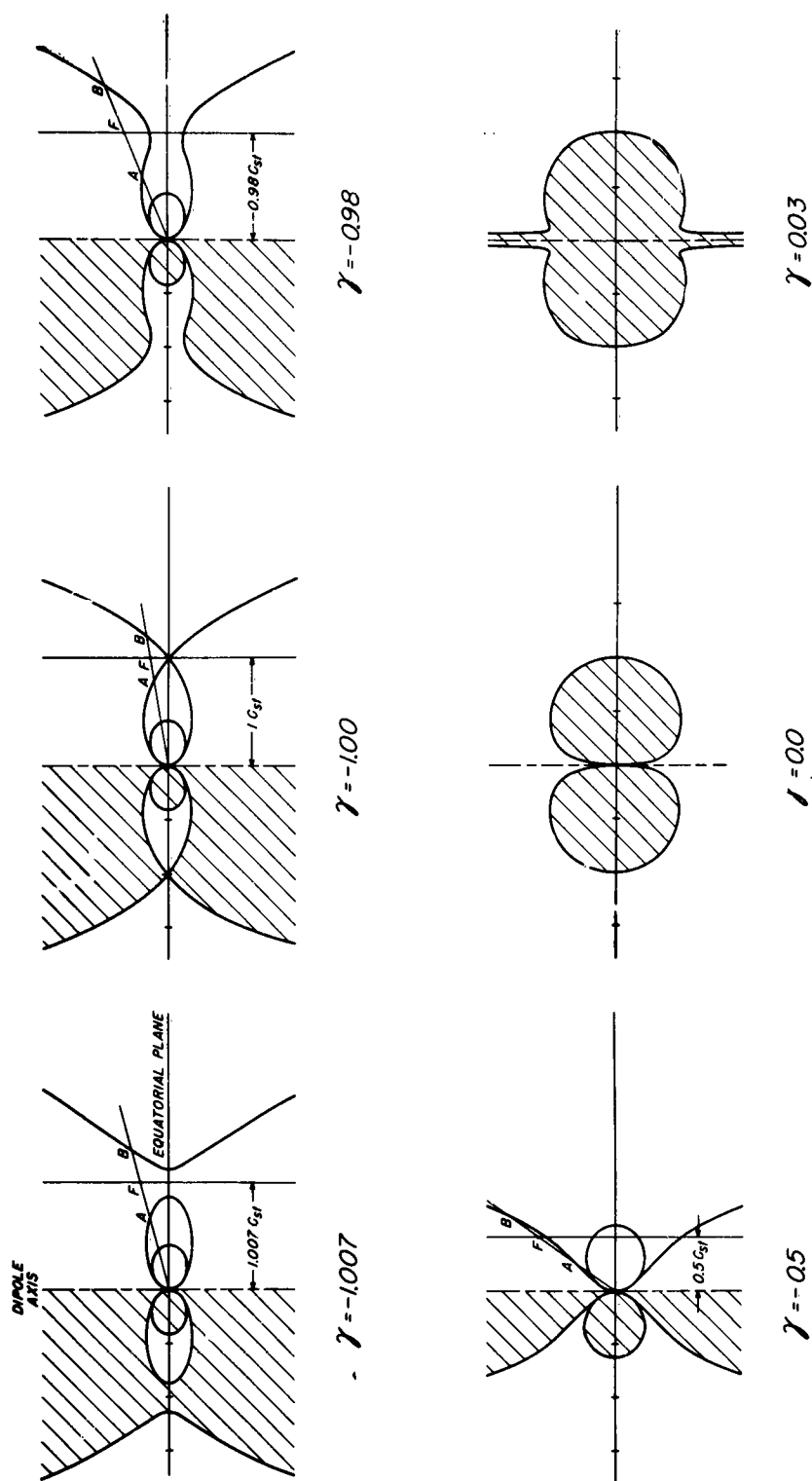


Fig. 4.5 Regions Forbidden to Particles of a Single Energy Moving in a Magnetic Dipole Field for Various Values of the Angular Momentum Constant  $\gamma$ .

the volume of  $A(\gamma')$  when  $\gamma' > -1$  is always greater than the volume of  $A(-1)$ . Also the region  $A(-1)$  is always included in  $A(\gamma')$  ( $\gamma' > -1$ ). In the equatorial plane  $\sin \theta = 1$ , and the intersection of the region  $B(-1)$  with the equatorial plane is a circle of radius  $1 C_{st}$ . From these considerations it may be seen that, for a particular Störmer unit (i. e., a particular dipole moment and particle energy), the region  $A(-1)$  is forbidden to all unbound particles, no matter what their value of  $\gamma$ . The boundary of region  $A(-1)$  is given by

$$\frac{r}{C_{st}} = \frac{-1 + (1 + \sin^3 \theta)^{1/2}}{\sin \theta} \quad (4.18)$$

This region is toroidal in shape with its major radius equal to  $\sqrt{2}-1 = 0.414$  Störmer units.

Besides the completely shielded region whose boundary is given by Eq. (4.18), there is a partially shielded region which can be entered only by those particles from infinity having values of  $\gamma$  between  $-1$  and about  $0.03$ . This is the region lying between the outer forbidden region  $B(-1)$  and the absolutely forbidden region  $A(-1)$ . It is also toroidal, its major radius is a full Störmer unit, and its boundary is given by

$$\frac{r}{C_{st}} = \frac{1 - (1 - \sin^3 \theta)^{1/2}}{\sin \theta} \quad (r \leq C_{st}). \quad (4.19)$$

The two regions represented by Eqs. (4.18) (4.19) are shown in Fig. 4.6. Determination of the degree of shielding provided by regions, such as that of Eq. (4.19), forbidden to particles having values of canonical angular momentum in a certain range can be made by detailed examination of particle trajectories.

The volume of the totally shielded region whose boundary is given by Eq. (4.18) can be determined as follows. Through the transformation equations  $\varpi = r \sin \theta$ ,  $z = r \cos \theta$ , we find the equation for the boundary

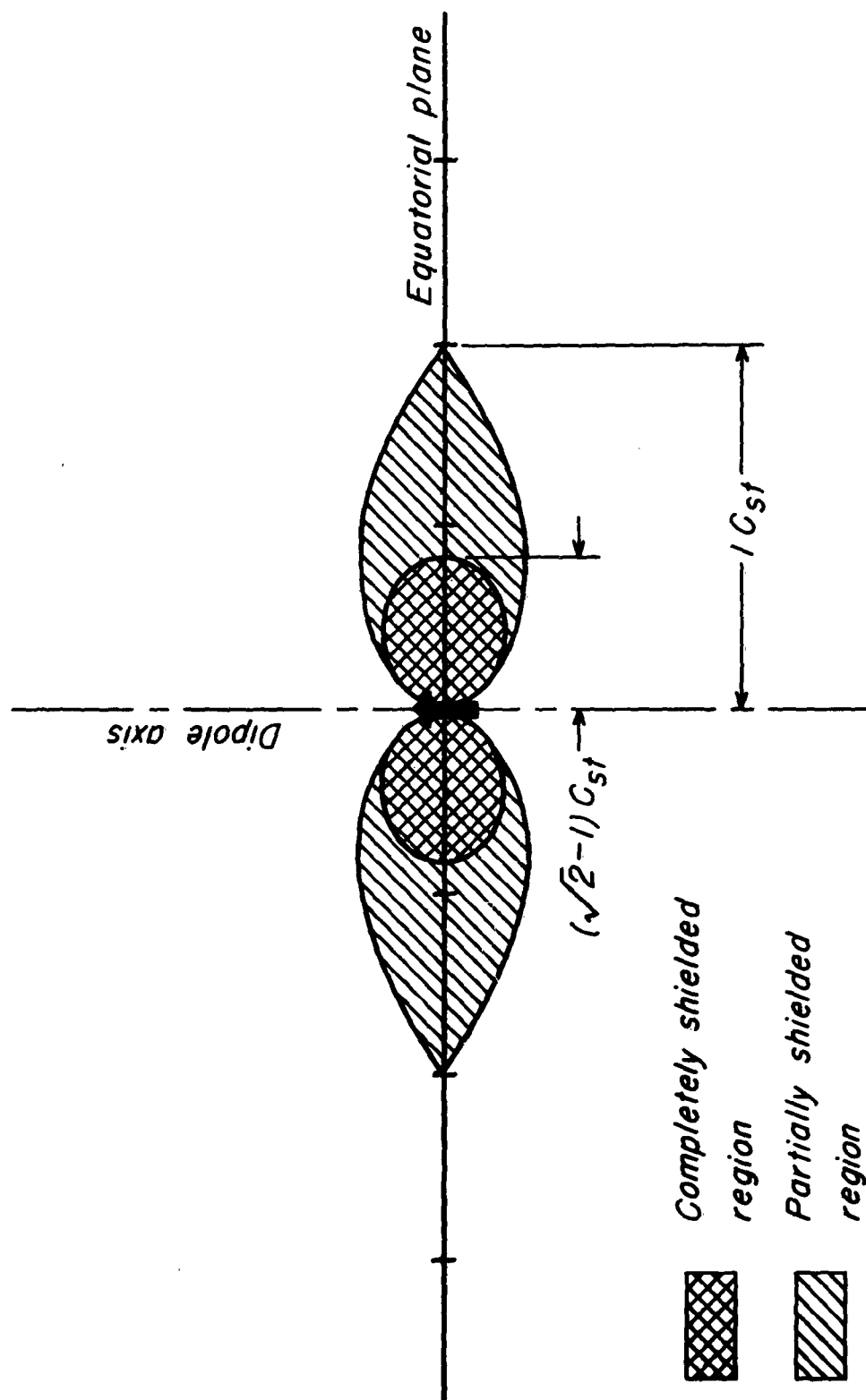


Fig. 4.6 Completely and Partially Shielded Regions for Particles of a Single Energy Moving in a Magnetic Dipole Field.

in cylindrical coordinates:

$$z^2 = \left( \frac{C_{st}^2 \omega^2}{\omega + 2 C_{st}} \right)^{2/3} - \omega^2. \quad (4.20)$$

Using the shell method of integration, it may be seen that the volume of the region A(-1) is given by

$$V_{A(-1)} = 4\pi \int_0^{\omega_{\max}} z \omega d\omega = 4\pi C_{st}^3 \int_0^1 \left[ \left( \frac{x^2}{x+2} \right)^{2/3} - x^2 \right]^{1/2} x dx,$$

where  $\omega_{\max} = C_{st} \Lambda = C_{st}(\sqrt{2}-1)$ . A ten-step integration by Simpson's rule gives approximately

$$V_{A(-1)} \approx 0.144 C_{st}^3 \quad (4.21)$$

for the volume of the shielded region.

#### Shielding Effectiveness

Calculations were performed giving the range of particle energies over which the shielding provided by a solenoid of reasonable magnetic moment would be effective. There is a change of viewpoint involved here: previously the particle energy was supposed to be held constant and the spherical coordinates  $\underline{r}$ ,  $\underline{\theta}$  were allowed to vary, thereby generating a toroidally shaped region protected from particles of the given energy. One may also prescribe a certain closed surface (representing the spaceship cabin) by giving  $\underline{r}$  as a function of  $\underline{\theta}$  and  $\underline{\phi}$  and obtain limiting values of energy for particles kept from entering the cabin.

The case of a spherical spaceship cabin of radius  $\underline{r}$  about the dipole center was considered for simplicity. Feasibility can be shown quickly by considering the shielding in the equatorial plane of the dipole. This gives the order of magnitude of the particle energies and size of shielded region

for which a solenoid of given magnetic moment would be adequate. In the equatorial plane,  $\theta = \pi/2$  and Eq. (4.18) for the completely shielded region reduces to

$$r = (\sqrt{2}-1) \left\{ \frac{ea}{E_{\min}} \left[ 1 - \left( \frac{m_0 c^2}{E_{\min}} \right)^2 \right]^{-1/2} \right\}^{1/2}, \quad (4.22)$$

whereas Eq. (4.19) for the partially shielded region becomes

$$r = \left\{ \frac{ea}{E_{\max}} \left[ 1 - \left( \frac{m_0 c^2}{E_{\max}} \right)^2 \right]^{-1/2} \right\}^{1/2}. \quad (4.23)$$

Equations (4.22) (4.23) give the limiting values  $E_{\min}$  and  $E_{\max}$  for the energies shielded by a dipole of moment  $a$  in a circular enclosure of radius  $r$ . The meaning of the (relativistic) energies  $E_{\min}$  and  $E_{\max}$  is as follows. A point a distance  $r$  from the dipole can be approached from any direction in the equatorial plane by particles with energy exceeding  $E_{\max}$ . A point at the same distance is forbidden from all directions in the equatorial plane for particles with energy less than  $E_{\min}$ . Particles with energy between  $E_{\min}$  and  $E_{\max}$  can approach the point  $r$  from certain allowed directions only. In other words, the point  $r$  is completely shielded from particles with energies below  $E_{\min}$  and partially shielded from particles with energies between  $E_{\min}$  and  $E_{\max}$ . For particles of energy greater than  $E_{\max}$ , no shielding is provided.

To use the energies  $E_{\min}$  and  $E_{\max}$  to evaluate the effectiveness of shielding provided by a particular solenoid, it is necessary to make some choice of the size of spacecraft to be shielded, since this prescribes the distance from the dipole center. A sphere of diameter 2 meters was chosen as an elementary model for the vehicle. A value of  $3 \times 10^{11}$  gauss cm<sup>3</sup> was chosen as a value of magnetic moment that might be achieved using a superconducting "air core" solenoid. Values of kinetic energy corresponding to  $E_{\min}$  and  $E_{\max}$  were found for protons and electrons as follows:

	Protons	Electrons
$E_{\min}^{\text{kin}}$	866 Mev	1.54 Bev
$E_{\max}^{\text{kin}}$	8.1 Bev	9 Bev

The shielding calculations can be extended to include directions other than the equatorial plane with the aid of results given in Reference 6, pp. 276-281. The basic equation

$$P(\lambda, \omega) = P_{\max} \frac{\cos^4 \lambda}{[(g^2 - \cos \omega \cos^3 \lambda)^{1/2} + g]^2} \quad (4.24)$$

gives the smallest initial momentum for a particle to reach a point a distance  $r$  from the dipole center at a latitude  $\lambda$  through an angle  $\omega$  in the east-west direction. The quantity  $P_{\max}$  is the momentum corresponding to the energy  $E_{\max}$ , found by using the energy-momentum relation

$$E^2 = P^2 c^2 + m_0^2 c^4. \quad (4.25)$$

Values of  $g$  appropriate to various latitudes  $\lambda$  have been tabulated by Lemaitre and Vallarta;<sup>61</sup> for our present purposes we shall take  $g = 1$ .

Some special cases of Eq. (4.24) are

(a) Particles with momentum greater than  $P(\lambda, 0)$  can approach the observer at latitude  $\lambda$  from all directions.

$$P(\lambda, 0) = P_{\max} \frac{\cos^4 \lambda}{[(g^2 - \cos^3 \lambda)^{1/2} + g]^2} \approx P_{\max} \cos^4 \lambda. \quad (4.24a)$$

The effect of the approximation used in Eq. (4.24a) is to give slightly higher values for both momentum and energy, but retains the stronger latitude dependence given by  $\cos^4 \lambda$  term.

(b) Particles with momentum less than  $P(\lambda, \pi)$  are forbidden for all directions at latitude  $\lambda$ .

$$P(\lambda, \pi) = P_{\max} \frac{\cos^4 \lambda}{[(g^2 + \cos^2 \lambda)^{1/2} + g]^2} \approx P_{\max} \frac{\cos^4 \lambda}{5.84}. \quad (4.24b)$$

(c) The limiting momentum in the vertical direction is

$$P(\lambda, \pi/2) = P_{\max} \frac{\cos^4 \lambda}{(2g)^2} \approx P_{\max} \frac{\cos^4 \lambda}{4}. \quad (4.24c)$$

In conclusion, all particles with momentum greater than  $P_{\max} \cos^4 \lambda$  are assumed to reach the sphere of radius  $r$ , and all particles with momentum less than  $P_{\min} \cos^4 \lambda / 5.84$  are excluded from the sphere. The results (in terms of limiting energies) for the former conditions discussed for other than the equatorial plane are given in Table 4.1.

Table 4.1. Limiting values of energy for complete and partial shielding at a latitude  $\lambda$ . The magnetic moment is  $3 \times 10^{11}$  gauss  $\text{cm}^3$  and the spherical region under consideration has radius 200 cm.

	Protons		Electrons	
	$E_{\max}^{\text{kin}}$ (Mev)	$E_{\min}^{\text{kin}}$ (Mev)	$E_{\max}^{\text{kin}}$ (Mev)	$E_{\min}^{\text{kin}}$ (Mev)
$0^\circ$	8113	866	9000	1540
$10^\circ$	7575	790	8460	1450
$20^\circ$	6165	594	7040	1210
$30^\circ$	4205	339	5050	865
$40^\circ$	2305	140	3100	531
$50^\circ$	865	36	1540	264
$60^\circ$	165	0	570	10
$70^\circ$	8	0	125	2.2
$80^\circ$	0	0	9	1.6
$90^\circ$	0	0	0	0

The shielding effectiveness is strongly dependent on the size and shape of the solenoid and spacecraft. The particles, some of which are prevented from approaching the protected area, have energies comparable to those encountered in the radiation belt and protons associated with solar flares. The example considered does not shield high energy cosmic rays effectively.

It is important to determine the effectiveness of shielding for a given magnetic moment and spacecraft size for energies lying between  $E_{\min}$  and  $E_{\max}$ . For instance, in the example cited, the kinetic energy of protons below which all particles were kept out of the region in question was less than about 1 Bev, whereas the kinetic energy of protons above which particles could enter from any direction was the high value of about 8 Bev. In the range from 1 Bev to 8 Bev nothing was said about whether the particles could or could not enter, except that if they did enter it would be from certain allowed directions only. These allowed directions can be determined by study of particle trajectories. The trajectories can only be obtained by numerical integration of the equations of motion, since a third constant of the motion, besides energy and canonical angular momentum, has never been found.

#### Particle Trajectories — Numerical Integration

In this section we shall be concerned with the calculation by numerical integration of the charged particle trajectories in a dipole field. The particles initially form a parallel beam. As this beam enters the region near the dipole, deflection of the particles occurs and the motion of each is strongly dependent on its impact parameters. The incident beam of particles will be characterized in the following way. At distances far from the dipole, the orbit of a charged particle is a straight line because the field falls off to zero at infinity. The actual orbit of the particle, which is in general a complicated three-dimensional curve, is asymptotic to this straight line. Imagine the asymptote for each trajectory to be continued until it intersects a plane passing through the dipole center and normal to the direction of the incident beam. All particles in the beam will be supposed to have the same initial velocity (the same initial speed and the same initial direction), but the points at which the asymptotes to each trajectory pierce the plane through the dipole center perpendicular to the incident direction will be different. For example, the

intersection points may be assumed to form a network of squares or concentric circles. We are interested in following each trajectory by numerical integration until it recedes to infinity.

A few remarks orienting the present work with other investigations are in order. Störmer, to whom we are indebted for the first researches into the motion of a charged particle in a dipole field,<sup>75</sup> found the trajectories passing through the dipole center characterized by different values of his integration constant  $\gamma$  which is proportional to the angular momentum at infinity about the dipole axis. He also found that the problem can be scaled for different particle energies by means of the Störmer unit, and studied the regions forbidden to particles having various values of angular momentum. The trajectories which he studied were ordered according to the value of the angular momentum and were, in general, incident from a wide variety of directions. An extension of this problem was considered by Lemaitre and Vallarta.<sup>61-65</sup> A charged particle intersects a sphere surrounding the dipole at a certain point having velocity in a certain direction, all of which are considered known. If the strength of the dipole is known, then the problem is to find the incident direction of the particle. This problem is of interest in the study of cosmic rays incident on the earth, whose magnetic field closely approximates that of an ideal dipole at altitudes less than a few earth radii. At greater altitudes the geomagnetic field is distorted by streams of plasma from the sun and the analysis no longer applies exactly. The results which one obtains for the incident direction of a charged particle depend strongly on the point at which the particle orbit pierces the sphere surrounding the dipole and the direction of the orbit at that point, and a wide variety of initial directions for trajectories are found

We have seen that, for a given particle energy, there exists a toroidal region into which particles cannot penetrate. [The boundary of this region is given by Eq. (4.18).] Other regions are shielded from particles having certain values of angular momentum. In order to study in more detail the nature of the shielding provided by a dipole field, it is necessary to consider an isotropic flux of particles having a continuous energy spectrum. For purposes of analysis this may be broken down into the study of beams of noninteracting particles having the same energy and incident from the same direction. Thus it is desirable to consider a homogenous beam of particles ordered with

respect to their initial direction, and observe what happens to this beam as it moves in the dipole field. The behavior of such a uniform beam has been studied by Schlüter<sup>67</sup> and more recently by Kelsall.<sup>72</sup> Schlüter determined the behavior of a beam initially parallel to the equatorial plane of the dipole. Kelsall studied trajectories which initially make angles between  $0^\circ$  and  $35^\circ$  with the equatorial plane, corresponding to particles from the sun moving in the geomagnetic field.

In previous work, the trajectories have been found by specifying as initial conditions the position of the particles in a plane perpendicular to the parallel beam at some finite distance from the dipole. Kelsall, for example, used a plane 6 Störmer units away from the dipole. The interval of numerical integration must be set by continuous examination of the orbit's curvature. Difficulties are experienced setting stopping conditions, since one wants some assurance that the whole trajectory has been obtained. In the present report a method is given whereby the trajectories can be computed all the way from infinity and boundary conditions applied directly to the asymptotes of the orbits. The computed points get closer together as the neighborhood of the dipole is reached; when the particle moves away from the dipole the integration steps increase once again. The trajectory along its whole length from infinity to the dipole region and back out to infinity is computed. There is no difficulty with a stopping condition and the accuracy at any point along the trajectory can be made as good as desired. Whereas in some cases the imposition of initial conditions concerning position and direction of velocity at a finite distance from the dipole is probably a good enough approximation, yet there exist some instances (e.g., particles near the equatorial plane aimed at nearly one Störmer unit from the dipole, particles aimed near the dipole axis) where the shape of the trajectory is very sensitive to small changes in the impact parameters. The representation of a uniform beam of particles by uniformly distributed asymptotes gives a more nearly correct representation in such cases. The theoretically correct specification of impact parameters in terms of asymptotes also gives more confidence in the study of quasi-trapped trajectories, which are of interest in connection with the Van Allen regions.

We obtain an expression for the magnetic field in a Cartesian coordinate system inclined at an angle  $\chi$  with the original Cartesian system. In such a rotated coordinate system it is easy to describe the initial position and

velocity of a particle incident from some arbitrary direction. The coordinates chosen are obtained from the usual Cartesian coordinates by rotation about some convenient axis lying in the equatorial plane of the dipole. We arbitrarily choose the x-axis about which to rotate and let

$$\left. \begin{aligned} \xi &= x \\ \eta &= -y \cos \chi + z \sin \chi \\ \zeta &= y \sin \chi + z \cos \chi \end{aligned} \right\}. \quad (4.26)$$

Here  $\chi$  is the angle between the  $\zeta$ -axis and the z-axis. In the application we have in view it is the angle between the initial velocity of a particle incident from infinity and the dipole axis. Because the transformation (4.26) is orthogonal, the expression for the distance from the origin is invariant, i. e.,

$$r^2 = x^2 + y^2 + z^2 = \xi^2 + \eta^2 + \zeta^2. \quad (4.27)$$

Using the transformation inverse to (4.26), we see that the expression (4.27) for the magnetic field in the  $(\xi, \eta, \zeta)$  system is, if  $\hat{e}_\xi, \hat{e}_\eta, \hat{e}_\zeta$  are unit vectors in the three coordinate directions,

$$\begin{aligned} \vec{H} = & -\hat{e}_\xi a \frac{3\xi(\eta \sin \chi + \zeta \cos \chi)}{(\xi^2 + \eta^2 + \zeta^2)^{3/2}} \\ & -\hat{e}_\eta a \frac{(2\eta^2 - \xi^2 - \zeta^2) \sin \chi + 3\eta\zeta \cos \chi}{(\xi^2 + \eta^2 + \zeta^2)^{3/2}} \\ & -\hat{e}_\zeta a \frac{(2\zeta^2 - \xi^2 - \eta^2) \cos \chi + 3\eta\zeta \sin \chi}{(\xi^2 + \eta^2 + \zeta^2)^{3/2}}. \end{aligned} \quad (4.28)$$

Let us obtain the equations of motion in the coordinate system (4.26). In doing so we sacrifice some of the simplicity inherent in spherical coordinates, notably that of the angular momentum integral (4.13), but we gain an easier

way to prescribe initial conditions representing particles incident in a parallel beam at some arbitrary orientation with respect to the dipole axis. We make the angle of inclination  $\chi$  equal to the angle between a line parallel to the incident asymptote and the dipole axis (the angle  $\chi$  of Fig. 4.4). The two Cartesian coordinate systems are aligned with respect to the dipole and the initial direction of the particle velocity according to the following construction:

1. The z-axis of the (x, y, z) system is selected so that it lies along the dipole axis.
2. The system (x, y, z) is translated along the z-axis until its origin coincides with the dipole center.
3. The system (x, y, z) is rotated about the z-axis until the x-axis is perpendicular to the direction of the particle's initial velocity.
4. The coordinates are rotated about the x-axis of the (x, y, z) system through an angle  $\pi/2 - \chi$  to form a new system ( $\xi, \eta, \zeta$ ) such that the  $\zeta$ -axis is parallel to the direction of the particle's initial velocity. The  $\xi$ -axis of the new system is identical with the x-axis of the old. If the particle's velocity at infinity is parallel to the equatorial plane of the dipole, then there need be no rotation of coordinates and the  $\zeta$ -axis is the same as the y-axis.

The initial position of a particle is given by specifying finite values of  $\xi(s)$  and  $\eta(s)$  when  $s \rightarrow -\infty$ . The initial value of  $\zeta(s)$  at  $s \rightarrow -\infty$  is infinite, but the value of  $d\zeta/ds$  is initially -1. The negative sign arises because the particle is directed toward, rather than away from, the dipole. The initial values of  $d\xi/ds$  and  $d\eta/ds$  are both zero.

In deriving the equations of motion by working out the cross product  $\vec{v} \times \vec{H}$ , it is essential to note that the ( $\xi, \eta, \zeta$ ) coordinates taken in that order comprise a left-handed system. The equations of motion in the rotated Cartesian system are, in terms of the arc length  $s$  as the independent variable,

$$\begin{aligned} \frac{d^2\xi}{ds^2} &= C_{st}^2 \left[ \frac{(2\xi^2 - \eta^2 - \zeta^2)\cos\chi + 3\eta\zeta\sin\chi}{(\xi^2 + \eta^2 + \zeta^2)^{5/2}} \frac{d\eta}{ds} - \frac{(2\eta^2 - \xi^2 - \zeta^2)\sin\chi + 3\eta\zeta\cos\chi}{(\xi^2 + \eta^2 + \zeta^2)^{5/2}} \frac{d\zeta}{ds} \right] \\ \frac{d^2\eta}{ds^2} &= C_{st}^2 \left[ \frac{3\xi\eta\sin\chi + 3\xi\zeta\cos\chi}{(\xi^2 + \eta^2 + \zeta^2)^{5/2}} \frac{d\zeta}{ds} - \frac{(2\xi^2 - \eta^2 - \zeta^2)\cos\chi + 3\eta\zeta\sin\chi}{(\xi^2 + \eta^2 + \zeta^2)^{5/2}} \frac{d\xi}{ds} \right] \\ \frac{d^2\zeta}{ds^2} &= C_{st}^2 \left[ \frac{(2\eta^2 - \xi^2 - \zeta^2)\sin\chi + 3\eta\zeta\cos\chi}{(\xi^2 + \eta^2 + \zeta^2)^{5/2}} \frac{d\xi}{ds} - \frac{3\xi\eta\sin\chi + 3\xi\zeta\cos\chi}{(\xi^2 + \eta^2 + \zeta^2)^{5/2}} \frac{d\eta}{ds} \right] \end{aligned} \quad (4.29)$$

As possible aids to the solution of the set (4.29) we have two "first integrals". The first expresses the conservation of particle speed and appears in the form

$$\left(\frac{d\xi}{ds}\right)^2 + \left(\frac{d\eta}{ds}\right)^2 + \left(\frac{d\zeta}{ds}\right)^2 = 1. \quad (4.30)$$

The second is derived from Störmer's first integral (4.13) by transforming first from cylindrical coordinates to Cartesian coordinates (x, y, z) and then to the rotated Cartesian coordinates ( $\xi, \eta, \zeta$ ). It is

$$\begin{aligned} & \frac{1}{C_{st}} \left[ \sin \chi \left( \xi \frac{d\zeta}{ds} - \zeta \frac{d\xi}{ds} \right) + \cos \chi \left( \eta \frac{d\xi}{ds} - \xi \frac{d\eta}{ds} \right) \right] \\ &= 2\gamma + C_{st} \frac{\xi^2 + \eta^2 \cos^2 \chi + \zeta^2 \sin^2 \chi - 2\eta\zeta \sin \chi \cos \chi}{(\xi^2 + \eta^2 + \zeta^2)^{3/2}}. \end{aligned} \quad (4.31)$$

As  $s \rightarrow -\infty$ ,  $d\xi/ds$  and  $d\eta/ds$  both go to zero, while  $d\zeta/ds \rightarrow -1$ . Also  $\zeta \rightarrow +\infty$  and the fraction on the right hand side of Eq. (4.31) goes to zero as  $1/\zeta$ . In this limit, Eq. (4.31) reduces to

$$-\frac{1}{C_{st}} \sin \chi \xi(-\infty) = 2\gamma. \quad (4.32)$$

This is identical with Eq. (4.16) if we put  $\xi(-\infty) = P_0$ .

In an ordinary scattering problem, such as that of unbounded motion in a central field of force, the trajectory (including the scattering angle) is completely determined by a single impact parameter for a given particle energy. This permits the essential features of the encounter to be described by the cross section as a function of energy. The problem of scattering by a magnetic dipole is sufficiently more complicated that three impact parameters

are necessary to specify the motion. These are: the angle of inclination  $\chi$  between the initial velocity and the dipole axis, and the initial coordinates  $P_0 = \xi(-\infty)$ ,  $Q_0 = \eta(-\infty)$  of the particle in a plane at infinity perpendicular to the trajectory's asymptote. The geometric meaning of these quantities is given in Fig. 4.4.

In mathematical terms the problem of finding the trajectory of a charged particle incident from infinity in the field of a magnetic dipole is the following. We are to solve a set of three coupled nonlinear differential equations of the second order in which the second derivatives appear only once in each equation:

$$\left. \begin{aligned} P'' &= F_1(P, Q, R; P', Q', R') \\ Q'' &= F_2(P, Q, R; P', Q', R') \\ R'' &= F_3(P, Q, R; P', Q', R') \end{aligned} \right\}. \quad (4.33)$$

In what follows all equations will be expressed in terms of the dimensionless variables  $P = \xi / C_{st}$ ,  $Q = \eta / C_{st}$ ,  $R = \zeta / C_{st}$ , and  $S = s / C_{st}$ . This means that all distances are measured using the Störmer distance as a unit of length. We wish to find  $P(S)$ ,  $Q(S)$ , and  $R(S)$  such that the system (4.1) is satisfied subject to the "initial" conditions

$$\left. \begin{aligned} P(-\infty) &= P_0, & Q(-\infty) &= Q_0, & R(-\infty) &= \infty, \\ P'(-\infty) &= 0, & Q'(-\infty) &= 0, & R'(-\infty) &= -1. \end{aligned} \right\} \quad (4.34)$$

Here, for example,  $P'(-\infty)$  means  $P'(S) = dP/dS$  evaluated as  $S \rightarrow -\infty$ . From the last of the initial conditions (4.34) we note that  $\underline{S}$  and  $\underline{R}$  diverge in the opposite sense but at equal rates, i. e.,

$$\lim_{S \rightarrow -\infty} \frac{R}{S} = -1. \quad (4.35)$$

Because of the complexity and nonlinearity of the system (4.33) [Cf. the parent equations (4.29)] it is necessary to perform the integration by numerical methods on an electronic digital computer. The method for solution of ordinary differential equations of the type (4.33) most convenient for use on an automatic digital machine is the Runge-Kutta method,<sup>94</sup> In order to apply this method to a system having the form (4.33) but with initial conditions given in finite terms at some finite value of  $\underline{S}$ , it is necessary to choose a small interval of integration and evaluate each of the functions  $F_1, F_2, F_3$  from arguments derived from points in this small interval, including the end points. The solution is started at the initial point  $S_0$  where all the functions  $\underline{P}, \underline{Q}, \underline{R}$  and their first derivatives are given as boundary conditions, and proceeds to find the values of the unknown functions and their first derivatives at  $S_0 + \Delta S$ . Then the new values are taken as initial conditions and the functions with their derivatives are calculated at a new point  $S_0 + 2\Delta S$ . This process may be continued as long as desired, and for a machine computation it is in general difficult to formulate a suitable stopping condition.

Because of the non-finite boundary conditions (4.34), it is not possible to use the Runge-Kutta method directly for the dipole trajectory problem. For the greatest accuracy in the method, it is necessary to take  $\Delta S$  to be a very small quantity. This means that the integration proceeds on the computer over very small increments with printout of the values of the solution occurring at, say, every 16 or 32 steps (for a binary-based computer). But since the boundary conditions are imposed at negative infinity, it would require an infinite number of small integration steps to reach the region in which the trajectory changes appreciably and in which the interesting features of the motion occur. It is necessary to make some transformation of the variables in order that the boundary conditions (4.34) and (4.35) may be expressed in finite terms.

It is desired to make transformations on  $\underline{R}$  and  $\underline{S}$  having the following properties: (a) when  $\underline{R}$  or  $\underline{S}$  becomes infinite in either the positive or negative sense, the new variables must remain finite, (b) the transformed variables must distinguish between plus and minus infinity in the physical variables  $\underline{R}, \underline{S}$ , and (c) when  $\underline{R}$  or  $\underline{S}$  has magnitude of order unity the new variables must

have comparable values. As a pair of transformations satisfying these conditions, we have chosen the following:

$$\mu = \arctan R = \arctan (\zeta/C_{st}), \quad (4.36)$$

$$\sigma = \arctan S = \arctan (z/C_{st}). \quad (4.37)$$

By "arc tan" we mean the principal value of the function  $\tan^{-1}$ , that is the value lying between  $-\pi/2$  and  $+\pi/2$ . When  $\underline{R}$  or  $\underline{S}$  approaches negative infinity,  $\underline{\mu}$  or  $\underline{\sigma}$  approaches  $-\pi/2$ . When  $\underline{R}$  or  $\underline{S}$  approaches positive infinity,  $\underline{\mu}$  or  $\underline{\sigma}$  (as the case may be) approaches  $+\pi/2$ . When  $\underline{R}$  or  $\underline{S}$  is in the neighborhood of zero, the slope of the curve is nearly unity, and  $\underline{\mu}$  or  $\underline{\sigma}$  has values in the neighborhood of zero. These values are therefore comparable with the values of  $\underline{R}$  or  $\underline{S}$ .

We wish to transform the system (4.33) of equations in  $\underline{P}$ ,  $\underline{Q}$ ,  $\underline{R}$  considered as functions of  $\underline{S}$  into a new system in which  $\underline{P}$ ,  $\underline{Q}$ , and  $\underline{\mu}$  are regarded as functions of  $\underline{\sigma}$ . In doing so it is necessary to find expressions for the old derivatives  $dR/dS$ , etc., in terms of new derivatives like  $d\mu/d\sigma$ , and to determine the boundary conditions on the new quantities and their derivatives. Moreover in order to start the Runge-Kutta solution, it is necessary to find the second derivatives at the initial point. As we shall see later, the second derivatives must be evaluated from the differential equations by a limiting process rather than by direct calculation, because of the nature of the boundary conditions.

In order to obtain the various derivatives that will be needed in transforming the differential equations (4.1), we need the derivative  $d\sigma/dS$ , which can be calculated directly; thus

$$\frac{d\sigma}{dS} = \frac{1}{1+S^2} = \cos^2 \sigma. \quad (4.38)$$

The derivative  $dR/dS$  may be expressed in terms of the transformed quantities by using Eq. (4.6) as follows:

$$\frac{dR}{dS} = \frac{d\sigma}{dS} \frac{d\mu}{d\sigma} \frac{dR}{d\mu} = \frac{\cos^2 \sigma}{\cos^2 \mu} \frac{d\mu}{d\sigma}. \quad (4.39)$$

Solving for  $d\mu/d\sigma$  and evaluating this expression as  $\sigma \rightarrow -\pi/2$ , we have, since  $dR/dS$  and  $R/S$  both go to  $-1$  initially,

$$\mu'(-\pi/2) = \lim_{\sigma \rightarrow -\pi/2} \frac{d\mu}{d\sigma} = \lim_{S \rightarrow -\infty} \frac{1+S^2}{1+R^2} (-1) = -1 \quad (4.40)$$

as the initial condition on  $d\mu/d\sigma$ . By a second differentiation,  $d^2R/dS^2$  may be expressed in terms of  $d^2\mu/d\sigma^2$  and  $d\mu/d\sigma$ .

$$\begin{aligned} \frac{d^2R}{dS^2} &= \frac{d\sigma}{dS} \frac{d}{d\sigma} \left( \frac{\cos^2 \sigma}{\cos^2 \mu} \frac{d\mu}{d\sigma} \right) \\ &= \frac{\cos^4 \sigma}{\cos^3 \mu} \frac{d^2\mu}{d\sigma^2} + 2 \frac{\cos^4 \sigma \sin \mu}{\cos^3 \mu} \left( \frac{d\mu}{d\sigma} \right)^2 - 2 \frac{\cos^3 \sigma \sin \sigma}{\cos^2 \mu} \frac{d\mu}{d\sigma}. \end{aligned} \quad (4.41)$$

The derivatives of  $\underline{P}$  and  $\underline{Q}$  with respect to the new variable  $\sigma$  are easier to calculate but one must be more careful in establishing the initial conditions on them. In fact it is necessary to use the parent equations (4.29) with  $\xi, \eta, \zeta, s$  replaced by  $P, Q, R, S$  (and  $C_{st}$  set equal to unity) to establish correctly the initial values of  $dP/d\sigma$  and  $dQ/d\sigma$ . We have

$$\frac{dP}{dS} = \frac{d\sigma}{dS} \frac{dP}{d\sigma} = \cos^2 \sigma \frac{dP}{d\sigma}. \quad (4.42)$$

The initial value of  $dP/d\sigma$  is found by solving Eq. (4.42) for  $dP/d\sigma$ , taking the limit as  $\sigma \rightarrow -\pi/2$ , and using L'Hospital's rule since numerator and

denominator both go to zero:

$$\begin{aligned}
 P'(-\pi/2) &= \lim_{\sigma \rightarrow -\pi/2} \frac{dP}{d\sigma} = \lim_{\substack{\sigma \rightarrow -\pi/2 \\ S \rightarrow -\infty}} \frac{1}{\cos^2 \sigma} \frac{dP}{dS} \\
 &= \lim_{\substack{\sigma \rightarrow -\pi/2 \\ S \rightarrow -\infty}} \frac{-1}{2 \sin \sigma \cos \sigma} \frac{d}{d\sigma} \frac{dP}{dS} = \lim_{\substack{\sigma \rightarrow -\pi/2 \\ S \rightarrow -\infty}} \frac{-1}{2 \sin \sigma \cos \sigma} \frac{dS}{d\sigma} \frac{d^2 P}{dS^2}. \quad (4.43)
 \end{aligned}$$

After noticing from the dimensionless form of Eq. (4.29a) that  $d^2 P/dS^2$  goes to zero like  $-\sin \chi/R^3$  as  $S \rightarrow -\infty$ , and that

$$\lim_{\sigma \rightarrow -\pi/2} \frac{1}{\sin \sigma \cos^3 \sigma} = \lim_{S \rightarrow -\infty} \frac{(1+S^2)^2}{S} = \lim_{S \rightarrow -\infty} S^3$$

we have

$$P'(-\pi/2) = \lim_{S \rightarrow -\infty} -\frac{1}{2} S^3 \frac{\sin \chi}{R^3} (-1) = -\frac{1}{2} \sin \chi. \quad (4.44)$$

The derivative  $d^2 P/dS^2$  is found in terms of the new variables and their derivatives by a method analogous to the derivation of Eq. (4.41).

$$\begin{aligned}
 \frac{d^2 P}{dS^2} &= \frac{d\sigma}{dS} \frac{d}{d\sigma} \frac{dP}{dS} = \cos^2 \sigma \frac{d}{d\sigma} \left( \cos^2 \sigma \frac{dP}{d\sigma} \right) \\
 &= \cos^4 \sigma \frac{d^2 P}{d\sigma^2} - 2 \sin \sigma \cos^3 \sigma \frac{dP}{d\sigma}. \quad (4.45)
 \end{aligned}$$

The derivatives  $dQ/dS$  and  $d^2 Q/dS^2$  in terms of the transformed variables

may be written down in strict analogy to Eqs. (4.42) (4.45):

$$\frac{dQ}{dS} = \cos^2 \sigma \frac{dQ}{d\sigma}. \quad (4.46)$$

$$\frac{d^2Q}{dS^2} = \cos^4 \sigma \frac{d^2Q}{d\sigma^2} - 2 \sin \sigma \cos^3 \sigma \frac{dQ}{d\sigma}. \quad (4.47)$$

We obtain the limiting initial value for  $dQ/d\sigma$  in a manner analogous to the derivation of Eq. (4.44), but in this case  $d^2Q/dS^2$  goes to zero faster than  $1/R^3$  as  $S \rightarrow -\infty$ , so that

$$Q'(-\pi/2) = \lim_{\sigma \rightarrow -\pi/2} \frac{dQ}{d\sigma} = \lim_{S \rightarrow -\infty} -\frac{1}{2} S^3 \frac{d^2Q}{dS^2} = 0. \quad (4.48)$$

Using the expressions  $R = \tan \mu$ , (4.39) (4.41) (4.42) (4.45) (4.46) (4.47), we find that the equations of motion (4.29) written in dimensionless notation assume the following form in terms of the transformed variables.

$$\begin{aligned} \cos^2 \sigma \frac{d^2P}{d\sigma^2} = & 2 \sin \sigma \cos \sigma \frac{dP}{d\sigma} + \frac{(2 \tan^2 \mu - P^2 - Q^2) \cos \chi + 3Q \sin \chi \tan \mu}{(P^2 + Q^2 + \tan^2 \mu)^{3/2}} \frac{dQ}{d\sigma} \\ & - \frac{(2Q^2 - P^2 - \tan^2 \mu) \sin \chi + 3Q \cos \chi \tan \mu}{(P^2 + Q^2 + \tan^2 \mu)^{3/2}} \frac{1}{\cos^3 \mu} \frac{d\mu}{d\sigma}, \end{aligned} \quad (4.49a)$$

$$\begin{aligned} \cos^2 \sigma \frac{d^2Q}{d\sigma^2} = & 2 \sin \sigma \cos \sigma \frac{dQ}{d\sigma} + \frac{3PQ \sin \chi + 3P \cos \chi \tan \mu}{(P^2 + Q^2 + \tan^2 \mu)^{3/2}} \frac{1}{\cos^3 \mu} \frac{d\mu}{d\sigma} \\ & - \frac{(2 \tan^2 \mu - P^2 - Q^2) \cos \chi + 3Q \sin \chi \tan \mu}{(P^2 + Q^2 + \tan^2 \mu)^{3/2}} \frac{dP}{d\sigma}, \end{aligned} \quad (4.49b)$$

$$\begin{aligned}
\frac{\cos^2 \sigma}{\cos^2 \mu} \frac{d^2 \mu}{d\sigma^2} = & 2 \frac{\sin \sigma \cos \sigma}{\cos^2 \mu} \frac{d\mu}{d\sigma} - 2 \frac{\cos^2 \sigma \sin \mu}{\cos^3 \mu} \left( \frac{d\mu}{d\sigma} \right)^2 \\
& + \frac{(2Q^2 - P^2 - \tan^2 \mu) \sin \chi + 3Q \cos \chi \tan \mu}{(P^2 + Q^2 + \tan^2 \mu)^{3/2}} \frac{dP}{d\sigma} \\
& - \frac{3PQ \sin \chi + 3P \cos \chi \tan \mu}{(P^2 + Q^2 + \tan^2 \mu)^{3/2}} \frac{dQ}{d\sigma}.
\end{aligned} \tag{4.49c}$$

The numerical integration problem is to find  $P(\sigma)$ ,  $Q(\sigma)$ ,  $\mu(\sigma)$ ;  $P'(\sigma) = dP/d\sigma$ ,  $Q'(\sigma)$ ,  $\mu'(\sigma)$  subject to the initial conditions

$$\begin{aligned}
P(-\pi/2) &= P_0, & P'(-\pi/2) &= -\frac{1}{2} \sin \chi, \\
Q(-\pi/2) &= Q_0, & Q'(-\pi/2) &= 0, \\
\mu(-\pi/2) &= \pi/2, & \mu'(-\pi/2) &= -1,
\end{aligned} \tag{4.50}$$

for various values of  $\chi$ .

In order to solve the system (4.49) subject to the initial conditions (4.50), it is necessary to know the values of the second derivatives at the initial value of the independent variable. Ordinarily these can be gotten by direct substitution of the initial values of the dependent variables and their first derivatives into the differential equation. This can be done in the present case only by the use of limit processes. It is convenient to evaluate the second derivatives using the expressions (4.41) (4.45) (4.47) and the original differential equations (4.29) instead of the rather cumbersome equations (4.49). In what follows we

shall have occasion to use the limit relations

$$\lim_{\sigma \rightarrow -\pi/2} \cos \mu = \lim_{R \rightarrow +\infty} \frac{1}{\sqrt{1+R^2}} = \lim_{R \rightarrow +\infty} \frac{1}{R}, \quad (4.51a)$$

$$\lim_{\sigma \rightarrow -\pi/2} \cos \sigma = \lim_{S \rightarrow -\infty} \frac{1}{\sqrt{1+S^2}} = \lim_{S \rightarrow -\infty} -\frac{1}{S}. \quad (4.51b)$$

To evaluate  $d^2\mu/d\sigma^2$  we solve Eq. (4.41) for this quantity, remembering that  $d\mu/d\sigma$  approaches -1 as  $\sigma \rightarrow -\pi/2$ .

$$\mu''(-\pi/2) = \lim_{\sigma \rightarrow -\pi/2} \left[ \frac{\cos^2 \mu}{\cos^4 \sigma} \frac{d^2 R}{dS^2} - 2(\tan \sigma + \tan \mu) \right]. \quad (4.52)$$

We use Eqs. (4.50) (4.51) to evaluate the cosines appearing in the first term. The last two terms are evaluated directly from Eqs. (4.26) (4.37). The second derivative  $d^2 R/dS^2$  is given in the limit by those terms of Eq. (4.29a) (in its dimensionless form) which involve negative powers of  $\underline{R}$ . Thus, since  $dP/dS$  and  $dQ/dS$  are bounded,

$$\lim_{\sigma \rightarrow -\pi/2} \frac{\cos^2 \mu}{\cos^4 \sigma} \frac{d^2 R}{dS^2} = \lim_{S \rightarrow -\infty} \frac{S^4}{R^2} O\left(\frac{1}{R^3}\right) = 0. \quad (4.53)$$

We therefore obtain for the limiting value of  $d^2\mu/d\sigma^2$  as  $\sigma \rightarrow -\pi/2$ ,

$$\mu''(-\pi/2) = \lim_{S \rightarrow -\infty} -2(R+S) = 0. \quad (4.54)$$

$\underline{S}$  and  $\underline{R}$  cancel each other in the limit because of Eq. (4.35).

The evaluation of  $d^2P/d\sigma^2$  is similar except that the inverse powers of  $R$  in the expression for  $d^2P/dS^2$  is not sufficient to cancel the fourth power of  $S$ . Solving Eq. (4.45) for  $d^2P/d\sigma^2$ , using Eq. (4.51), remembering that  $\tan \sigma = S$  and using Eq. (4.44), we have

$$P''(-\pi/2) = \lim_{S \rightarrow -\infty} \left[ S^4 \frac{d^2P}{dS^2} + 2S \left( -\frac{1}{2} \sin \chi \right) \right]. \quad (4.55)$$

The second derivative  $d^2P/dS^2$  is given in the limit by those terms in Eq. (4.29a) having powers in  $R$  equal to -3 and -4. Substituting this result in (4.55) one obtains

$$P''(-\pi/2) = \lim_{S \rightarrow -\infty} \left( \frac{S^4}{R^4} \cdot 3Q_0 \cos \chi - \frac{S^4}{R^3} \sin \chi - S \sin \chi + \frac{S^4}{R^3} \cdot 2 \cos \chi \frac{dQ}{dS} \right). \quad (4.56)$$

Since  $S/R$  goes to -1 in the limit as  $S \rightarrow -\infty$ , the quotient  $S^4/R^3$  goes to - $S$  and  $S^4/R^4$  goes to +1. This means that the second and third terms on the right of Eq. (4.56) cancel. The first term is just  $3Q_0 \cos \chi$ . The last term must be evaluated using L'Hospital's rule, as follows:

$$\lim_{S \rightarrow -\infty} -S \frac{dQ}{dS} = \lim_{S \rightarrow -\infty} - \frac{dQ/dS}{1/S} = \lim_{S \rightarrow -\infty} \frac{d^2Q/dS^2}{1/S^2} = 0. \quad (4.57)$$

The limit is zero because no powers of  $R$  greater than -3 occur in the limiting equation for  $d^2Q/dS^2$  obtained from Eq. (4.29b). Hence from Eq. (4.56) we see that  $d^2P/d\sigma^2$  has the finite value

$$P''(-\pi/2) = 3Q_0 \cos \chi \quad (4.58)$$

in the limit as  $\sigma \rightarrow -\pi/2$ .

Finally we need to evaluate  $d^2Q/d\sigma^2$ ; this will require a multiple use of the L'Hospital rule. Solving Eq. (4.47) for  $d^2Q/d\sigma^2$ , taking the limit as  $\sigma \rightarrow -\pi/2$ , and using (4.51), one finds

$$\lim_{\sigma \rightarrow -\pi/2} \frac{d^2Q}{d\sigma^2} = \lim_{S \rightarrow \infty} S^2 \frac{d^2Q}{dS^2} + \lim_{\sigma \rightarrow -\pi/2} 2 \frac{dQ/d\sigma}{1/S}. \quad (4.59)$$

The first term is evaluated by retaining only those powers of  $R$  greater than -4 in the limiting expression for  $d^2Q/dS^2$  gotten from Eq. (4.29b); L'Hospital's rule is applied to the second term.

$$\lim_{\sigma \rightarrow -\pi/2} \frac{d^2Q}{d\sigma^2} = -3P_0 \cos \chi + \lim_{S \rightarrow \infty} 2S \cos \chi \frac{dP}{dS} + \lim_{\sigma \rightarrow -\pi/2} 2 \frac{d^2Q/d\sigma^2}{\frac{d}{d\sigma} \left( \frac{1}{S} \right)}. \quad (4.60)$$

The quantity  $S(dP/dS)$  can be evaluated in the limit by a method similar to that in Eq. (4.57); the limit is zero because no powers of  $R$  greater than -3 occur in the limiting equation for  $d^2P/dS^2$ . For the denominator in the last term we have

$$\lim_{\sigma \rightarrow -\pi/2} \frac{d}{d\sigma} \left( \frac{1}{S} \right) = \lim_{\sigma \rightarrow -\pi/2} \frac{d}{d\sigma} \cot \sigma = \lim_{\sigma \rightarrow -\pi/2} \frac{-1}{\sin^2 \sigma} = -1. \quad (4.61)$$

Accordingly Eq. (4.60) becomes

$$\lim_{\sigma \rightarrow -\pi/2} \frac{d^2Q}{d\sigma^2} = -3P_0 \cos \chi - \lim_{\sigma \rightarrow -\pi/2} 2 \frac{d^2Q}{d\sigma^2}. \quad (4.62)$$

This equation is solved to give the desired initial value for the second derivative  $Q''(\sigma)$ :

$$Q''(-\pi/2) = -P_0 \cos \chi. \quad (4.63)$$

The system (4. 49) of differential equations may be integrated subject to the initial conditions (4. 50) now that the starting values (4. 54) (4. 58) (4. 63) of the second derivatives have been determined. The initial conditions are not separate entities from the differential equations: It was for convenience in imposing the initial conditions that the equations of motion were written in the form (4. 29) using the rotated Cartesian coordinate system. The equations of motion were rewritten in the transformed variables  $\mu$  and  $\sigma$  because the initial conditions were imposed at infinity. The differential equations (4. 29) were used strongly in setting up the new initial values (4. 50) for the system (4. 49). And the equivalents of the differential equations (4. 49) were used in evaluating the starting values for the second derivatives.

In practice the integration is performed by choosing values of impact parameters  $\chi$ ,  $P_0$ ,  $Q_0$  and the integration step size  $\Delta\sigma$  for the independent variable. The variable of integration  $\sigma$  is permitted to take on values from  $-\pi/2$  to  $+\pi/2$ . A convenient interval accurate enough for most cases was found to be  $\Delta\sigma = \pi/100$ . Thus 100 points are computed for each trajectory. The points in  $\underline{P}$ ,  $\underline{Q}$ ,  $\underline{R}$  space which are distant from the dipole are far apart; as the trajectory gets closer to the dipole the points get closer together. The closest spacing of the physical points occurs in the neighborhood of  $S = 0$ ; this point is determined uniquely by the condition that  $\underline{R}$  and  $\underline{S}$  are initially equal in absolute value. As the trajectory moves away from the dipole the points get farther apart again. The computation is stopped when  $\sigma = +\pi/2$ , which corresponds to  $S = +\infty$ . For most trajectories the complicating features, such as loops, spirals, etc., occur in the vicinity of  $S = 0$ . Occasionally a trajectory is so complicated that the radius of curvature is small in the region where the interval between points is becoming large. Such trajectories are recomputed using a smaller value for  $\Delta\sigma$  in order to obtain the correct shape of the curve.

Figure 4. 7 shows a group of trajectories moving in the equatorial plane of the dipole. The dipole is supposed to be directed out of the paper which means that the magnetic field lines are going into the paper. If particles start out in the equatorial plane, they remain in it, because the magnetic lines of force are always perpendicular to the equatorial plane. The impact parameters  $P_0$ ,  $Q_0$  marked on each trajectory are in Störmer units of length. For all particles in the figure, which are assumed to be positively charged particles,

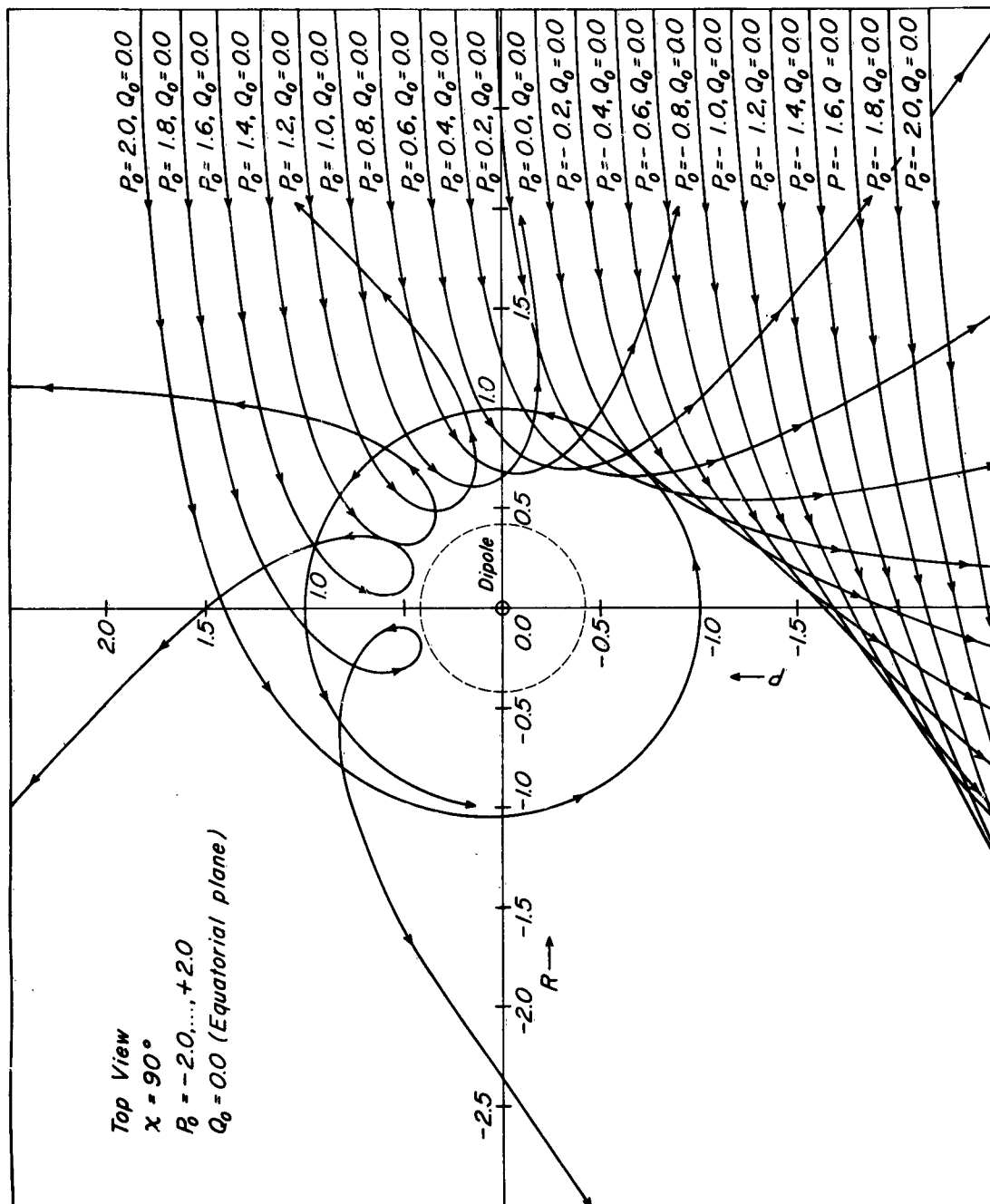


Fig. 4.7 Trajectories in the Equatorial Plane of the Dipole.

the initial velocity  $\vec{v}$  is directed from right to left,  $\vec{H}$  is always into the paper, and thus  $\vec{v} \times \vec{H}$  is downward. The trajectories in the equatorial plane can be calculated in closed form using elliptic integrals, but they were obtained by numerical integration so as to check the method by comparison with previous work of Störmer. Trajectories in the equatorial plane have the interesting property that the radius of curvature at a given point (measured in Störmer units) is equal to the cube of the distance (also measured in Störmer units) from the dipole. One trajectory is spirally asymptotic to a circle of radius one Störmer unit with center at the dipole.

Figure 4.8 shows a group of trajectories incident parallel to the dipole axis and in a plane passing through the dipole axis. Although the trajectories lie initially in a plane, the magnetic forces soon move most of them out of that plane, and they become skew curves in space, of which Fig. 4.8 and the illustrations to follow merely give two-dimensional orthographic representations. An exception is the particle aimed directly at the dipole center; it is undeflected by the magnetic field and moves along the dipole axis. This figure shows an example of the magnetic mirror effect discussed earlier. The trajectories on the left side of the illustration are symmetric with those on the right in this particular case, and are omitted for the sake of simplicity.

Figure 4.9 shows the behavior of a beam of particles making an angle of  $22\frac{1}{2}^\circ$  with the dipole axis. The impact parameters of one particle are such as to put that particle in a magnetic mirror orbit.

Figure 4.10 illustrates some trajectories starting out at an angle of  $45^\circ$  with the dipole axis. Other trajectories at  $45^\circ$  with impact parameters different from those shown here get involved in magnetic mirrors. The trajectories in this figure show particularly well the shielding properties of a dipole field in deflecting particles away from a toroidal region centered on the dipole.

In Fig. 4.11 the behavior of a beam from  $67\frac{1}{2}^\circ$  is shown. These particular trajectories show a tendency to form complicated nodes above and below the dipole. This behavior is different from the magnetic mirror effect and is common for trajectories initially making angles of  $90^\circ$  plus or minus about  $30^\circ$  with the dipole axis.

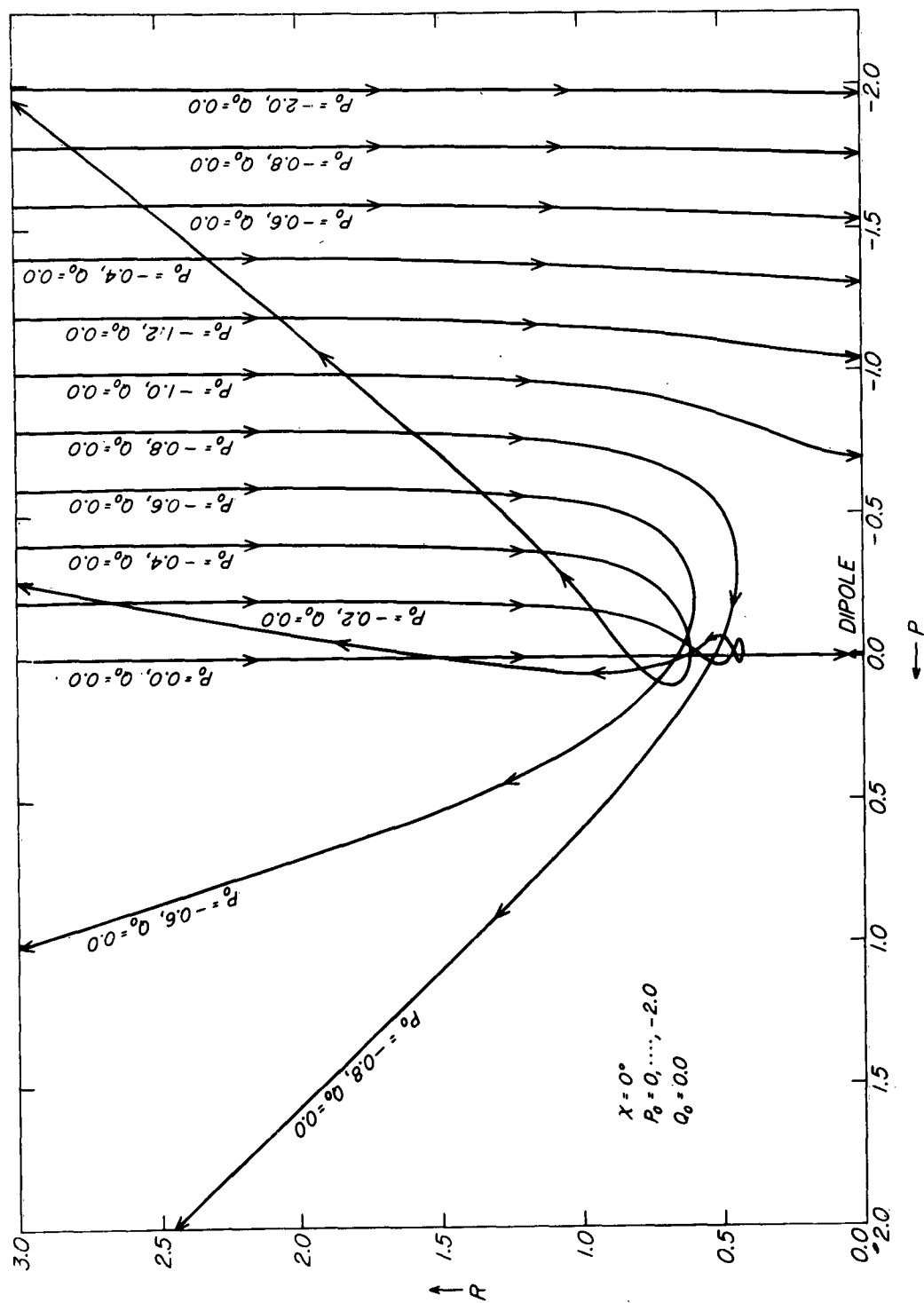


Fig. 4.8 Trajectories Incident Parallel to the Dipole Axis.

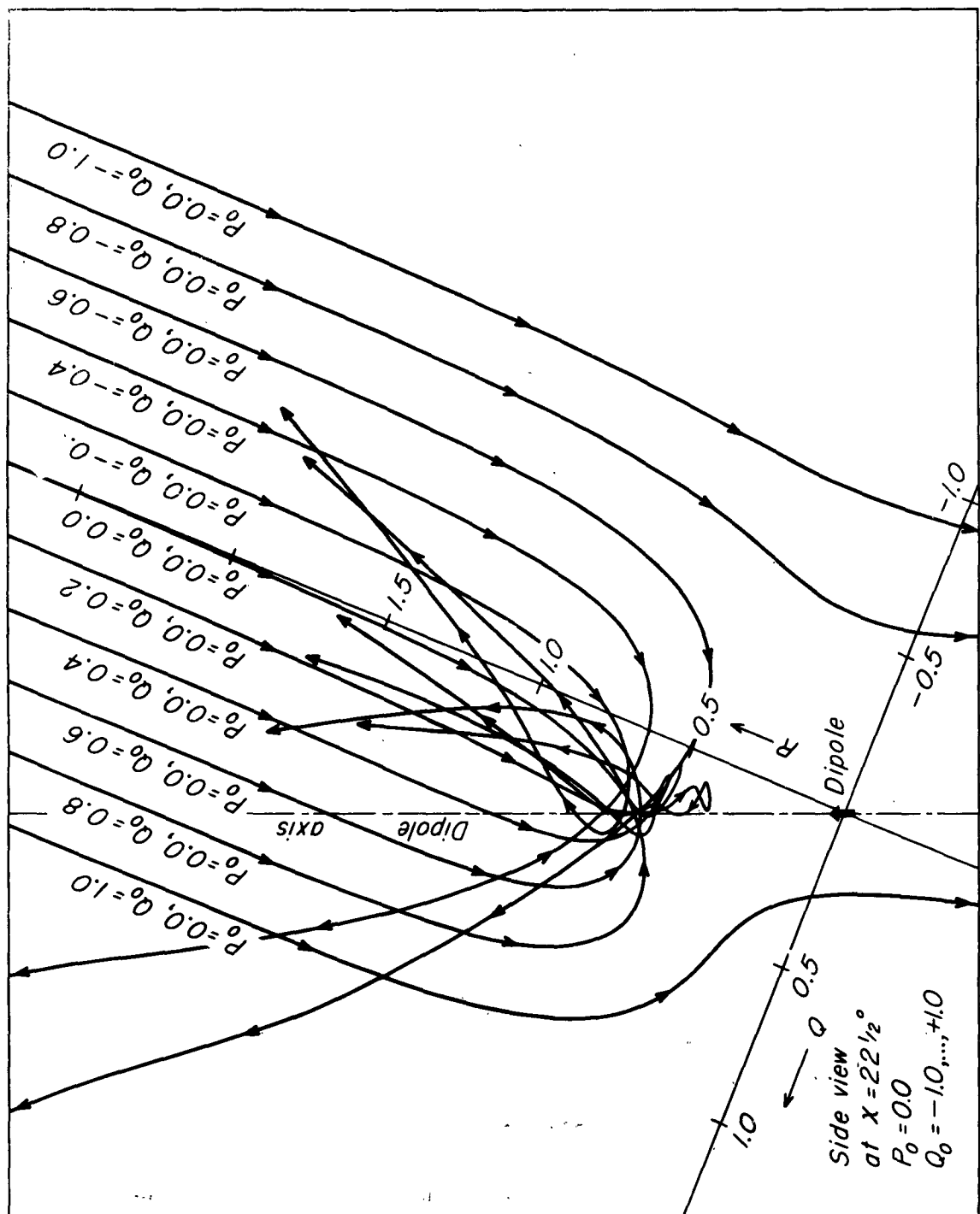


Fig. 4.9 Trajectories of Particles Incident at an Angle of  $22\frac{1}{2}^\circ$  With the Dipole Axis.

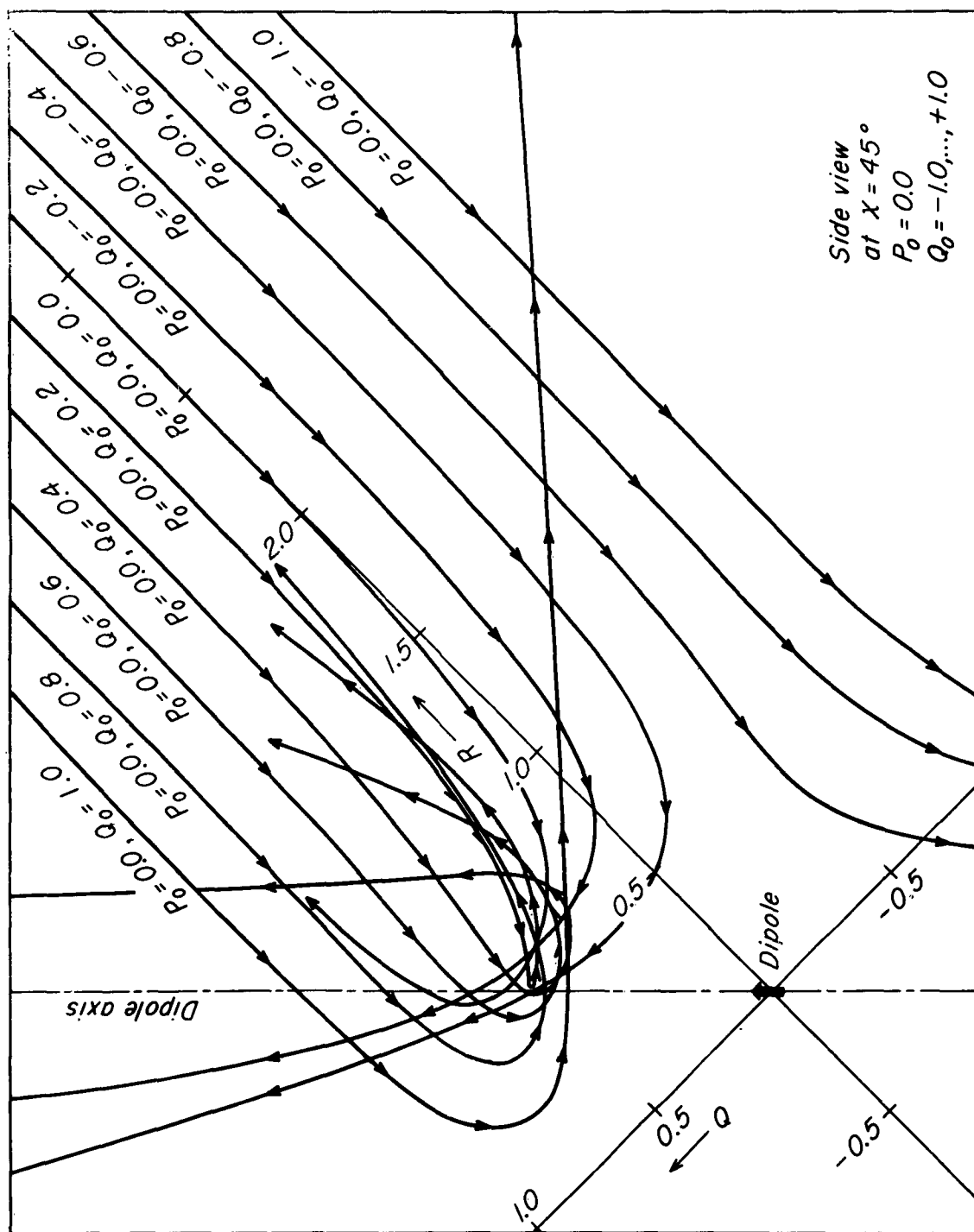


Fig. 4. 10 Trajectories of Particles Incident at an Angle of  $45^\circ$  With the Dipole Axis.

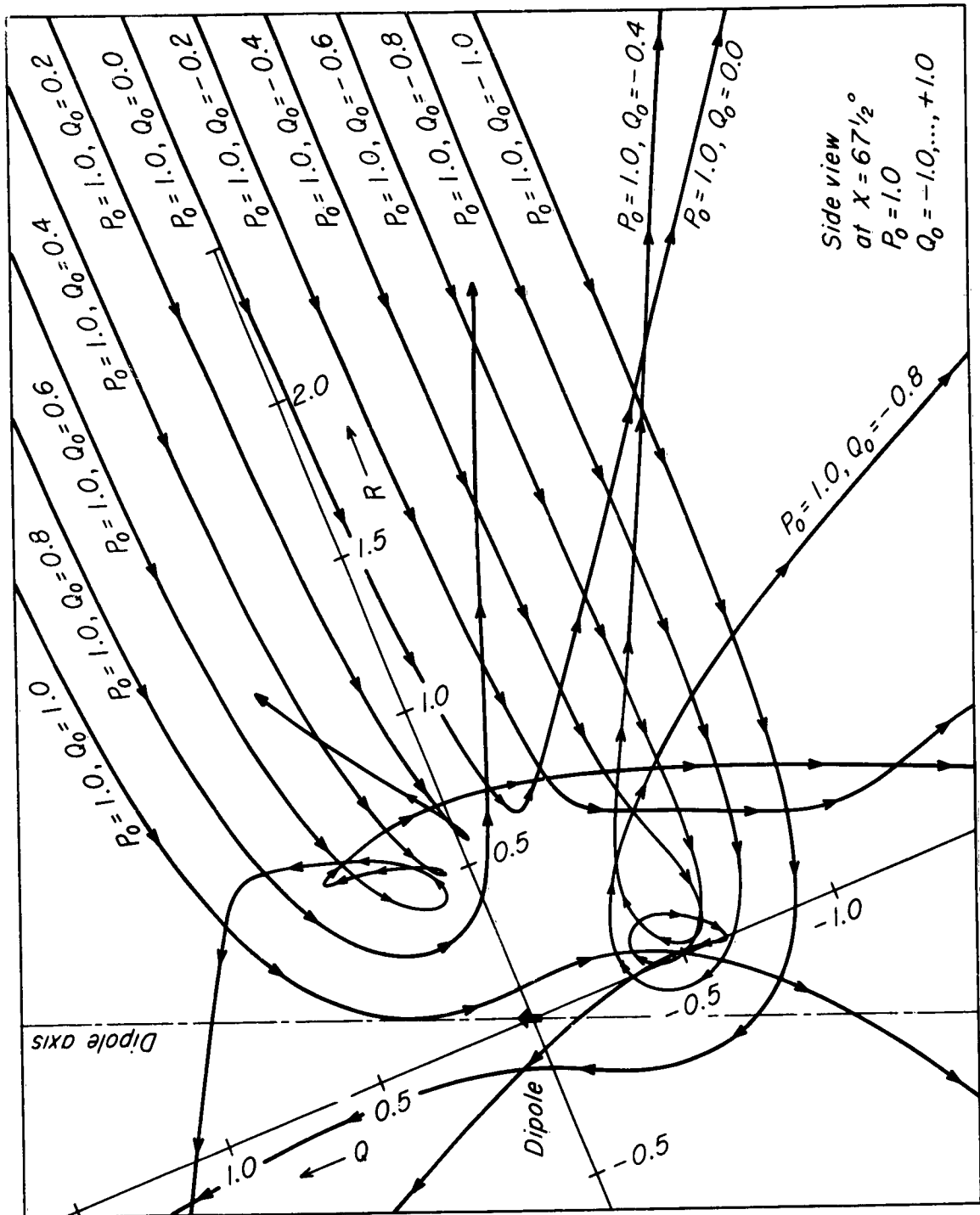


Fig. 4.11 Trajectories of Particles Incident at an Angle of  $67\frac{1}{2}^\circ$  With the Dipole Axis.

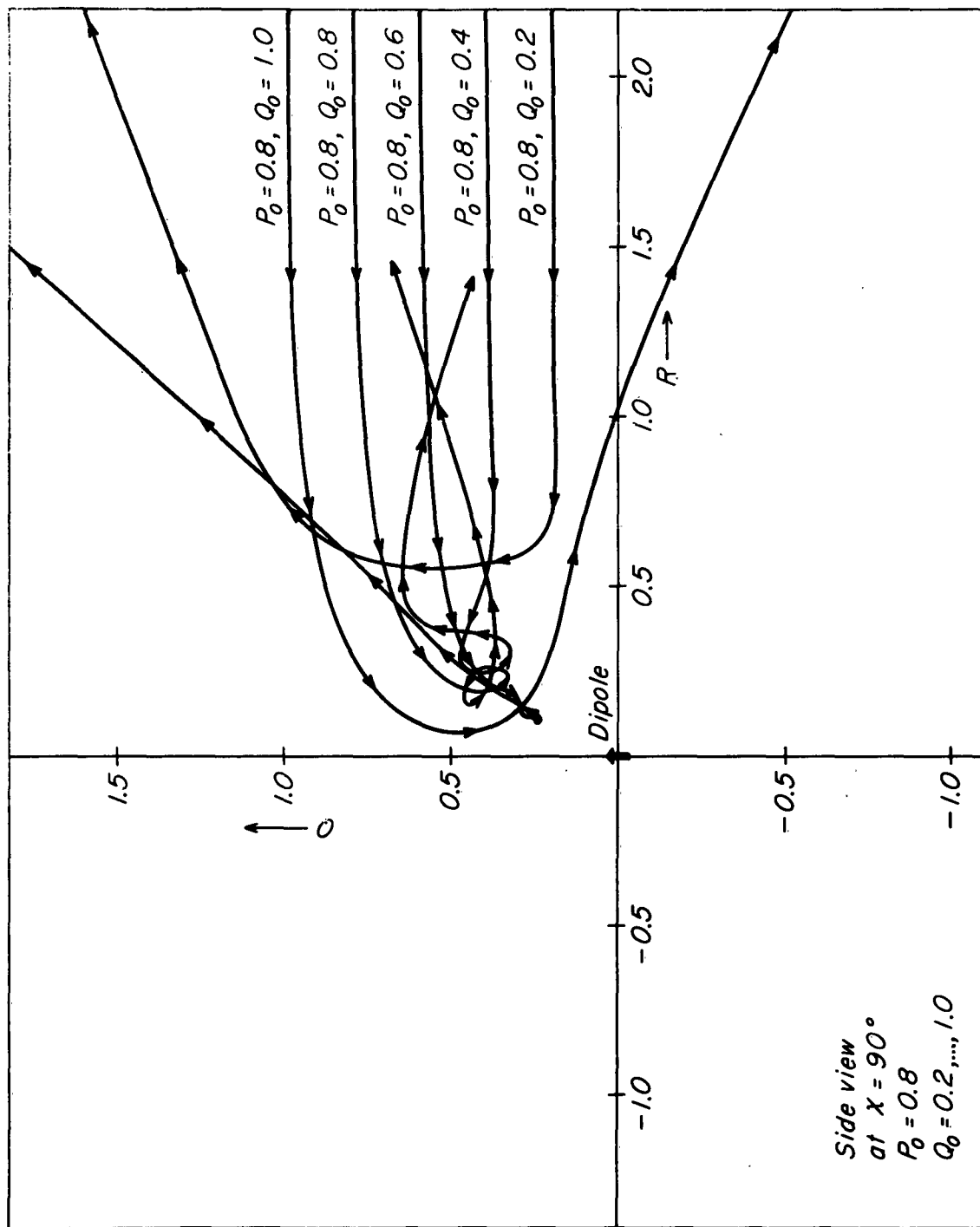


Fig. 4.12 Trajectories of Particles Incident at Right Angles to the Dipole Axis (Parallel to the Equatorial Plane).

Figure 4. 12 shows a side view of a beam incident parallel to the equatorial plane, making an angle of  $90^\circ$  with the dipole axis. The equatorial plane is represented by the straight horizontal line. The trajectories below this plane are mirror images of the ones above, and are not shown. Appearing in Fig. 4. 12 are complicated space-filling trajectories (called by Kelsall "quasi-trapped" orbits) as well as particle paths exhibiting the magnetic mirror effect.

#### Extension to General Axisymmetric Fields

If the Störmer radius [given by Eq. (4. 10)] is comparable with the dimensions of the coil producing the magnetic field, then the analysis of shielding effectiveness based on the dipole approximation given above is no longer valid. Since this situation obtains when reasonable values of dipole strength ( $\approx 10^{12}$  gauss  $\text{cm}^3$ ) and proton kinetic energy ( $\approx 1$  Bev) are considered, it is worthwhile to indicate how the shielding calculations can be extended to include all physically realizable axially symmetric fields.

An axially symmetric magnetic field can be derived from a vector potential having only an azimuthal component which is independent of the  $\phi$  - coordinate. In cylindrical coordinates  $(\alpha, \phi, z)$ ,

$$\vec{A} = \hat{e}_\phi A_\phi(\alpha, z). \quad (4. 64a)$$

The vector potential of an axially symmetric current distribution is proportional to the dipole moment  $\underline{a}$  of the distribution, so that we can write

$$\vec{A} = \hat{e}_\phi a \frac{A_\phi(\alpha, z)}{a}, \quad (4. 64b)$$

in which the quotient  $A_\phi/a$  does not involve the dipole moment explicitly.

The energy of a charge in a static magnetic field remains constant as before. With the vector potential given by Eq. (4. 64) one obtains for the

equation of motion, instead of (4. 8),

$$\frac{E}{c^2} \frac{d\vec{v}}{dt} = \frac{ea}{c} \vec{v} \times \text{curl} \left( \hat{e}_\phi \frac{A_\phi}{a} \right). \quad (4. 65)$$

This equation may be written in dimensionless form by reintroducing the Störmer unit  $C_{st}$  defined by Eq. (4. 10), but the simple interpretation of the Störmer unit as the radius of a circular orbit in the equatorial plane of the current distribution no longer holds as in the dipole case.

The axisymmetry permits a generalization of the angular momentum conservation expressed by Eq. (4. 13). The Lagrangian function for the general axially symmetric case, is in cylindrical coordinates,

$$\mathcal{L} = -m_0 c^2 \left[ 1 - \frac{1}{c^2} (\dot{\omega}^2 + \omega^2 \dot{\phi}^2 + \dot{z}^2) \right]^{1/2} + \frac{e}{c} \omega \dot{\phi} A_\phi(\omega, z) \quad (4. 66)$$

instead of (4. 12). Since the Lagrangian is independent of  $\phi$ , the momentum conjugate to  $\phi$  is conserved. An expression for this momentum is

$$p_\phi \equiv \frac{\partial \mathcal{L}}{\partial \dot{\phi}} = \frac{E}{c^2} \left[ \omega^2 \dot{\phi} + v C_{st}^2 \omega \frac{A_\phi(\omega, z)}{a} \right] = 2\gamma \frac{E}{c^2} v C_{st}. \quad (4. 67)$$

Equation (4. 14) introducing the Störmer angular momentum constant  $\gamma$  has been used unchanged, and the interpretation (4. 16) of  $\gamma$  in terms of the impact parameters  $P_0$  and  $\chi$  remains valid in the general case providing the vector potential goes to zero at infinity.

The forbidden regions may be obtained by rearranging Eq. (4. 67) in a form analogous to (4. 15):

$$Q(\gamma; \omega, z) \equiv \frac{\omega \dot{\phi}}{v} = -C_{st}^2 \frac{A_\phi(\omega, z)}{a} + 2\gamma \frac{C_{st}}{\omega}. \quad (4. 68)$$

Since  $Q$  is the ratio of the azimuthal component of velocity to the total speed, its magnitude must be less than or equal to unity. Those points  $(\omega, \phi, z)$  for which  $|Q(Y')|$  is greater than unity are forbidden to all particles having angular momentum characterized by  $Y = Y'$ . So the forbidden regions are given by

$$\left. \begin{array}{l} A(Y): \quad Q(Y; \omega, z) > +1 \\ B(Y): \quad Q(Y; \omega, z) < -1 \end{array} \right\} \quad (4.69)$$

In the dipole field, a point where the vector potential is arbitrarily strong can always be found in a sufficiently small neighborhood of the origin, so that a forbidden region  $A(Y)$  exists for all values of  $Y$ . If in the case of a finite current distribution it should happen that the vector potential has no singularities, then it is no longer clear that such a forbidden region need exist for certain values of  $C_{st}$  and  $Y$ . This requires examination for each case separately.

A further requirement for the existence of an absolutely shielded region (a region protected from all particles, independent of their values of angular momentum) for a given particle energy and dipole moment is a topological behavior of  $A(Y)$  and  $B(Y)$  for changing  $Y$  analogous to that shown in Fig. 4.5 for the dipole case. Although particles in nature have a distribution of energies, and a region totally shielded against particles of a certain energy may be only partially shielded against particles of higher energy, still it is felt that the existence of a completely protected region for particles of moderate energy is important for any magnetic shielding system.

There are presently two cases of axially symmetric fields of the type (4.64) more complicated than the dipole field about which something of the shielding properties are known. The first is the field of a single turn, considered by Levy.<sup>77</sup> The vector potential of this field has a singularity at the wire, so that a forbidden region of type  $A(Y)$  exists for all  $Y$ . If the coil radius is much longer than the Störmer radius the volume of the resulting (toroidal) shielded region becomes very small. This feature gives an indication of similar effects to be expected when more complicated current

distributions are considered. In practice the large currents required cannot flow in the infinitesimally thin single turn, but the required field can be approximated very simply by making the conductor in the form of a hollow tube which just fits inside an absolutely forbidden region for particles of some chosen energy. This can be done in cases where a radial cross-section of a forbidden region approximates a magnetic field line reasonably closely. Difficulties with this design include the necessities of providing openings for access to the passenger compartment and surrounding the crew space with cryogenic helium. Distortion of the field sufficient to cause interference with the shielding could result from straightforward attempts to solve these difficulties.

A second example, on which work has recently begun at our laboratory, is the field of a cylindrical solenoid whose dimensions are not small compared with the Störmer radius. Now the shielding provided by an ideal dipole can be determined simultaneously for all values of particle energy and magnetic moment because all such problems can be scaled in terms of the Störmer unit—we have a "zero-parameter family of solutions". With the single turn the ratio of coil radius to Störmer radius enters, and one has a one-parameter family of solutions. In the case of a cylindrical solenoid an additional parameter, the ratio of radius to length of the coil, appears, and a much more intricate two-parameter family of solutions is obtained. In the single-turn case, the ratio of coil radius to Störmer radius can be fixed by minimizing the structural weight for a given shielded volume. It is to be expected that similar optimization procedures would be able to select a particular radius to length ratio for the cylindrical solenoid.

Whereas an expression for the magnetic field of a cylindrical solenoid is known for points both on and off the axis,<sup>96</sup> an expression giving the vector potential in closed form everywhere does not seem to be available in the literature. Accordingly we outline here the derivation of an expression for  $A_\phi(\omega, z)$  appropriate to a finite solenoid in terms of elliptic integrals.

The vector potential of a single turn of radius  $R$  carrying a current  $I$  is, at a point  $(\omega, \phi, z)$  (Reference 2, p. 270)

$$A_\phi(\omega, z) = 2I \int_0^\pi \frac{R \cos \phi \, d\phi}{(z^2 + \omega^2 + R^2 - 2R\omega \cos \phi)^{1/2}}.$$

The potential of a cylindrical current-sheet of length  $L$  constructed from a large number  $N$  of circular turns each carrying a current  $I$  is obtained by integrating this expression in the axial direction

$$A_{\phi}(\omega, z) = \frac{2NI R}{L} \int_{-L/2}^{L/2} dz' \int_0^{\pi} \frac{\cos \phi \, d\phi}{[(z-z')^2 + \omega^2 + R^2 - 2R\omega \cos \phi]^{1/2}}$$

$$= -\frac{2a}{\pi R L} \int_{\xi^-}^{\xi^+} d\xi \int_0^{\pi} \frac{\cos \phi \, d\phi}{(\xi^2 + \omega^2 + R^2 - 2R\omega \cos \phi)^{1/2}} \quad (4.70)$$

In the last way of writing the formula  $a = \pi R^2 NI$  has been used to evaluate the dipole moment of the current-sheet, a change of variables  $\xi = z - z'$  has been made, and the notation

$$\left. \begin{aligned} \xi^+ &= z + \frac{1}{2} L \\ \xi^- &= z - \frac{1}{2} L \end{aligned} \right\} \quad (4.71)$$

has been introduced. The integration with respect to  $\xi$  can be done first. Then an integration by parts can be performed to remove the resulting logarithmic expression; the result is

$$A_{\phi}(\omega, z) = \frac{2a\omega}{\pi L} \int_0^{\pi} \frac{\sin \phi \, d\phi}{[\xi + (\xi^2 + \omega^2 + R^2 - 2R\omega \cos \phi)^{1/2}](\xi^2 + \omega^2 + R^2 - 2R\omega \cos \phi)^{1/2}} \Big|_{\xi^-}^{\xi^+}.$$

Multiplying numerator and denominator of the integral by the expression  $(\xi^2 + \omega^2 + R^2 - 2R\omega \cos \phi)^{1/2} - \xi$ , simplifying, and noting that the term not involving  $\xi$  drops out when evaluated at the limits  $\xi^+$  and  $\xi^-$ , we obtain for the vector potential

$$A_{\phi}(\omega, z) = -\frac{2a\omega}{\pi L} \xi \, I(\xi) \Big|_{\xi^-}^{\xi^+}, \quad (4.72)$$

where

$$I(\xi) \equiv \int_0^\pi \frac{\sin^2 \phi \, d\phi}{(\omega^2 + R^2 - 2R\omega \cos \phi)(\xi^2 + \omega^2 + R^2 - 2R\omega \cos \phi)^{1/2}} \quad (4.73)$$

By means of the substitution  $t = \cos \phi$  it is possible to break up the integral  $I(\xi)$  into three simpler integrals

$$\left. \begin{aligned} I(\xi) &= \frac{\omega^2 + R^2}{4R\omega^2} I_1(\xi) + \frac{1}{2R\omega} I_2(\xi) - \left( \frac{\omega^2 - R^2}{2R\omega} \right)^2 I_3(\xi) \\ I_1(\xi) &= \int_{-1}^{+1} \frac{dt}{\sqrt{(A-Bt)(1-t)(1+t)}} \\ I_2(\xi) &= \int_{-1}^{+1} \frac{t \, dt}{\sqrt{(A-Bt)(1-t)(1+t)}} \\ I_3(\xi) &= \int_{-1}^{+1} \frac{dt}{(D-Bt)\sqrt{(A-Bt)(1-t)(1+t)}} \end{aligned} \right\} \quad (4.74)$$

where

$$\left. \begin{aligned} A &\equiv \xi^2 + \omega^2 + R^2 \\ B &\equiv 2R\omega \\ D &\equiv \omega^2 + R^2 \end{aligned} \right\}.$$

The integrals in (4.74) can be expressed in terms of complete elliptic integrals of the first, second, and third kinds, respectively. Using Formulas

234.00, 234.06, 315.02, 234.18, and 339.01 of Reference 95, we get

$$I_1(\xi) = \frac{k}{\sqrt{R\omega}} K(k) \quad (4.75)$$

$$I_2(\xi) = \frac{2}{k\sqrt{R\omega}} \left[ \left(1 - \frac{1}{2}k^2\right) K(k) - E(k) \right] \quad (4.76)$$

$$\begin{aligned} I_3(\xi) &= \frac{k}{(\omega - R)\sqrt{R\omega}} \int_0^{K(k)} \frac{dn^2 u \, du}{1 + \beta^2 k^2 \operatorname{sn}^2 u} \\ &= -\frac{k K(k)}{\xi^2 \sqrt{R\omega}} + \frac{4R\omega k}{\xi^2 (\omega - R)\sqrt{R\omega}} \frac{k'^2}{k^2} \Pi(-\beta^2 k^2, k) \end{aligned} \quad (4.77)$$

where  $K(k)$ ,  $E(k)$  and  $\Pi(-\beta^2 k^2, k)$  are complete elliptic integrals with modulus  $k$  given by

$$k^2 = \frac{4R\omega}{\xi^2 + (\omega + R)^2}, \quad (4.78)$$

$k' = (1 - k^2)^{1/2}$  is the complementary modulus, and

$$\beta = \left| \frac{\xi}{\omega - R} \right|. \quad (4.79)$$

Substituting into Eqs. (4.74) and (4.72) we obtain the expression for the vector potential of a solenoid of radius  $\underline{R}$  and length  $\underline{L}$  in the form

$$A_\phi(\omega, z) = -\frac{I_a}{\pi L} \left( \frac{\omega}{R} \right)^{1/2} \frac{k'^2}{k\xi} \left\{ \frac{2K(k)}{k^2} - \frac{\xi^2 E(k)}{2k'^2 R\omega} - \frac{(\omega + R)^2}{2R\omega} \Pi(-\beta^2 k^2, k) \right\} \Bigg|_{\xi^-}^{\xi^+}. \quad (4.80)$$

Equation (4.80) can be put in a form more convenient for calculation by using Formula 410.01 of Reference 95 to express the complete elliptic integral of the third kind in terms of complete and incomplete elliptic integrals of the first and second kinds:

$$A_{\Phi}(\omega, z) = -\frac{2a}{\pi R \omega} \left(\frac{\omega}{R}\right)^{1/2} \xi \left\{ \left[ 1 + \frac{(\omega - R)^2 k^2}{4 R \omega} K(k) - E(k) \right. \right. \\ \left. \left. - \frac{k(\omega + R)}{2\sqrt{R\omega}} \left| \frac{\omega - R}{\xi} \right| \frac{\pi}{2} \Lambda_0(\psi, k) \right] \right\} \Big|_{\xi^-}^{\xi^+} \quad (4.81)$$

Here

$$\sin \phi = \frac{k|\xi|}{2k'\sqrt{R\omega}} \quad (4.82)$$

and

$$\frac{\pi}{2} \Lambda_0(\psi, k) = E(k)F(\psi, k') + K(k)E(\psi, k') - K(k)F(\psi, k') \quad (4.83)$$

(called "Heuman's Lambda Function") is a tabulated function (Reference 95, pp. 344-349).

In the equatorial plane  $z = 0$  and Eq. (4.81) reduces to

$$A_{\Phi}(\omega, 0) = -\frac{2a}{\pi R \omega} \left(\frac{\omega}{R}\right)^{1/2} \frac{1}{k} \left\{ \left[ 1 + \frac{(\omega - R)^2 k^2}{4 R \omega} K(k) - E(k) \right. \right. \\ \left. \left. - \frac{k|\omega^2 - R^2|}{L\sqrt{R\omega}} \frac{\pi}{2} \Lambda_0(\psi, k) \right] \right\}, \quad (4.84)$$

where now

$$k^2 = \frac{16 R \omega}{L^2 + 4(\omega + R)^2}, \quad \sin \phi = \frac{k L}{4 k' \sqrt{R \omega}}. \quad (4.85)$$

For  $L = 0$  Eq. (4.84) reduces to the expression given by Smythe (Reference 2, p. 271) for the potential of a single turn with  $z = 0$ . Also, when  $\omega, z \gg R, L$  Eq. (4.81) reduces to the expression (4.3) for the vector potential of a dipole field.

A plot of the vector potential (4.84) for  $z = 0$  as a function of radial distance is given in Fig. 4.13. Since neither of the two values of  $k^2$  in the equatorial plane given by Eq. (4.85a) can equal unity (except for  $L = 0$ ), Eq. (4.84) for the vector potential contains no singularities. Certain shielded regions  $A(\gamma)$  will shrink to zero for sufficiently high values of particle energy. Detailed examination of the shielded regions is necessary for a range of values of  $R/C_{st}$  and  $L/R$ .

The expression (4.80) for the vector potential everywhere does contain a singularity at  $z = L/2, \omega = R$ , i.e., around the edges of the solenoid. Thus the edges of the solenoid must fall within a forbidden region.

The inequalities (4.69) for a cylindrical solenoid are much more complicated than the corresponding ones for the dipole or the single turn, so that determination of shielded regions for a solenoid by methods analogous to those used in the other cases is difficult. Fig. 4.14 shows the shielded regions for the case  $R/L = 1.00$ ,  $R/C_{st} = 0.40$ , and  $\gamma = -1.03$ . The inner forbidden region  $A(\gamma)$  is a torus centered roughly on the equatorial plane and the circumference of the solenoid. The singularity at the rim of the solenoid falls within the outer forbidden region  $B(\gamma)$ , which sends down a protuberance to meet it.

Further information concerning the forbidden regions of solenoids must await the programming of the problem for a large-scale digital computer.

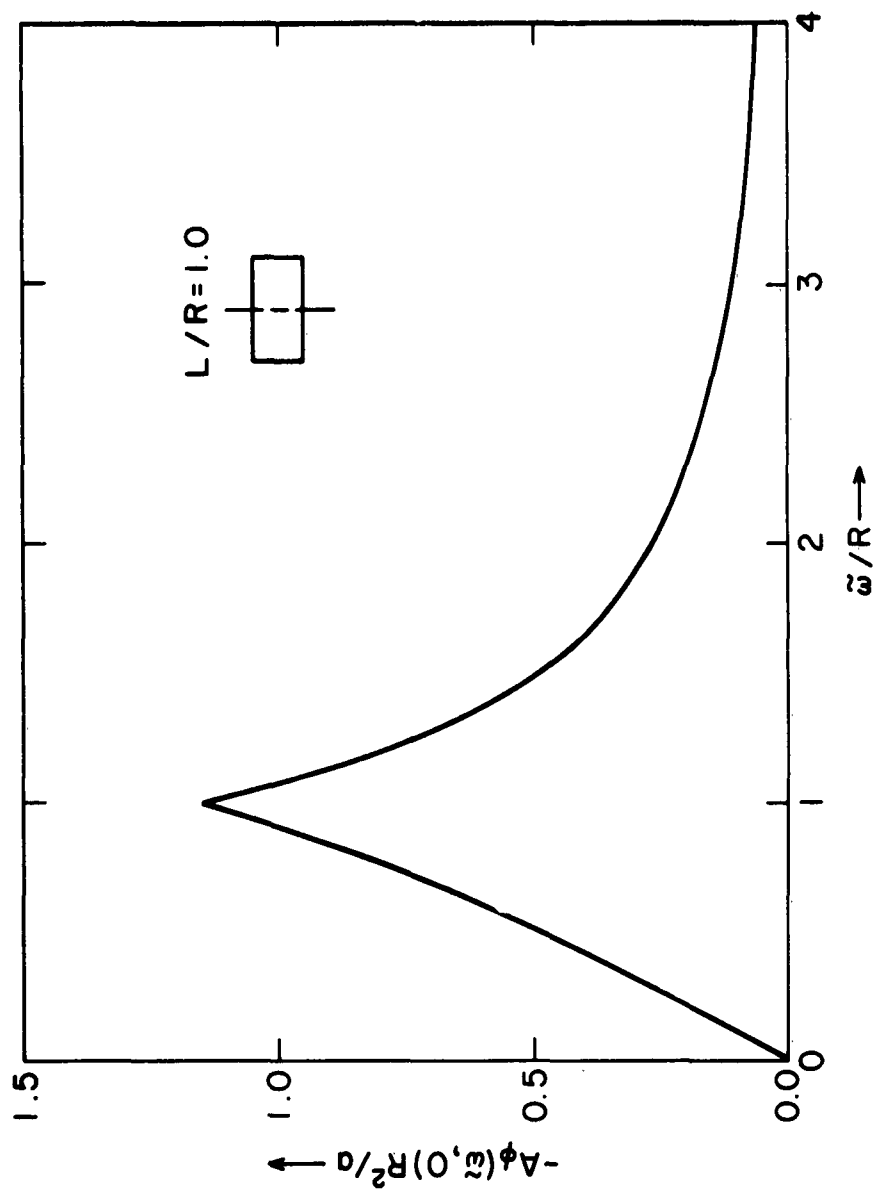


Fig. 4.13 Vector Potential of a Cylindrical Solenoid in the Equatorial Plane as a Function of Radial Distance.

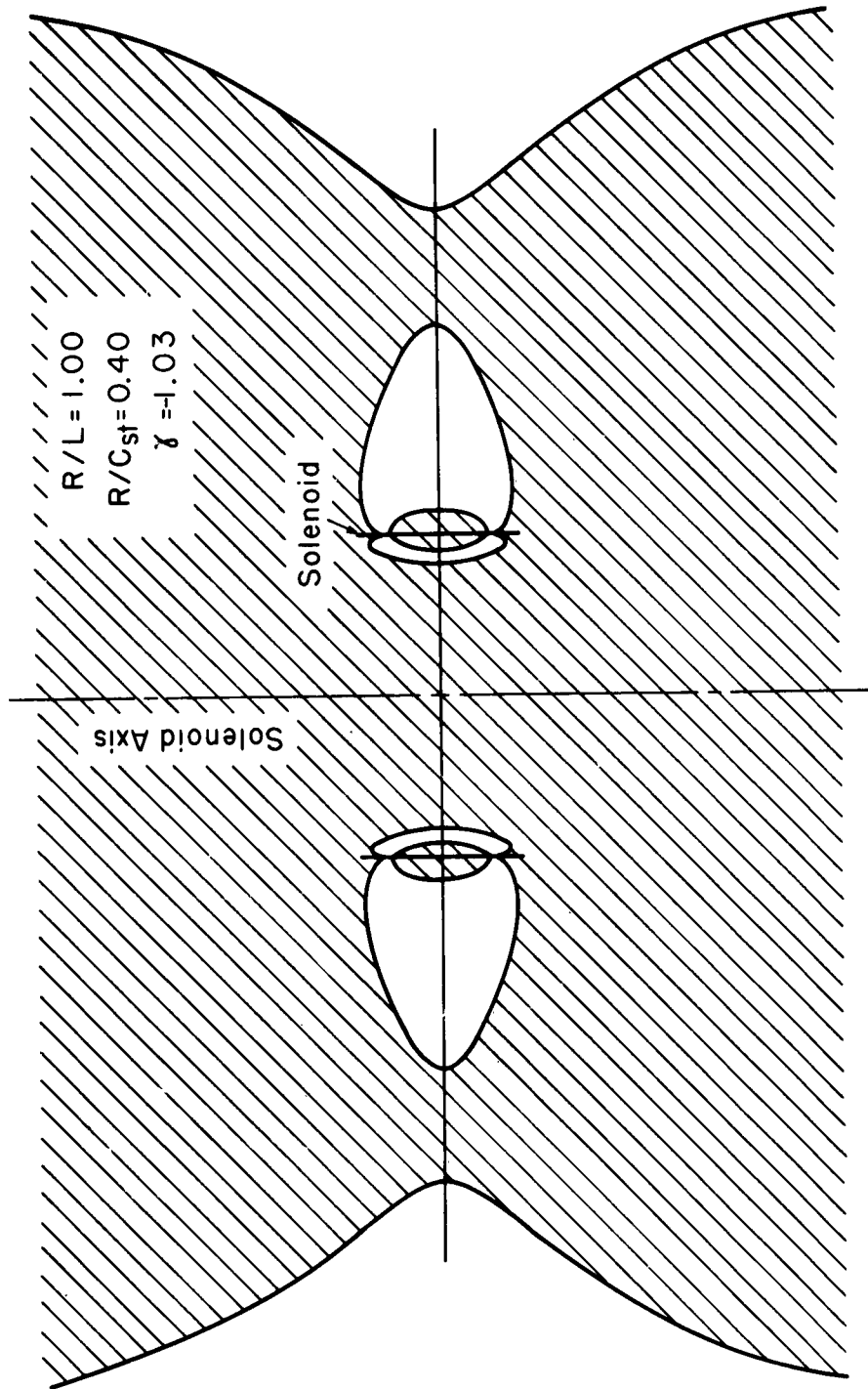


Fig. 4. 14 Shielded Regions for a Cylindrical Solenoid Whose Dimensions are Comparable With the Störmer Radius, for  $\gamma = 1.03$ .

## 5. MAGNETIC SHIELDING—MAGNET DESIGN

### Characteristics of Superconducting Materials

The recent discovery of materials which remain superconducting in strong magnetic fields opens up the possibility of shielding electromagnets aboard space vehicles. The reason for the importance of superconductors in this context is that power is dissipated if the windings are made of an ordinary conductor such as silver or copper. As the current flows through the conductor the electrical energy is converted into (Joule) heat due to the resistance of the metallic path. If the magnet is to operate at high field strengths, or if the volume of the intense field region is to be large, both of which conditions would obtain in magnets used for spacecraft shielding, then the energy losses due to Joule heating represent major practical problems. Also the weight of the large volume of ordinary conducting material necessary to sustain the required fields would make the use of non-superconducting magnets unfeasible for space vehicle applications. In summary the reasons which make superconducting magnets mandatory for spacecraft shielding are

- (1) The power requirements are kept at a minimum; no electrical power is required to sustain the magnetic field once the current has been started.
- (2) The weight requirements are minimized since the cross section of wire necessary to transmit a given current is much smaller than that of an ordinary conductor.

The most promising of the new superconducting materials are the niobium-zirconium alloys and the niobium-tin intermetallic compound  $\text{Nb}_3\text{Sn}$ . These materials have been discussed in the open literature by Kunzler<sup>86</sup> and members of his group at Bell Laboratories.<sup>85</sup> Most of the information used herein concerning these materials has been taken from the review article by Kunzler.<sup>86</sup> While it is to be expected that progress will continue in the development of superconducting materials, the design procedures for solenoids will remain essentially the same. The data regarding the characteristics of the superconductors will have the same form although the numerical values will probably change. Accordingly we give estimates based on niobium-zirconium or niobium-tin using data presented by Kunzler's group, but the calculations

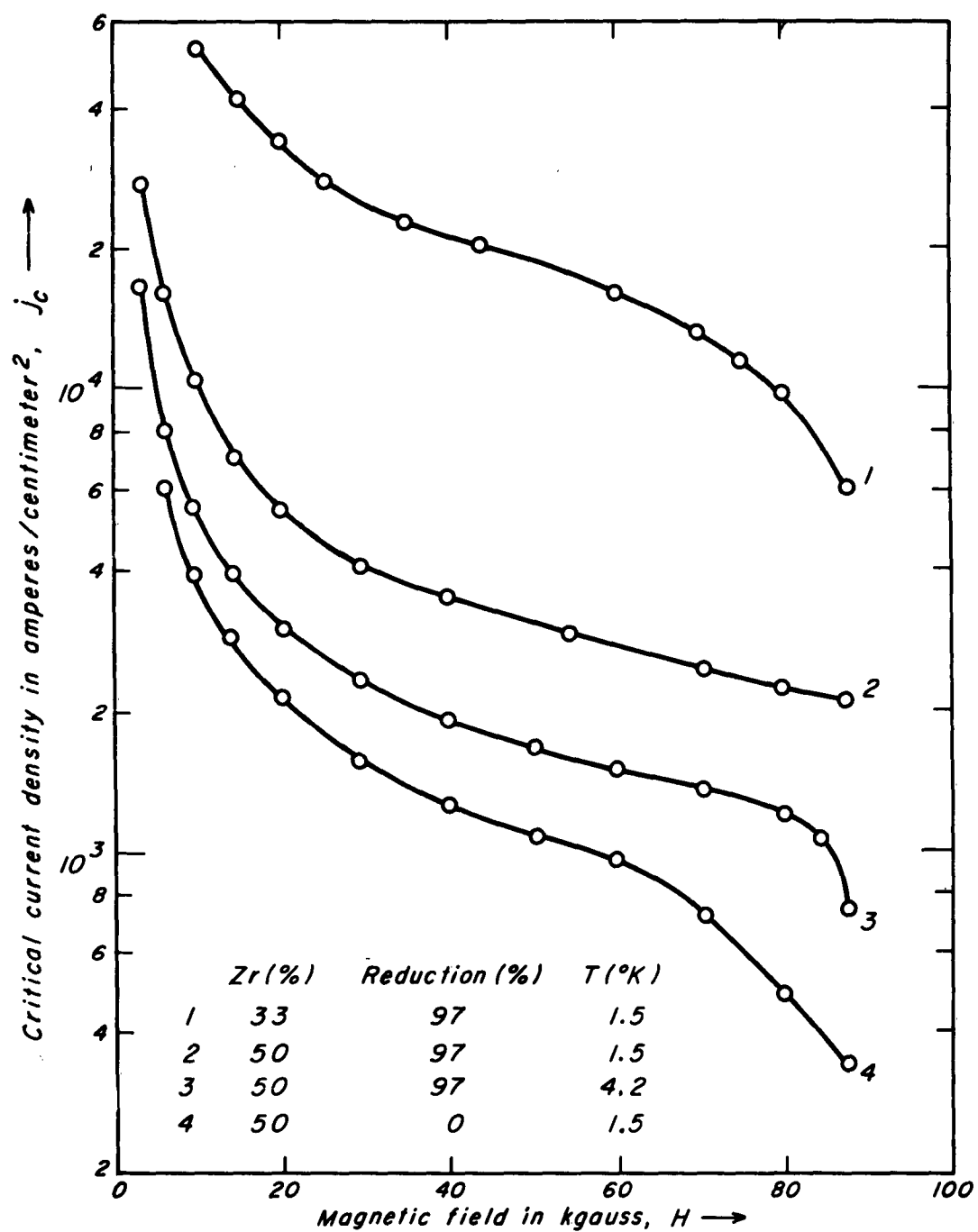


Fig. 5.1 Critical Current Density vs. Applied Magnetic Field for Some Niobium-Zirconium Alloys.

will be readily adaptable to solenoids constructed of other materials as they become available.

From the standpoint of magnet design, the most useful information about a superconductor is a plot of the critical current flowing through a given wire sample as a function of the applied magnetic field. The critical current at a given magnetic field strength is that current above which the wire sample loses its superconductivity, and represents the maximum current that can be passed through the sample at a given magnetic field. Often the current density or current per unit cross sectional area corresponding to a wire sample is given for comparison purposes between different materials.

The critical current density for various niobium-zirconium alloys is given as a function of applied magnetic field in Fig. 5.1. The physical quantities which make the curves different from one another are the percentage of zirconium in the alloy, the degree of reduction by cold-rolling, and the temperature. The critical magnetic field (field above which the material loses its superconductivity) of the niobium-zirconium alloys increases with increasing zirconium concentration, reaches a maximum somewhere between 65 and 75 percent zirconium, and drops rapidly thereafter. The critical current increases with decreasing zirconium content, reaches a maximum between 25 and 35 percent zirconium, and falls off rapidly at lower concentrations.

Although the critical magnetic field and current densities of niobium-zirconium alloys are smaller than those of niobium-tin, the niobium-zirconium alloys are ductile, easier to fabricate into wire, have a much higher tensile strength, and in general are much easier to work with than the niobium-tin compound. It is expected that most laboratory superconducting magnets for use on the ground where weight is not a problem will have niobium-zirconium windings.

The brittle intermetallic niobium-tin compound  $\text{Nb}_3\text{Sn}$  with its high transition temperature near  $18^\circ\text{K}$  was discovered by Matthias *et. al.* in 1954.<sup>85</sup> The high critical temperature suggested immediately that the critical field might be high for this compound. This conjecture was strengthened by the susceptibility observations of Bozorth *et. al.*; they concluded that the critical field for  $\text{Nb}_3\text{Sn}$  might be as high as 70 kgauss at  $4.2^\circ\text{K}$ . Investigations of the current carrying capacity of  $\text{Nb}_3\text{Sn}$  in high magnetic fields have been made

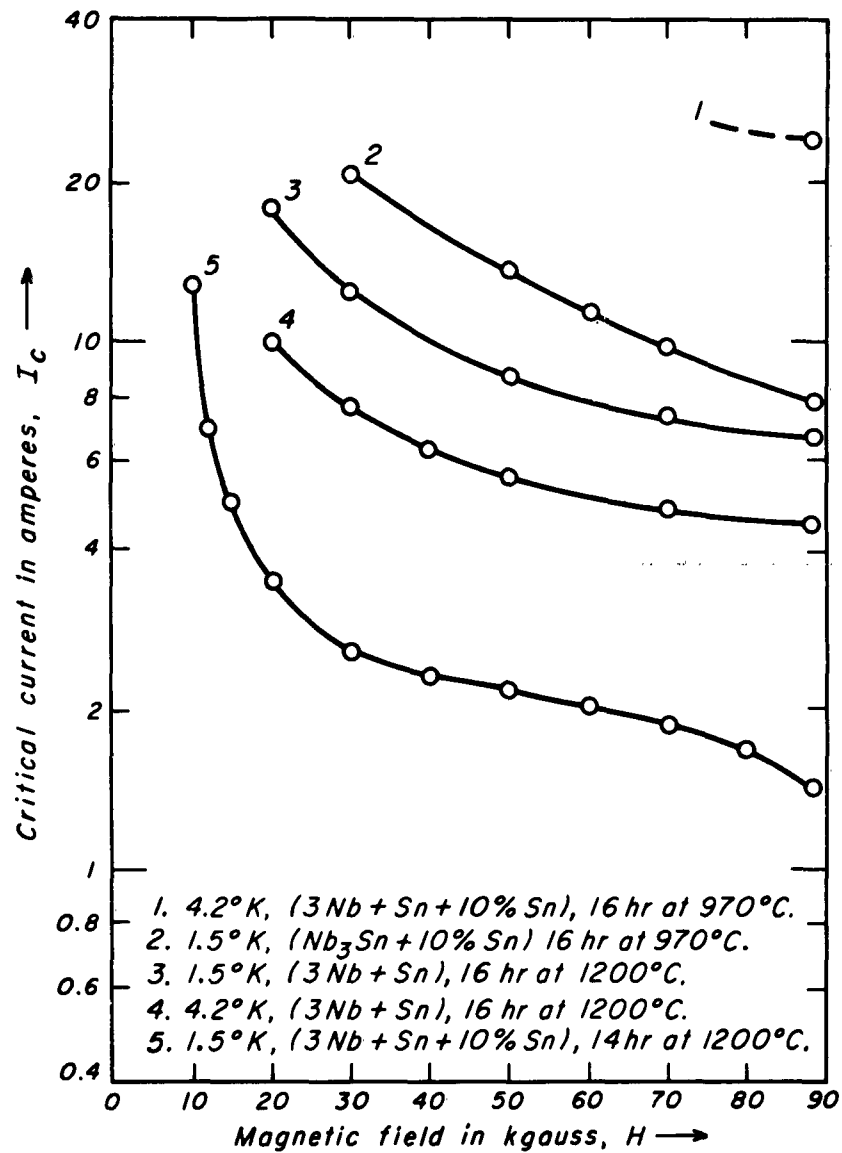


Fig. 5.2 Critical Current vs. Applied Magnetic Field for Nb<sub>3</sub>Sn "Wires".

using samples of bulk  $\text{Nb}_3\text{Sn}$  and  $\text{Nb}_3\text{Sn}$  "wire" samples. The bulk material remained superconducting in a field of 88 kgauss with a current density of about  $3000 \text{ amp/cm}^2$ . The "wire" samples remained superconducting at 88 kgauss but could sustain a current density about 50 times as great as the bulk samples. Current density figures for  $\text{Nb}_3\text{Sn}$  are more reliable than for other superconductors because the current flows in "filaments" throughout the material rather than being concentrated near the surface; however, we have given values of current in Fig. 5.2 for the sake of convenience.

The so-called "wire" samples of  $\text{Nb}_3\text{Sn}$  may be prepared by taking a rod of niobium about 1/4 inch in diameter and drilling a 1/8 inch hole through it. The hole is filled with a mixture of niobium and tin powders in stoichiometric proportion and the ends of the tube are plugged. The niobium tube packed with the powders is reduced to a fine tube or "wire" form by mechanical swaging. In the samples used at Bell Laboratories the outer diameter of the tubing was 0.38 mm and the core diameter was 0.15 mm. In this form the niobium and tin powders are unreacted and the outer tube can be bent and otherwise worked into the form of a coil. Reaction of the elements to form the compound  $\text{Nb}_3\text{Sn}$  is done after forming is complete.

The critical current for  $\text{Nb}_3\text{Sn}$  wires clad with niobium is given as a function of applied magnetic field in Fig. 5.2. The physical parameters which characterize the curves are: the composition of the cores, the temperature at which the reaction took place, and the temperature at which the measurements were made. When ten percent more tin by weight than is required to form  $\text{Nb}_3\text{Sn}$  (assuming no reaction with the niobium tube) was added, the critical current was considerably higher than for other cases. However, it was possible to take only one experimental point, the one at 88 kgauss. If the curve corresponding to this composition has a shape similar to the other curves in Fig. 5.2, then we may extrapolate critical currents as high as 50 amperes at fields of about 50 kgauss for "wires" of the dimensions stated. The experimental point under discussion was taken at a temperature of  $4.2^\circ\text{K}$ , whereas some of the other curves were taken at the somewhat lower temperature of  $1.5^\circ\text{K}$  with improvement in current-carrying capability over than at  $4.2^\circ\text{K}$ .

For further discussion of the properties and the materials of superconductivity see, in addition to the references already given, Reference 97. For alternative treatments of solenoid design, see References 88-91.

### Solenoid Parameters

In this section the physical parameters of a superconducting solenoid to be used for space vehicle shielding are discussed. Those design variables which we shall consider are the magnetic moment of the coil, the radius and length of the coil, the cross sectional area of the superconducting wire used in the windings and the electric current passing through a single turn of the conductors. The magnetic moment of the coil is to be determined from the size of the shielded region and the energy of particles against which shielding is desired via the Störmer distance as determined from studies of particle trajectories. The radius and length of the coil are governed by the shape of the desired shielded region; for calculations based on a dipole field the length of the solenoid should be chosen small compared with the Störmer radius. The current chosen should be less than the critical current for a wire of the assumed cross section operating at the chosen magnetic field.

For shielding against protons of energy 500 Mev, it is necessary to have a magnetic moment of  $6 \times 10^{11}$  gauss cm<sup>3</sup>; this gives a Störmer radius of about 3.8 meters (see Fig. 4.3). It would be desirable to have a magnetic moment of  $6 \times 10^{12}$  gauss cm<sup>3</sup>; for a proton of the above energy the Störmer radius is about 13 meters. For an electron the Störmer radius corresponding to a given magnetic moment is larger than for a proton of the same energy. Thus a 500 Mev electron will have a Störmer radius of 6 meters in the field of a dipole having a moment of  $6 \times 10^{11}$  gauss cm<sup>3</sup>. In nature the energies of electrons are much lower than 500 Mev. For an electron of 1 Mev kinetic energy, the Störmer radius for a dipole moment of  $6 \times 10^{11}$  gauss cm<sup>3</sup> is 110 meters, and for  $6 \times 10^{12}$  gauss cm<sup>3</sup> it is about 350 meters. For electrons of moderate energy the dipole model is capable of providing a good analysis of the shielded volume. For high energy protons the dipole approximation breaks down; for instance, for a proton having 1 Bev kinetic energy the magnetic moment necessary to give a Störmer radius of 10 meters is  $5.66 \times 10^{12}$  gauss cm<sup>3</sup>, and magnets of reasonable weight giving such a dipole moment would have to have dimensions comparable with the 10 meters figure. Studies of particle trajectories in a dipole field have shown that the region shielded against particles of a given energy is a toroid with major radius

equal to about 41 percent of the Störmer unit corresponding to that energy. However, a toroidal region whose major radius is 50 percent of a Störmer unit will be shielded against 97 percent of the particles of given energy, and a toroid whose major radius is a full Störmer unit will be shielded against about 70 percent of the particles of given energy.

For calculations of the weight of the superconducting material and the structure needed to sustain the solenoid against magnetic forces, it is necessary to have knowledge of the densities of the superconducting material and the material used in the supporting structure. One must also know the tensile yield strength of the structural material. From the standpoint of weight, the most desirable superconductors are those with the smallest ratio of mass density to critical current density for the magnetic fields being used. In our examples we have chosen  $\text{Nb}_3\text{Sn}$ , which has a density of  $8.0 \text{ grams/cm}^3$  and a critical current density of the order of  $10^5 \text{ amps/cm}^2$  for magnetic fields of  $10^5$  gauss. The most desirable structural materials are those with the smallest ratio of density to yield strength. It will be shown later that the structure takes up about 90 percent of the solenoid mass, so that the development of better structural materials is more important for magnetic shielding than the discovery of better superconductors. The material used in our examples is the titanium alloy Ti-6Al-4V ELI, which has a density of  $4.46 \text{ grams/cm}^3$  and a yield strength of 263,000 psi.

The mass of the solenoid may be divided into three components: the mass of the conductors, the mass of the supporting structure, and the mass of the cryogenic system. Although most of the mass is taken up by the structure, we will also be concerned with the mass of the coil windings. It will be assumed that the thickness of the windings and the spacing of the turns are small compared with the other dimensions of the solenoid, so that in effect we may regard the solenoid as a cylindrical current sheet. This configuration is desirable in that it gives a large dipole moment for a reasonable volume, although it is not to be regarded necessarily as a final design. At first we will assume that the structure is intimately associated with the windings, so that the geometry of the structure is essentially that of the coil itself. This structure balances the forces tending to expand

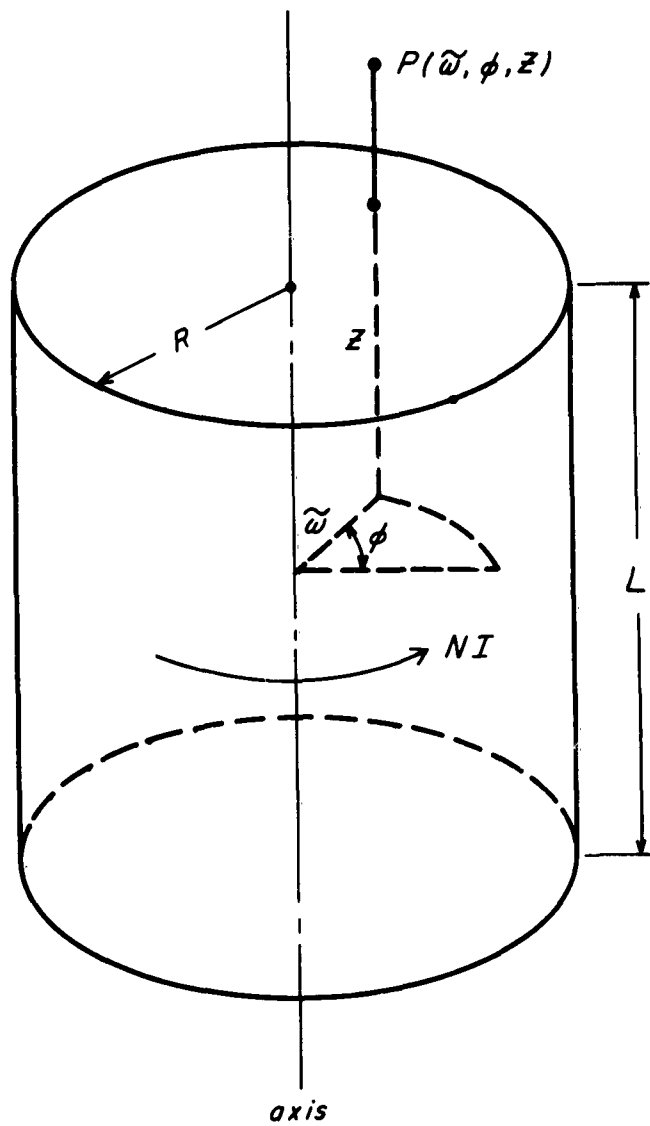


Fig. 5.3 Definition of Coordinates and Geometrical Parameters for a Cylindrical Solenoid.

the windings azimuthally and to compress them axially. Later we will consider a structure made of a series of thin disks having the same radius as the solenoid and separated by compressive members. The disks balance the forces tending to expand the windings both azimuthally and radially and the spacing members balance the axial compressive forces.

#### Mass of the Conductors

We consider the magnetic field due to the cylindrical current sheet of radius  $R$  and length  $L$  shown in Fig. 5.3. The components of the field in the radial and axial directions at a point  $(\omega, \phi, z)$  in cylindrical coordinates are given (in Gaussian units) by<sup>96</sup>

$$H_{\omega}(\omega, z) = \frac{4\pi NI}{L} \left(\frac{R}{\omega}\right)^{1/2} \frac{1}{k} \left[ \left(1 - \frac{1}{2}k^2\right) K(k) - E(k) \right] \Big|_{\xi^-}^{\xi^+}, \quad (5.1)$$

$$H_z(\omega, z) = \frac{NI}{L} \left[ \frac{\xi k}{\sqrt{R\omega}} K(k) + 2 \frac{\xi(R-\omega)}{[\xi(R-\omega)]} \frac{\pi}{2} \lambda_0(\vartheta, k) \right] \Big|_{\xi^-}^{\xi^+}. \quad (5.2)$$

Here  $\xi^{\pm} = z \pm \frac{1}{2} L$ ,

$$k^2 = \frac{4R\omega}{\xi^2 + (\omega + R)^2}, \quad \vartheta = \arctan \left| \frac{\xi}{R - \omega} \right|, \quad (5.3)$$

$N$  is the number of turns each of which carries a current  $I$ ,  $E(k)$  and  $K(k)$  are complete elliptic integrals, and  $\lambda_0(\vartheta, k)$  is Heuman's function defined as in Eq. (4.83).

Putting  $\omega = 0 = z$ , we obtain the axial field at the center of the coil:

$$H_z(0, 0) = \frac{4\pi NI}{\sqrt{L^2 + 4R^2}}. \quad (5.4)$$

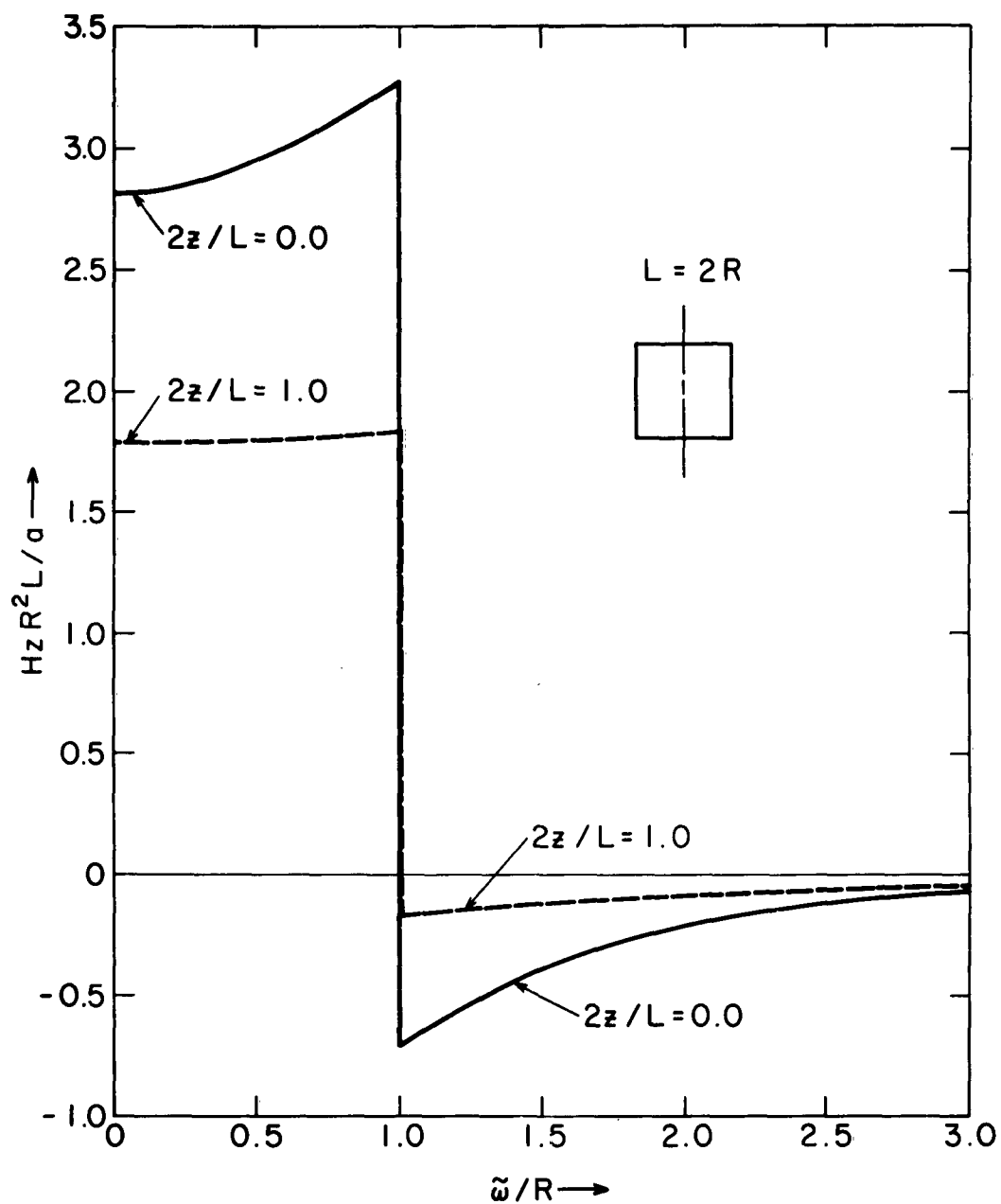


Fig. 5.4 Variation of Magnetic Field With Radial Distance for a Cylindrical Solenoid.

Expressed in terms of the dipole moment  $a = \pi R^2 NI$  of the solenoid, this field is

$$H_z(0,0) = \frac{4a}{R^2 \sqrt{L^2 + 4R^2}}. \quad (5.5)$$

This is the expression for the field we shall use in determining the critical current flowing through a single turn. Actually one should use the field at the wire, given by the more complicated formulas (5.1) (5.2). For a coil whose radius is half its length, Eq. (5.2) shows that the maximum axial field at the wire is about 1.16 times the value at the center given by (5.4) (Cf. Reference 96). To offset this factor one should use somewhat conservative values for the critical current density. Also the results of Kunzler *et al.* indicate that the maximum current-carrying capacity of  $Nb_3Sn$  increases some 50 percent from 4.2°K to 1.5°K.<sup>85</sup>

If we assume each turn carries a current  $I_c$  equal to the critical current corresponding to the field (5.5), then an estimate of the mass of superconducting wire may be made as follows:

$$m_w = 2\pi R N \sigma_w \rho_w = 2a \sigma_w \rho_w / R I_c = 2a \rho_w / R j_c. \quad (5.6)$$

Here  $\sigma_w$  and  $\rho_w$  are the cross sectional area and density of the superconducting wire. The quantity  $j_c = I_c / \sigma_w$  represents the critical current density corresponding to the magnetic field at the center. It may be seen from Eq. (5.6) that the "figure of merit" for a superconducting wire material is the ratio  $\rho_w / j_c$ .

As an example, we consider a coil having a magnetic moment  $a = 5.66 \times 10^{12}$  gauss cm<sup>3</sup> (giving a Störmer radius of 10 meters for 1 BeV protons), a radius of 400 cm, and a length 800 cm carrying a critical current  $I_c = 20$  amperes through  $Nb_3Sn$  wire ( $\rho_w = 8.0$  gram/cm<sup>3</sup>) of cross section  $\sigma_w = 1.77 \times 10^{-4}$  cm<sup>2</sup> (corresponding to a wire diameter of 0.15 mm as

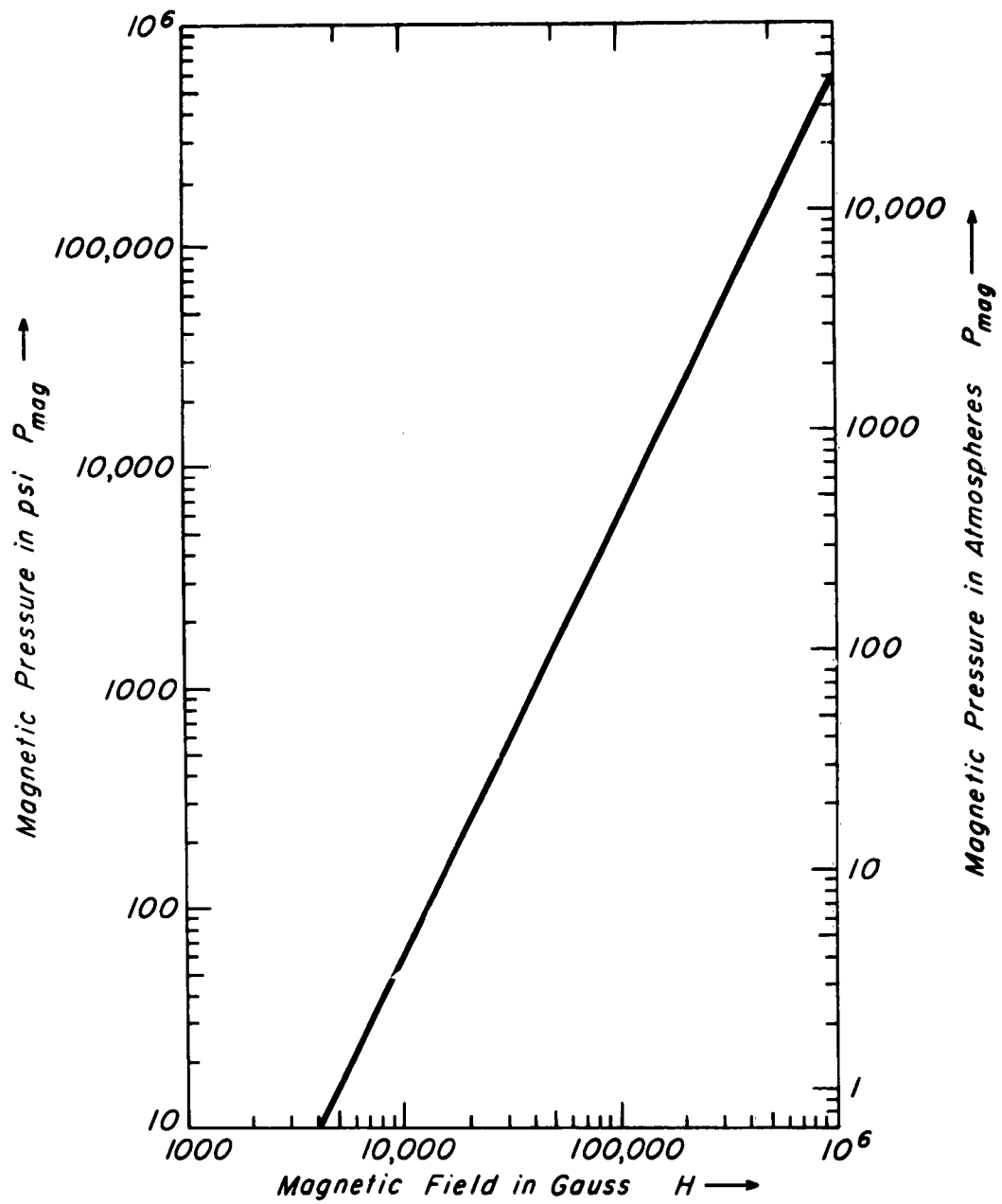


Fig. 5.5 Magnetic Pressure as a Function of Magnetic Field Strength.

reported by Kunzler). The magnetic field calculated from Eq. (5.5) is  $1.23 \times 10^5$  gauss. The assumed value of  $I_c = 20$  amperes at this field can be taken as an extrapolation of curve I in Fig. 5.2. The corresponding critical current density is  $j_c = 1.13 \times 10^4$  abamps/cm<sup>2</sup>. We get for the mass  $m_w$  of the wire according to Eq. (5.6) a value 20,000 kg or about 44,000 lb.

In the estimate above the wire was assumed to be uniformly wound both radially and axially, so that each turn carried the same current. Now the magnetic field varies considerably in the vicinity of the coil windings; it is a maximum just inside the solenoid and decreases with distance from the equatorial plane. Just outside the coil it has a value (large for short solenoids) opposite in direction to that just inside (see Fig. 5.4). Actually the discontinuity in the field shown in the graph for a current sheet does not exist; instead the field drops continuously but rapidly from its maximum just inside the windings to its negative maximum just outside. Where the field is smaller one may use a higher value of critical current and decrease the number of turns in that region. The overall reduction in the amount of wire required can be considerable—of the order of 30 to 50 percent, depending on the dimensions and dipole moment of the coil.<sup>89</sup> For example, if we assume that the critical current varies exponentially with the magnetic field (This would appear as a linear plot in Fig. 5.2) and consider the variation of the field in the equatorial plane of the sample solenoid discussed above, we obtain a reduced wire mass of about 30,000 lb. A further reduction in the wire mass could also be obtained if the variation of the field in the axial direction were taken into account.

If one could operate at a temperature of 1.5°K instead of 4.2°K an additional wire saving of about 30 percent should be possible.<sup>86</sup> The use of a variable wire composition may also reduce the mass somewhat by permitting a portion of the tensile stress to be carried by the superconducting wire.<sup>97</sup>

#### Mass of the Structure

The current-carrying elements of a high-field electromagnet are subject to forces arising from  $\vec{j} \times \vec{H}$  interaction with their own field. A contained magnetic field  $\vec{H}$  can be thought to exert a pressure  $H^2/8\pi$  normal to its lines of force and an equal tension along its lines of force. A plot giving the magnetic pressure  $P_{\text{mag}} = H^2/8\pi$  in psi or atmospheres as a function of the

magnetic field in gauss is shown in Fig. 5.5. A magnetic field of 5,000 gauss is equivalent to a pressure of about 1 atmosphere. Because the pressure varies directly as the square of the field, the magnetic pressure rises rapidly with increasing field strength. The magnetic pressure corresponding to 100,000 gauss is about 5,780 psi. Fields of  $10^6$  gauss have magnetic pressures beyond the working stresses of known materials and are therefore unrealizable, at least in the steady state.

Although in general the coil windings cannot support much tensile stress, they can and do support compressive stresses. To the extent that this reduces the compressive stresses in the structure, the estimates given below for the overall structural mass could be reduced.

The structure we shall consider first is a thin-walled cylinder having the same radius and length as the solenoid. This structure is supposed to be closely associated with the coil windings; the means of fastening the windings to the structure and providing channels for liquid helium coolant will not be discussed here.

Because of the cylindrical symmetry the stresses on the structure can be resolved into three principal components: an azimuthal tensile stress  $S_t$ , an axial compressive stress  $S_L$ , and a radial compressive stress  $S_R$ . The principle stress is  $S_t$ , which arises from forces in the structure required to balance the outward radial stress produced by the magnetic field. Calculation of the structural mass may be simplified by neglecting the radial compressive stress  $S_R$  by comparison with  $S_t$ . This may be justified as follows: The compressive radial stress is at most equal to the magnetic pressure  $H^2/8\pi$  at the coil windings, which is limited by the critical field  $H_c$  of the superconducting wire. For a value  $H_c$  equal to  $10^5$  gauss this pressure is about 5780 psi. On the other hand, the tensile stress  $S_t$  is of the order of the yield strength  $S_y$  of the structural material.\* For the titanium alloy Ti-6Al-4V ELI considered in the present application  $S_y$  is over 250,000 psi, so that  $S_R$  is at most 2 or 3 percent of  $S_t$ . If the structural material had a considerably

---

\*The tensile yield strength  $S_y$  is the maximum stress that can be developed in a material without causing more than a specified deformation or set; a set of 0.10 or 0.20 percent (which means an elongation of 0.001 or 0.002 in per in) is considered permissible for metals.

smaller yield strength, the radial compressive stress could not be neglected.

The axial compressive stress may not be neglected in general. It contributes to the structural mass because it in effect reduces  $S_t$  from its maximum value  $S_y$ . To compute this effect we utilize the relation from plasticity theory<sup>93</sup>

$$\left(\frac{S_y}{S_t}\right)^2 = 1 + \frac{S_L}{S_t} + \left(\frac{S_L}{S_t}\right)^2. \quad (5.7)$$

To estimate the mass of the structure we ignore detailed design features and restrict our consideration to overall forces and average stresses. These can be determined accurately from the expression for the total magnetic energy  $E_{\text{mag}}$  of the system. We have

$$E_{\text{mag}} = \frac{1}{2} \mathcal{L} I^2 \quad (5.8)$$

where  $I$  is the current in a single turn and  $\mathcal{L}$  [not to be confused with the Lagrangian  $\mathcal{L}$  of Eqs. (4.12) and (4.66)] is the inductance of the coil [Reference 98, Eq. (2.26)]

$$\mathcal{L} = \frac{8\pi N^2 R}{3k} \left[ K(k) - E(k) + \frac{k^2}{k'^2} \{E(k) - k\} \right]. \quad (5.9)$$

Here  $K(k)$  and  $E(k)$  are complete elliptic integrals with modulus  $k$  given by

$$k^2 = \frac{4R^2}{L^2 + 4R^2} \quad (5.10)$$

and  $k'^2 = 1 - k^2$  [Notice that  $k$  has a somewhat different form here than the  $k$  in Eqs. (4.78) (5.3)].

The average pressure  $\underline{P}$  tending to expand the cylinder radially can be obtained by equating the change  $\Delta E_{\text{mag}}$  in magnetic energy due to an expansion  $\Delta R$  of the solenoid-and-structure to the radial force  $2\pi RLP$  times the displacement  $\Delta R$ . Thus

$$P = \frac{1}{2\pi RL} \frac{\partial E_{\text{mag}}}{\partial R}. \quad (5.11)$$

Substituting Eqs. (5.8) (5.9) into Eq. (5.11) and performing the indicated differentiation, we obtain

$$P = \frac{N^2 I^2}{R^2} \frac{k^2}{k'^2} [E(k) - k]. \quad (5.12)$$

The pressure on the cylinder must be balanced by the tensile stress within the cylinder; accordingly we use the hoop-stress formula

$$t S_t = RP, \quad (5.13)$$

where  $t$  is the thickness of the cylindrical shell, to obtain the azimuthal tensile stress.

We get compressive axial stress in a similar manner. The compressive force on the cylinder is

$$2\pi R t S_L = - \frac{\partial E_{\text{mag}}}{\partial L}, \quad (5.14)$$

whence

$$t S_L = \frac{N^2 I^2}{3 R k'} \left[ \frac{2 k^2}{k'^2} \{E(k) - k\} - K(k) + E(k) \right]. \quad (5.15)$$

Dividing (5.15) by (5.13) with (5.12) substituted, we obtain an expression for the ratio  $S_L/S_t$ :

$$\frac{S_L}{S_t} = \frac{2}{3} - \frac{k'^2}{3 k^2} \frac{K(k) - E(k)}{E(k) - k}. \quad (5.16)$$

This ratio is plotted as a function of  $L/R$  in Fig. 5.6. For very short solenoids  $S_L/S_t$  is near zero; the longitudinal compressive stress is small compared to the azimuthal stress. For long solenoids  $S_L/S_t$  tends asymptotically to the value 0.5; thus the longitudinal stress is at most one-half the azimuthal stress.

The ratio  $S_y/S_t$  is obtained from  $S_L/S_t$  by means of Eq. (5.7);  $S_y/S_t$  is also plotted against  $L/R$  in Fig. 5.6. For very short solenoids  $S_y/S_t$  tends to unity; the longitudinal stress is not effective in reducing  $S_y$ . The ratio  $S_y/S_t$  increases slowly as  $L/R$  increases and tends asymptotically to  $\sqrt{1.75} = 1.324$  for large  $L/R$ . Thus the maximum increase in structural mass required in view of longitudinal compressive effects is about 32 percent, and this will occur only for very long solenoids.

The expression for  $S_y/S_t$  may be used in combination with the hoop-stress formula (5.13) to obtain the thickness  $t$  of the cylindrical shell in terms of the working stress  $S_y$ . The structural mass is

$$m_{st} = 2\pi R L t \rho_{st} \quad (5.17)$$

where  $\rho_{st}$  is the density of the structural material. If we now substitute

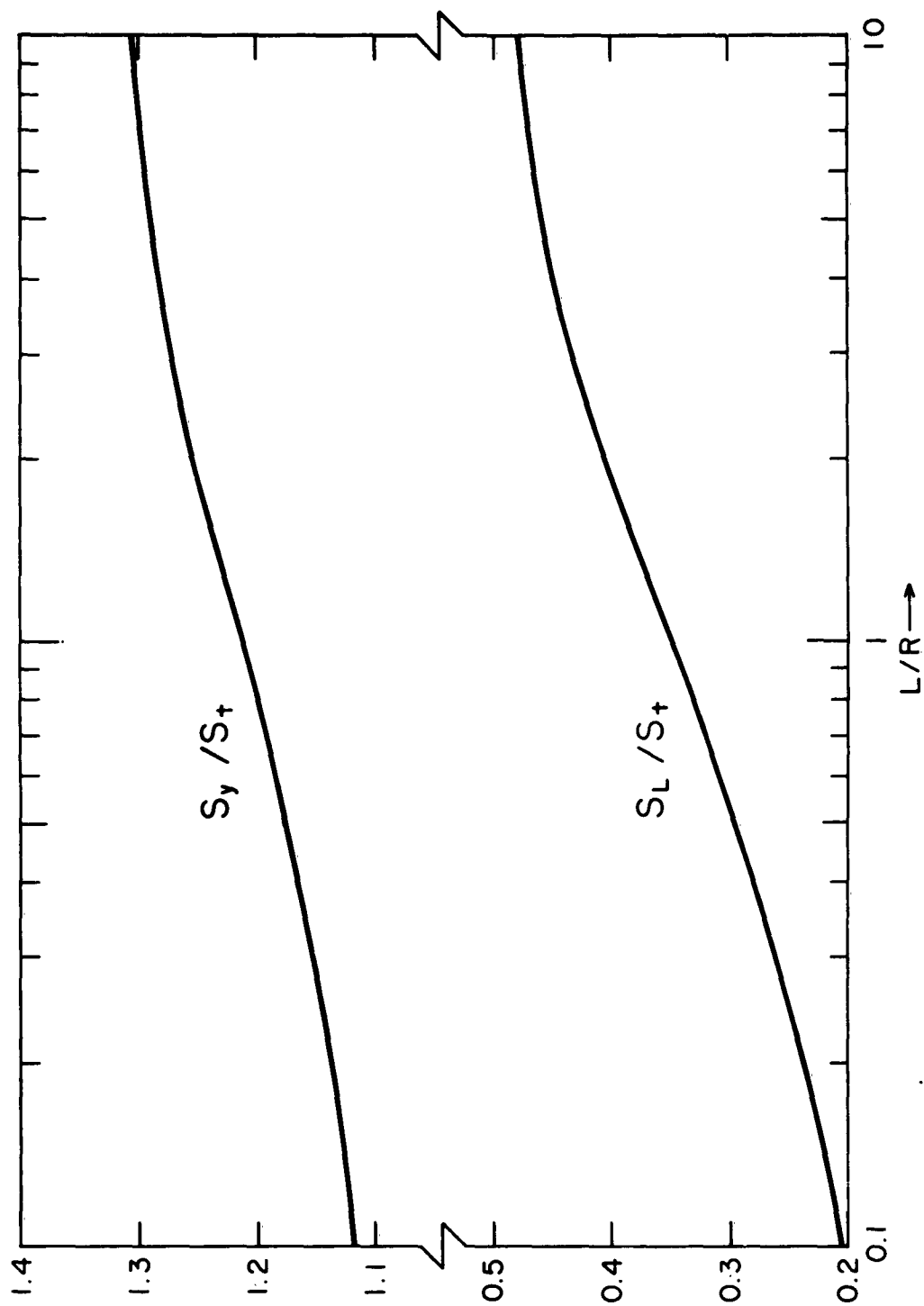


Fig. 5.6 Ratios of Working Stress to Azimuthal Stress and Longitudinal Stress to Azimuthal Stress for Cylindrical Solenoid Structures as Functions of  $L/R$ .

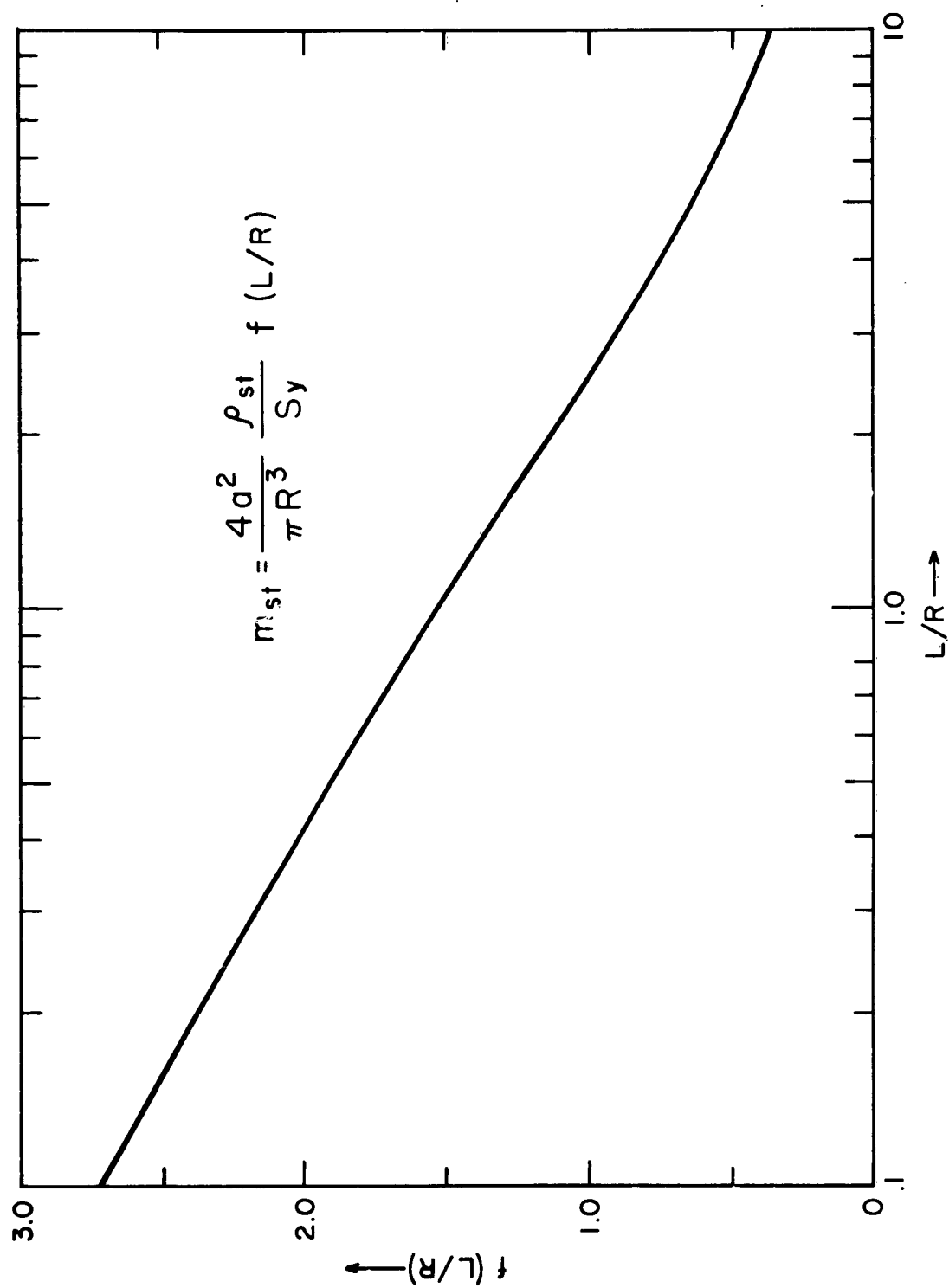


Fig. 5.7 Mass of the Cylindrical Structure  $C_1$  as a Function of  $L/R$ .

for  $\underline{t}$  and introduce the magnetic moment  $a = \pi R^2 NI$ , we have finally

$$m_{st} = \frac{4a^2}{\pi R^3} \frac{f_{st}}{S_y} \left[ 1 + \frac{S_L}{S_t} + \left( \frac{S_L}{S_t} \right)^2 \right]^{1/2} \frac{k}{k'^2} [E(k) - k], \quad (5.18)$$

where  $S_L/S_t$  is given by Eq. (5.16).

The variation of  $m_{st}$  with  $L/R$  is shown in Fig. 5.7. As an example, the mass of a solenoid designed to shield against 1-BeV protons, and having a magnetic moment of  $5.66 \times 10^{12}$  gauss  $\text{cm}^3$ , a radius of 400 cm, and a length 800 cm is found to be 180,000 kg or 394,000 lb. The thickness of the structure is about 20 cm. For these calculations we have used an extrapolated value

$$f_{st}/S_y = 2.46 \times 10^{-10} \text{ grams/erg}$$

appropriate to the titanium alloy Ti-6Al-4V ELI at a temperature of  $4^\circ\text{K}$ .

If we divide Eq. (5.18) for the structural mass by the expression for magnetic energy obtained from (5.8) (5.9), we obtain a relation of the form

$$\frac{m_{st}}{E_{mag}} = \frac{f_{st}}{S_y} g\left(\frac{L}{R}\right)$$

in which the factor  $g(L/R)$  depends on the shape of the coil. For a given  $L/R$ , the structural mass is proportional to the magnetic energy. If however  $L/R$  varies, then  $m_{st}/E_{mag}$  will also vary, by a factor of about 2.6 as we go from a flat solenoid to a very long solenoid. Thus the structural mass is not, strictly speaking, proportional to the magnetic energy stored in the coil, except for coils of constant shape. In what follows we will see that the factor  $g$  depends also on the structural configuration chosen, and for suitable structures can actually be made less than unity.

We have seen that for the solenoid there are two principal forces to be balanced by the supporting structure: an outward radial force  $\partial E_{\text{mag}}/\partial R$  and an inward axial force  $-\partial E_{\text{mag}}/\partial L$ . In the analysis presented so far a simple structure consisting of a thin cylinder ( $C_1$ ) encasing the solenoid windings was assumed for the support of both of these forces. It is apparently possible, however, to find somewhat more complicated structural configurations of smaller mass that can support the forces on the solenoid.

Consider a structural arrangement consisting of a cylinder  $C_2$  at the windings supporting the axial force plus a series of disks inside this cylinder supporting the radial force. Let  $t_d$  represent the total thickness (in the axial direction) of all the disks. Considering the radial stresses on the disks alone, we have

$$2\pi R t_d S_y = \frac{\partial E_{\text{mag}}}{\partial R}.$$

The thickness  $t$  of the cylinder  $C_1$  described previously is given by

$$2\pi R t S_t = \frac{\partial E_{\text{mag}}}{\partial R}.$$

The ratio of the volume of the disks to the volume of the cylinder  $C_1$  is

$$\frac{\text{Volume of disks}}{\text{Volume of } C_1} = \frac{\pi R^2 t_d}{2\pi R L t} = \frac{1}{2} \frac{S_t}{S_y}. \quad (5.19)$$

Now consider the cylinder  $C_2$  necessary to support the axial force, and let  $t_c$  represent its thickness. Then\*

$$2\pi R t_c S_y = -\frac{\partial E_{\text{mag}}}{\partial L}.$$

---

\*We are assuming (see Reference 93) that  $S_y$  represents the maximum compressive stress as well as the maximum tensile stress.

Comparing this with the corresponding relation for the cylinder  $C_1$  withstanding both axial and radial stresses

$$2\pi R t S_L = - \frac{\partial E_{mag}}{\partial L},$$

we find for the ratio of the volume of  $C_2$  to that of  $C_1$

$$\frac{\text{Volume of } C_2}{\text{Volume of } C_1} = \frac{t_c}{t} = \frac{S_L}{S_y} = \frac{S_L}{S_t} \frac{S_t}{S_y}. \quad (5.20)$$

Let us first apply this design to the case of a long solenoid. Noting from Fig. 5.6 that  $S_t \approx 0.76 S_y$  for a long solenoid, we see from Eq. (5.19) that the volume of the disks is about 0.38 that of the cylinder  $C_1$ . Also for the long solenoid  $S_L \approx 0.5 S_t$ ; hence the mass of the cylinder  $C_2$  is, according to Eq. (5.20), also 0.38 times the mass of  $C_1$ . Thus the mass  $m'_{st}$  of the new structure consisting of a thinner cylinder  $C_2$  and an array of thin connecting disks is only 0.76 of the mass  $m_{st}$  of the single cylinder  $C_1$ .

Consider now the situation for shorter solenoids. As  $L/R$  decreases  $S_L$  decreases and  $S_t$  approaches  $S_y$ . For a very flat solenoid ( $L \ll R$ ),  $S_L$  becomes only a few percent of  $S_t$ , so that the mass of  $C_2$  becomes small in comparison with that of the disks. Hence the structural mass is approximately that of the disks alone, or about half the mass of the corresponding cylinder  $C_1$ .

From the foregoing we conclude that the use of a structure consisting of a cylinder at the solenoid windings and connecting disks inside can give a mass reduction over a single cylinder varying from about 24 percent for long solenoids to almost 50 percent for flat solenoids. In the case of the solenoid for which  $L = 2R$ , the saving is approximately 27 percent.

It is of special interest in the case of the very flat solenoid to compare the mass  $m'_{st}$  of the supporting disk structure with the magnetic energy of the coil. (This comparison is also applicable to the single-turn magnetic

shield proposed by Levy<sup>77</sup>). For such a coil we have approximately

$$E_{mag} = 2\pi R N^2 I^2 (\Lambda - \frac{1}{2})$$

$$m'_{st} = \frac{p_{st}}{S_y} \pi R N^2 I^2 (\Lambda + \frac{1}{2})$$

where  $\Lambda = \log (8R/L)$ . Hence

$$m'_{st} = \frac{1}{2} \frac{\Lambda + \frac{1}{2}}{\Lambda - \frac{1}{2}} \frac{p_{st}}{S_y} E_{mag}. \quad (5.21)$$

For a very flat solenoid the numerical coefficient approaches one-half.

The results above are in contradiction to a theorem of Petschek and Longmire (presented by Levy<sup>99</sup>) which states that

$$m_{st} \geq \frac{p_{st}}{S_y} E_{mag}. \quad (5.22)$$

Extending an analysis by Parker<sup>100</sup> on so-called force-free coils, Petschek and Longmire obtain the following interesting relation between the magnetic energy and the trace  $S_{ii}$  of the mechanical stress tensor  $S_{ij}$ :

$$E_{mag} = \iiint_{\substack{\text{all} \\ \text{space}}} S_{ii} dV = \iiint_{\substack{\text{coil and} \\ \text{structure}}} S_{ii} dV. \quad (5.23)$$

In deriving consequences of this relation Petschek and Longmire assume that each of the principal stresses is supported by an individual structural member; on this basis Eq. (5.22) is obtained. The possibility of a structural element supporting a tensile stress in more than one direction has apparently

been overlooked. For example, if each structural element were under tensile stress in two principal directions we would have, instead of (5.22),

$$m_{st} \geq \frac{1}{2} \frac{\rho_{st}}{S_y} E_{mag}. \quad (5.24)$$

If a structural configuration could be devised such that each structural element were under maximum isotropic tensile stress, the numerical factor would be further reduced from one-half to one-third.

An analysis of the supporting disks used in the design above shows them to be under equal tensile stress  $S_y$  in both the azimuthal and radial directions. Thus neglecting the compressive axial stress (which for a flat coil is only a few percent of  $S_y$ ), we obtain from the relation (5.23)

$$E_{mag} \approx \iiint (S_{\alpha\alpha} + S_{\phi\phi}) dV = 2S_y V_{structure},$$

whence

$$m_{st} \approx \frac{1}{2} \frac{\rho_{st}}{S_y} E_{mag}. \quad (5.25)$$

The results presented above are extremely important, for it means that the structural mass can be reduced considerably---27 percent for the solenoid in which  $L = 2R$  and approximately 50 percent for a flat solenoid. We find therefore that for 1-BeV protons the weight of a superconducting magnetic shield may be made almost an order of magnitude smaller than the weight of a passive shield. Furthermore, if a design can be found for which the structural material is subjected to a tensile stress in each of the principal directions, the structural mass could be reduced even further.

## 6. CONCLUSIONS

### Feasibility

The most important parameters for four sample cylindrical solenoid designs are given in Table 6.1. It is to be emphasized that these examples are given merely to show the way in which the magnetic field, wire mass, and structural mass vary as the dimensions of the solenoid are changed, and in no way represent optimized designs suitable for fabrication. In all four designs the magnetic dipole moment has been held constant at  $5.66 \times 10^{12}$  gauss cm<sup>3</sup>. This gives Störmer radii of 10 meters for 1-Bev protons, 12.6 meters for 500-Mev protons, 19.5 meters for 100-Mev protons, and 345 meters for 1-Mev electrons.

An important conclusion to be derived from Table 6.1 regarding the shielding against high-energy particles is that as the radius of the solenoid is made smaller than about 0.4 Störmer radii the mass of both the windings and structure becomes excessive. This is particularly true for Example 4, where the length is also small compared with the Störmer radius. It is not clear at this time whether or not the increased mass of the system is accompanied by a corresponding increase in the volume shielded against high energy ( $\sim 1$  Bev) particles.

All of the shielded volume estimates in Table 6.1 are made using the dipole approximation except for the figure ( $\sim 50$  meters<sup>3</sup>) given for 1-Bev protons in Example 3. This has been obtained using the plot of the actual shielded region of a cylindrical solenoid shown in Fig. 4.14. The volume was estimated by considering a cross section of the toroidal shielded region as an ellipse and multiplying the area of this ellipse by the circumference  $2\pi R$  of the solenoid. The blank spaces in the shielded volume categories represent gaps in our knowledge of the shielded regions of solenoids whose dimensions are not small compared with the Störmer radius.

The best case for magnetic shielding can be made for vehicles having cabin shapes compatible with the toroidal shielded regions of axially symmetric current distributions. For vehicles having a certain amount of aerodynamic streamlining or for cylindrical vehicles, it may be more advantageous to consider shielding magnets having a larger ratio of radius to length. For such

Table 6.1 Parameters of four sample solenoids.

	Example #1	Example #2	Example #3	Example #4
Magnetic moment $a$ (gauss $\text{cm}^3$ )	$5.66 \times 10^{12}$	$5.66 \times 10^{12}$	$5.66 \times 10^{12}$	$5.66 \times 10^{12}$
Radius R (meters)	4	3	4	3
Length L (meters)	8	6	4	3
Central magnetic field H (gauss)	$1.25 \times 10^5$	$2.96 \times 10^5$	$1.58 \times 10^5$	$3.75 \times 10^5$
Wire material	Nb <sub>3</sub> Sn	Nb <sub>3</sub> Sn	Nb <sub>3</sub> Sn	Nb <sub>3</sub> Sn
Wire diameter (mm)	0.15	0.15	0.15	0.15
Current in single turn I (amperes)	20	10	20	5
Wire mass $m_w$ (lb)	44,000	117,600	44,000	235,000
$S_L/S_t$	0.406	0.406	0.350	0.350
$S_y/S_t$	1.254	1.254	1.213	1.213
$f(L/R)$	1.142	1.142	1.541	1.541
Mass of cylindrical structure $m_{st}$ (lb)	394,000	935,000	532,000	1,260,000
$m_{st}/(m_w + m_{st})$ (percent)	90.0	88.8	92.4	84.3
Mass of disk structure $m'_{st}$ (lb)	285,000	675,000	373,000	883,000
$m'_{st}/(m_w + m'_{st})$ (percent)	86.6	85.2	89.4	79.0
Total mass $m_w + m_{st}$ (lb)	329,000	792,600	417,000	1,118,000
R/C <sub>st</sub> for 1-Bev protons	0.400	0.300	0.400	0.300
Shielded volume for 1-Bev protons (meters <sup>3</sup> )			~50	
R/C <sub>st</sub> for 500-Mev protons	0.317	0.238	0.317	0.238
Shielded volume for 500-Mev protons (meters <sup>3</sup> )		~289		~289
R/C <sub>st</sub> for 100-Mev protons	0.205	0.154	0.205	0.154
Shielded volume for 100-Mev protons (meters <sup>3</sup> )	~1070	~1070	~1070	~1070
R/C <sub>st</sub> for 1-Mev electrons	0.116	0.087	0.116	0.087
Shielded volume for 1-Mev electron (meters <sup>3</sup> )	$5.91 \times 10^6$	$5.91 \times 10^6$	$5.91 \times 10^6$	$5.91 \times 10^6$

magnets and particle energies of interest the dipole analysis is not a good approximation, and it would be desirable to carry out an exact analysis of shielded regions for a cylindrical coil before making any final statements concerning magnetic shielding for such vehicles.

#### Comparison With Passive Shielding

Magnetic Design No. 4 of Table 6.1, capable of providing complete shielding against 1-Bev protons, was selected for comparison with passive shielding. The weight of the magnetic system, assuming that it uses niobium-tin superconductor and cylindrical disk structure, would be of the order of 417,000 lb. Using range-energy data and neglecting the effects of secondaries, an estimate was made of a passive shielding weight for the same shielded volume. For a polyethylene shield, about 334 grams/cm<sup>2</sup> are required to stop 1-Bev protons. The region completely shielded by the magnetic system against such particles would be toroidal and would have a volume of about 50 meters<sup>3</sup>. For a spherical volume of 50 meters<sup>3</sup> (radius 2.28 meters) the weight of the polyethylene shield is  $2.195 \times 10^5$  kilograms, or about 482,000 lb. If the additional shielding necessary to protect against secondary neutrons were taken into account, the passive shield would be heavier than this.

The prospects of magnetic shielding as a weight-saving device compared to passive shielding appear good, particularly when the present work is correlated with that of Levy (References 77, 99). About 80 percent of the mass of a magnetic shielding system would be taken up by the structure. The mass of the structure is proportional to the ratio  $\rho_{st}/S_y$  of density to yield strength of the structural material. Levy considered a single turn coil (a cylindrical solenoid of negligible length) and found that, for an optimized ratio of coil radius to Störmer radius, and using aluminum as the structural material, the mass of a magnetic shield could be made about a factor of 2 less than the mass of a comparable water shield for 1-Bev protons (neglecting secondaries). For aluminum the ratio  $\rho_{st}/S_y$  is about  $7.71 \times 10^{-10}$  grams/erg. The use of structural materials with a more advantageous "figure of merit" would give a smaller mass for the active shield. For instance, the titanium alloy Ti-6Al-4V ELI considered in Section 5 has a  $\rho_{st}/S_y$  ratio of  $2.46 \times 10^{-10}$  grams/erg

at 4°K. A single-turn magnetic shield using Levy's structure could be made to weigh about a factor 3 less than Levy's estimate using this structural material, or about a factor 6 less than a corresponding passive shield. If the disk structure utilizing tensile stresses in two directions were used, a factor 1.7 could be gained (taking into account the compressive stresses neglected by Levy). This means that a single-turn magnetic shield could be made about 1/10 of the mass of a water shield for 1-Bev protons. For lower energy particles Levy's calculations indicate that the magnetic shield would not be favorable compared to the passive shield, but when the considerations outlined above are taken into account, it may be concluded that magnetic shielding would have a weight advantage over passive shielding for low-energy protons also.

The use of solenoids of finite length could give a further weight advantage over the single-turn shield. According to Fig. 5.7 the mass of a cylindrical solenoid shield with fixed magnetic moment and fixed ratio  $\rho_{st}/S_y$  goes down as the ratio of length to radius increases. Basically this is because, as a cylindrical coil is lengthened with the dipole moment remaining constant, the field strength decreases. An infinitely long coil would have an infinite dipole moment but only a finite magnetic field inside. For a given ratio of coil radius to Störmer radius (which depends only on the particle energy and the dipole moment of the coil) the shielded volume also goes down as the length of the coil is increased, but the way in which this variation takes place has not yet been studied. By determining the coil parameters so that the ratio of shielded volume to coil mass is optimum, it might be possible to gain a further advantage over passive shielding using a cylindrical coil of some finite length.

#### Recommendations for Future Work

The present study indicates that magnetic shielding is feasible and warranted, and can probably be accomplished with the technology of 1968 or 1970. Before detailed engineering design efforts are made, however, it will be necessary to consider the following further problems:

1. A computer analysis of the forbidden regions should be made for a large number of cases of the cylindrical solenoid. The dipole analysis is valid only for values of magnetic moment and particle energy such that the

Stormer radius is much larger than the dimensions of the coil. The analysis of the forbidden region for a cylindrical coil, for Stormer distances not small by comparison with the coil radius or length, would be valuable for determining the optimum shape of coil and strength of field for a particular shielding situation.

2. A study of partial shielding should be made on the basis of particle trajectories in the magnetic field of a cylindrical solenoid. The solenoid chosen should be the one with optimum shielded volume to mass ratio selected in Part 1 above. Also calculations of the particle flux should be made for this cylindrical solenoid using a sequence of forbidden regions based on a realistic spectrum of particle energies. Thus the reduction in dosage accomplished by a magnetic shield over the unshielded dosage could be calculated explicitly.

3. A more thorough comparison of magnetic shielding with passive shielding requires more information on the effect of secondaries. This needs to be done both for the active and the passive cases because the more promising cylinder-disc structure for magnetic shielding has its important components exposed to bombardment by the primary charged particles.

4. An integrated structural analysis should be made to take into account such effects as the structural properties of the superconducting wire, nonuniform winding to decrease the mass of the conductors, distribution of current density in the nonuniform magnetic field to best take into account the magnetic field-critical current relationships of the superconductor, etc. It is to be expected that a considerable saving in payload weight of the shielding system could be accomplished by such a careful analysis of the solenoid construction.

5. Analysis of the structural mass and shielded regions should be made for other current configurations. It is perhaps not appropriate to speculate at this time on the explicit form of these current-carrying elements, but it is possible that more favorable shielded volume to structural mass ratios could be obtained by designs more complicated than the cylindrical solenoid or (its special case) the single-turn coil. Of greatest interest are the possibilities of approaching more closely the limiting factor  $1/2$  in the theorem (5.24) by using a structural design under tension in two directions.

6. A laboratory investigation into the properties of, and the fabrication in long lengths of niobium-tin wires, or wires of newer superconductors having higher critical fields and current densities, should be made. Ultimately this should involve understanding the structure of hard superconductors better. The effect of various mechanical treatments, fabrication, and heat treatment on the superconductors should be investigated so that ways of making materials with the optimum electrical and tensile properties may be discovered.

7. A fairly large-sized model superconducting solenoid using niobium-tin wire should be constructed and tested in the laboratory. This is needed to give better insight into the problems of startup, cryogenic systems, safety factors when the superconductors accidentally become normal, and to test explicitly the functioning of the magnetic shielding system.

## REFERENCES

1. J. A. Stratton, Electromagnetic Theory, McGraw-Hill Book Company, Inc., New York (1941).
2. W. R. Smythe, Static and Dynamic Electricity, McGraw-Hill Book Company, Inc., New York (1950).
3. H. Goldstein, Classical Mechanics, Addison-Wesley Press, Inc., Cambridge, Mass. (1950).
4. L. Landau and E. M. Lifschitz, The Classical Theory of Fields, Addison-Wesley Press, Inc., Cambridge, Mass. (1951).
5. W. K. H. Panofsky and M. Phillips, Classical Electricity and Magnetism, 2nd Ed., Addison-Wesley Publishing Company, Inc., Reading, Mass. (1962).
6. L. Janossy, Cosmic Rays, Oxford: At the Clarendon Press (1949).
7. J. R. Winckler, "Primary Cosmic Rays," Radiation Research **14**, 521-539 (1956).
8. J. H. Atkinson, Jr. and B. H. Willis, "High Energy Particle Data, Volume II," UCRL-2426 (rev.), June 1957.
9. K. A. Anderson, Preliminary Study of Prediction Aspects of Solar Cosmic Ray Events, NASA TN D-700.
10. K. A. Anderson and C. E. Fichtel, Discussions of Solar Proton Events and Manned Space Flight, NASA TN D-671.
11. J. R. Winckler, et. al., "Auroral X-Rays, Cosmic Rays, and Related Phenomena During the Storm of February 10-11, 1958," Journal of Geophysical Research **64**, 597-610 (1959).
12. E. P. Ney, J. R. Winckler, and P. S. Freier, "Protons From the Sun on May 12, 1959", Physical Review Letters **3**, 183 (1959).
13. D. C. Hock, Physics of the Van Allen Radiation Belts, Air Force Special Weapons Center Report AFSWC TR-60-57 (1960).

14. C. Y. Fan, P. Meyer, and J. A. Simpson, "Trapped and Cosmic Radiation Measurements from Explorer VI", Space Research: Proceedings of the First International Space Science Symposium, North-Holland Publishing Company, Amsterdam (1960).
15. T. R. Riethof, Charged Particle Radiation in Space, General Electric Company TIS Report R 60SD391, Philadelphia (1960).
16. D. H. Robey, "Radiation Shield Requirements for Two Large Solar Flares", Astronautica Acta 6, 206-224 (1960).
17. W. N. Hess and A. J. Starnes, "Measurement of the Neutron Flux in Space", Physical Review Letters 5, 48-50 (1960).
18. S. Yoshida, G. H. Ludwig, and J. A. Van Allen, "Distribution of Trapped Radiation in the Geomagnetic Field", Journal of Geophysical Research 65, 807-813 (1960).
19. E. C. Ray, "On the Theory of Protons Trapped in the Earth's Magnetic Field", Journal of Geophysical Research 65, 1125-1134 (1960).
20. R. L. Arnoldy, R. A. Hoffman, and J. R. Winckler, "Observations of the Van Allen Radiation Regions During August and September 1959, Part I," Journal of Geophysical Research 65, 1361-1376 (1960).
21. S. C. Freden and R. S. White, "Particle Fluxes in the Inner Radiation Belt", Journal of Geophysical Research 65, 1377-1383 (1960).
22. W. O. Roberts and H. Zirin, "Recent Progress in Solar Physics", Journal of Geophysical Research 65, 1645-1659 (1960).
23. J. R. Winckler and P. D. Bhavsar, "Low Energy Cosmic Rays and the Geomagnetic Storm of May 12, 1959", Journal of Geophysical Research 65, 2637-2655 (1960).
24. K. A. Anderson and D. C. Enemark, "Observations of Solar Cosmic Rays Near the North Magnetic Pole", Journal of Geophysical Research 65, 2657-2671 (1960).
25. K. G. McCracken and R. A. R. Palmeira, "Comparison of Solar Cosmic Rays Injection Including July 17, 1959 and May 4, 1960", Journal of Geophysical Research 65, 2673-2683 (1960).

26. J. A. Van Allen and W. C. Lin, "Outer Radiation Belt and Solar Proton Observations with Explorer VII During March-April 1960", Journal of Geophysical Research 65, 2998-3003 (1960).
27. R. L. Arnoldy, R. A. Hoffman, and J. R. Winckler, "Solar Cosmic Rays and Soft Radiation Observed at 5,000,000 Kilometers from Earth", Journal of Geophysical Research 65, 3004-3007 (1960).
28. J. C. Anderson, et. al., "The Solar Cosmic-Ray Outburst of May 4, 1960", Journal of Geophysical Research 65, 3889-3894 (1960).
29. J. A. Van Allen, "Corpuscular Radiations in Space", Radiation Research 14, 540-550 (1961).
30. E. P. Morrison, "Origin of Cosmic Rays", Handbuch der Physik, Vol. XLVI/1, Cosmic Rays I, Springer-Verlag, Berlin (1961).
31. H. S. Appleman, "Radiation Effects on Manned Space Flights", Journal of Environmental Sciences 4, No. 6, 10-13 (1961).
32. J. E. Naugle, "Space Radiation Levels", Nucleonics 19, No. 4, 89-91 (1961).
33. A. H. Armstrong, et. al., "Charged Particles in the Inner Van Allen Radiation Belt", Journal of Geophysical Research 66, 351-357 (1961).
34. J. R. Winckler, P. D. Bhavsar, and L. Peterson, "The Time Variations of Solar Cosmic Rays During July 1959 at Minneapolis", Journal of Geophysical Research 66, 995-1022 (1961).
35. J. R. Winckler, A. J. Masley, and T. C. May, "The High-Energy Cosmic-Ray Flare of May 4, 1960", Journal of Geophysical Research 66, 1023-1033 (1961).
36. J. G. Roederer, et. al., "Cosmic Ray Phenomena During the November 1960 Solar Disturbances", Journal of Geophysical Research 66, 1603-1610 (1961).
37. H. S. Ghielmetti, "The Spectrum and Propagation of Relativistic Solar Flare Particles During July 17-18, 1959", Journal of Geophysical Research 66, 1611-1625 (1961).

38. A. Roseu and T. A. Farley, "Characteristics of the Van Allen Radiation Zones as Measured by the Scintillation Counter on Explorer XI", Journal of Geophysical Research 66, 2013-2028 (1961).
39. M. Walt and W. M. MacDonald, "Energy Spectrum of Electrons Trapped in the Geomagnetic Field", Journal of Geophysical Research 66, 2047-2052 (1961).
40. S. E. Forbush, D. Venkatesan, and C. E. McIlwain, "Intensity Variations in the Outer Van Allen Radiation Belt", Journal of Geophysical Research 66, 2275-2287 (1961).
41. J. B. Cladis, L. F. Chase, W. L. Imhof, and D. J. Knecht, "Energy Spectrum and Angular Distribution of Electrons Trapped in the Geomagnetic Field", Journal of Geophysical Research 66, 2297-2312 (1961).
42. C. Y. Fan, P. Meyer, and J. A. Simpson, "Dynamics and Structure of the Outer Radiation Belt", Journal of Geophysical Research 66, 2607-2640 (1961).
43. J. T. Wasson, "Radioactivity Produced in Discoverer XVII by November 12, 1960 Solar Protons", Journal of Geophysical Research 66, 2659-2663 (1961).
44. D. Adamson and R. E. Davidson, "Statistics of Solar Cosmic Rays as Inferred from Correlation with Intense Geomagnetic Storms", NASA TN D-1010, February 1962.
45. R. A. Hoffman, R. L. Arnoldy, and J. R. Winckler, "Observations of the Van Allen Radiation Regions During August and September 1959. 3. The Inner Belt", Journal of Geophysical Research 67, 1-12 (1962).
46. S. Biswas, P. S. Freier, and W. Stein, "Solar Protons and Alpha Particles From the September 3, 1960 Flares", Journal of Geophysical Research 67, 13-24 (1962).
47. S. C. Freden and R. S. White, "Trapped Proton and Cosmic-Ray Albedo Neutron Fluxes", Journal of Geophysical Research 67, 25-29 (1962).
48. K. G. McCracken, "The Cosmic-Ray Flare Effect", Journal of Geophysical Research 67, 423-458 (1962).

49. J. W. Freeman, "Detection of an Intense Flux of Low-Energy Protons or Ions Trapped in the Inner Radiation Zone", Journal of Geophysical Research 67, 921-928 (1962).
50. K. W. Ogilvie, D. A. Bryant, and L. R. Davis, "Rocket Observations of Solar Protons During the November 1960 Events, I", Journal of Geophysical Research 67, 929-927 (1962).
51. G. Pizzella, C. E. McIlwain, and J. A. Van Allen, "Time Variations of Intensity in the Earth's Inner Radiation Zone, October 1959 Through December 1960", Journal of Geophysical Research 67, 1235-1253 (1962).
52. H. H. Heckman and A. H. Armstrong, "Energy Spectrum of Geomagnetically Trapped Protons", Journal of Geophysical Research 67, 1255-1262 (1962).
53. W. N. Hess and J. A. Poirier, "Energy Spectrum of Electrons in the Outer Radiation Belt", Journal of Geophysical Research 67, 1699-1709 (1962).
54. E. P. Ney and W. A. Stein, "Solar Protons, Alpha Particles, and Heavy Nuclei in November 1960", Journal of Geophysical Research 67, 2087-2105 (1962).
55. R. L. Arnoldy, R. A. Hoffman, and J. R. Winckler, "Observation of the Van Allen Radiation Regions During August and September, 1959. 4. The Outer-Zone Electrons", Journal of Geophysical Research 67, 2595-2611 (1962).
56. S. Biswas, "The Flux of Heavy Nuclei in the July 10, 1959 Flare", Journal of Geophysical Research 67, 2613-2615 (1962).
57. A. J. Masley, T. C. May, and J. R. Winckler, "Analysis of Balloon Observations During the April 1960 Solar Cosmic-Ray Events", Journal of Geophysical Research 67, 3243-3268 (1962).
58. B. Maehlum and B. J. O'Brien, "Solar Cosmic Rays of July 1961 and Their Ionospheric Effects", Journal of Geophysical Research 67, 3269-3279 (1962).

59. G. Pizzella, C. D. Laughlin, and B. J. O'Brien, "Note on the Electron Energy Spectrum in the Inner Van Allen Belt", Journal of Geophysical Research 67, 3281-3287 (1962).

60. H. J. Schaefer, "Radiation Danger in Space", Astronautics, July 1960, p. 36; "Proton Radiation Hazards in Space", Astronautics, February 1961, p. 39; see also "Tissue Depth Doses in the High Intensity Proton Radiation Field of the Inner Van Allen Belt" and "Further Evaluation of Tissue Depth Doses in Proton Radiation Fields in Space", U. S. Naval School of Aviation Medicine, Bureau of Medicine and Surgery, Research Project MR005. 13-1002, Subtask 1, Reports No. 16 and 17.

61. G. Lemaitre and M. S. Vallarta, "On Compton's Latitude Effect of Cosmic Radiation", Physical Review 43, 87-91 (1933).

62. G. Lemaitre, M. S. Vallarta, and L. Bouckaert, "On the North-South Asymmetry of Cosmic Radiation", Physical Review 47, 434-436 (1935).

63. G. Lemaitre and M. S. Vallarta, "On the Geomagnetic Analysis of Cosmic Radiation", Physical Review 49, 719-726 (1936).

64. G. Lemaitre and M. S. Vallarta, "On the Allowed Cone of Cosmic Radiation", Physical Review 50, 493-504 (1936).

65. M. S. Vallarta, "Theory of the Geomagnetic Effects of Cosmic Radiation", Handbuch der Physik, Vol. XLVI/1, Cosmic Rays I, Springer-Verlag, Berlin (1961).

66. K. Dwight, "Solar Magnetic Moment and Diurnal Variation in Intensity of Cosmic Radiation", Physical Review 78, 40-49 (1950).

67. A. Schlüter, "Solare Ultrastrahlung and Erdmagnetfeld", Zeitschrift für Naturforschung 6a, 613-618 (1951).

68. J. Firor, "Cosmic Radiation Intensity-Time Variations and Their Origin. IV. Increases Associated With Solar Flares", Physical Review 94, 1017-1028 (1954).

69. F. S. Jory, "Selected Cosmic-Ray Orbits in the Earth's Magnetic Field", Physical Review 103, 1068-1075 (1956).

70. R. Lüst, "Impact Zones for Solar Cosmic-Ray Particles", Physical Review 105, 1827-1839 (1957).
71. J. E. Kasper, "Geomagnetic Effects on Cosmic Radiation for Observation Points Above the Earth", Journal of Geophysical Research 65, 39-53 (1960).
72. T. Kelsall, "Solar Proton Impact Zones", Journal of Geophysical Research 66, 4047-4070 (1961).
73. R. F. Tooper, "Trajectories of Charged Particles in a Magnetic Dipole Field", Bulletin of the American Physical Society 7, 467 (1962).
74. R. F. Tooper and W. O. Davies, Electromagnetic Shielding of Space Vehicles, IAS Paper No. 62-156, June 1962.
75. C. Störmer, The Polar Aurora, Oxford: At the Clarendon Press (1955).
76. N. F. Dow, "Structural Implications of the Ionizing Radiation in Space", Proceedings of the Manned Space Stations Symposium, Los Angeles, Calif., April 20-22 (1960).
77. R. H. Levy, "Radiation Shielding of Space Vehicles by Means of Superconducting Coils", ARS Journal 31, 1568-1570 (1961); see also AVCO Research Report 106 (1961).
78. N. F. Dow, S. P. Shen, and J. F. Heyda, "Evaluations of Space Vehicle Shielding", General Electric Space Sciences Laboratory Report R 62SD31, April 1962.
79. G. V. Brown, "Magnetic Radiation Shielding", Proceedings of the International Conference on High Magnetic Fields, M. I. T. Press and John Wiley and Sons, Inc. (1962), pp. 370-378.
80. S. W. Kash and R. F. Tooper, "Active Shielding for Manned Space Flight", Astronautics, September 1962, p. 68.
81. D. Shoenberg, Superconductivity, Cambridge University Press, London (1952).
82. B. Serin, "Superconductivity. Experimental Part", Handbuch der Physik, Vol. XV, Low Temperature Physics II, pp. 210-273, Springer-Verlag, Berlin (1956). In connection with this see also J. Bardeen, "Theory of Superconductivity", pp. 274-369 in the same volume.

83. K. Mendelssohn, Cryophysics, Interscience Publishers, Inc., New York (1960).
84. F. London, Superfluids. I. Macroscopic Theory of Superconductivity, 2nd Ed., Dover Publications, Inc., New York (1961).
85. J. E. Kunzler, E. Buehler, F. S. L. Hsu, and J. H. Wernick, "Superconductivity in  $\text{Nb}_3\text{Sn}$  at High Current Density in a Magnetic Field of 88 Kgauss", Physical Review Letters 6, 89-91 (1961).
86. J. E. Kunzler, "Superconductivity in High Magnetic Fields at High Current Densities", Reviews of Modern Physics 33, 1-9 (1961).
87. H. Kolm, B. Lax, F. Bitter, and R. Mills, ed., "Superconducting Materials", in Proceedings of the International Conference on High Magnetic Fields, M.I. T. Press and John Wiley and Sons, Inc., (1962), pp. 574-614.
88. D. B. Montgomery and J. Terrell, Some Useful Information for the Design of Air-Core Solenoids, AFOSR-1525, National Magnet Laboratory, Massachusetts Institute of Technology (1961).
89. R. W. Boom and R. S. Livingston, "Superconducting Solenoids", Proceedings of the IRE 50, 274-285 (1962).
90. R. F. Tooper and W. E. Zagotta, "Design of a Superconducting Solenoid for Magnetic Shielding", Electromagnetic Shielding Feasibility Study, Armour Research Foundation Report ARF 1196-9.
91. S. H. Autler, "Superconducting Magnets"; J. K. Hulm, M. J. Fraser, H. Riemersma, A. J. Venturino, and R. E. Wien, "A High Field Niobium-Zirconium Superconducting Solenoid"; R. R. Hake, T. G. Berlincourt, and D. H. Leslie, "A 59-Kilogauss Niobium-Zirconium Superconducting Solenoid"; L. J. Donadieu and D. J. Rose, "Conception and Design of a Large Volume Superconducting Solenoid"; Proceedings of the International Conference on High Magnetic Fields, M.I. T. Press and John Wiley and Sons, Inc., (1962) pp. 324-343, 358-369.
92. J. F. Watson, J. L. Christian, and J. Hertz, "Cryogenics: Selection Data for Structural Materials", Electro-Technology 68, 76-84 (1961).
93. A. Nadai, Plasticity, McGraw-Hill Book Company, Inc., New York (1931), pp. 182-185.

94. J. B. Scarborough, Numerical Mathematical Analysis, 4th Ed., Johns Hopkins Press, Baltimore (1958).

95. P. F. Byrd and M. D. Friedmann, Handbook of Elliptic Integrals for Engineers and Physicists, Springer-Verlag, Berlin (1954).

96. E. E. Callaghan and S. H. Maslen, The Magnetic Field of a Finite Solenoid, NASA TN D-465.

97. H. Riemersma, et. al., "A Variable Composition, High Field Superconducting Solenoid", Journal of Applied Physics 33, 3499-3504 (1962).

98. C. Snow, Formulas for Computing Capacitance and Inductance, National Bureau of Standards Circular 544 (1954), p. 31.

99. R. H. Levy, "Reply to Willinski's Comment on 'Radiation Shielding of Space Vehicles by Means of Superconducting Coils,'" ARS Journal, May 1962, p. 787.

100. E. N. Parker, "Reaction of Laboratory Magnetic Fields Against Their Current Coils", Physical Review 109, 1440 (1958).

<p>Aeronautical Systems Division, Dir/Advanced Systems Planning, Aerospace Vehicle Design Branch, Wright-Patterson AFB, Ohio. Rpt Nr ASD-TDR-63-194, ELECTROMAGNETIC SHIELDING FEASIBILITY STUDY. Final report, May 63. 143 p. incl illus., tables, 100 refs.</p> <p>Unclassified Report</p> <p>This report discussed the shielding of personnel against charged particles in space using electric or magnetic fields. The energy distribution and other characteristics of charged particles in space are summarized. The operation and stability of an electrostatic shield (two concentric charged conducting spheres) for protection against 1-Mev electrons and 500-Mev protons is discussed. Shielded regions for charges in a magnetic dipole field are described. A method is given for</p>	<p>Unclassified</p> <ol style="list-style-type: none"> <li>1. Electromagnetic shielding</li> <li>2. Feasibility study</li> <li>1. AFSC Project 1395, Task 139502</li> <li>2. Contract AF 33(616)-8489</li> <li>3. Armour Research Foundation, Chicago, Illinois</li> <li>4. Robert F. Tooper</li> <li>5. Avail fr OTS</li> <li>6. In ASTIA collection</li> </ol>
<p>Aeronautical Systems Division, Dir/Advanced Systems Planning, Aerospace Vehicle Design Branch, Wright-Patterson AFB, Ohio. Rpt Nr ASD-TDR-63-194, ELECTROMAGNETIC SHIELDING FEASIBILITY STUDY. Final report, May 63. 143 p. incl illus., tables, 100 refs.</p> <p>Unclassified Report</p> <p>This report discussed the shielding of personnel against charged particles in space using electric or magnetic fields. The energy distribution and other characteristics of charged particles in space are summarized. The operation and stability of an electrostatic shield (two concentric charged conducting spheres) for protection against 1-Mev electrons and 500-Mev protons is discussed. Shielded regions for charges in a magnetic dipole field are described. A method is given for</p>	<p>Unclassified</p> <ol style="list-style-type: none"> <li>1. Electromagnetic shielding</li> <li>2. Feasibility study</li> <li>1. AFSC Project 1395, Task 139502</li> <li>2. Contract AF 33(616)-8489</li> <li>3. Armour Research Foundation, Chicago, Illinois</li> <li>4. Robert F. Tooper</li> <li>5. Avail fr OTS</li> <li>6. In ASTIA collection</li> </ol>
<p>Aeronautical Systems Division, Dir/Advanced Systems Planning, Aerospace Vehicle Design Branch, Wright-Patterson AFB, Ohio. Rpt Nr ASD-TDR-63-194, ELECTROMAGNETIC SHIELDING FEASIBILITY STUDY. Final report, May 63. 143 p. incl illus., tables, 100 refs.</p> <p>Unclassified Report</p> <p>This report discussed the shielding of personnel against charged particles in space using electric or magnetic fields. The energy distribution and other characteristics of charged particles in space are summarized. The operation and stability of an electrostatic shield (two concentric charged conducting spheres) for protection against 1-Mev electrons and 500-Mev protons is discussed. Shielded regions for charges in a magnetic dipole field are described. A method is given for</p>	<p>Unclassified</p> <ol style="list-style-type: none"> <li>1. Electromagnetic shielding</li> <li>2. Feasibility study</li> <li>1. AFSC Project 1395, Task 139502</li> <li>2. Contract AF 33(616)-8489</li> <li>3. Armour Research Foundation, Chicago, Illinois</li> <li>4. Robert F. Tooper</li> <li>5. Avail fr OTS</li> <li>6. In ASTIA collection</li> </ol>